الجمهورية الجزائرية الديمقراطية الشعبية

République Algérienne Démocratique et Populaire

Ministère de L'Enseignement Supérieur et de la Recherche Scientifique

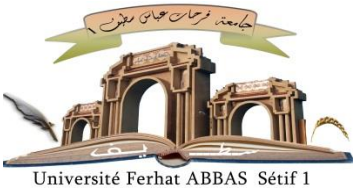

UNIVERSITÉ FERHAT ABBAS - SETIF1

FACULTÉ DE TECHNOLOGIE

THÈSE

Présentée au Département de génie civil

Pour l'obtention du diplôme de

DOCTORAT

Domaine : Sciences et Technologie

Filière : Génie civil

Option : Modélisation numérique en structures

Par

ABDESSELAM Abderrahmane

THÈME

Modélisation numérique des éléments structuraux linéaires en béton armé renforcés par des matériaux composites

Soutenue le 06/07/2024 devant le Jury:			
HADJI Rihab	**Professeur**	**Univ. Ferhat Abbas Sétif 1**	**Président**
MERDAS Abdelghani	**Professeur**	**Univ. Ferhat Abbas Sétif 1**	**Directeur de thèse**
BENZAID Riad	**Professeur**	**Univ. Jijel**	**Examinateur**
HEBBACHE Kamel	**M.C.A.**	**Univ. Ferhat Abbas Sétif 1**	**Examinateur**
YAHIAOUI Djarir	**Professeur**	**Univ , Batna 2**	**Examinateur**

الجمهورية الجزائرية الديمقراطية الشعبية

Democratic and Popular Republic of Algeria

Ministry of Higher Education and Scientific Research

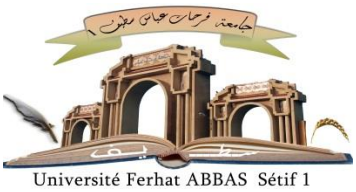

FERHAT ABBAS UNIVERSITY - SETIF1

FACULTY OF TECHNOLOGY

THESIS

Presented to the Department of Civil Engineering

For obtaining the degree of

DOCTORATE

Field: Science and Technology

Field: Civil Engineering **Option: Numerical Modeling in Structures**

By

ABDESSELAM Abderrahmane

THEME

Numerical modeling of linear reinforced concrete elements strengthened by composite materials

Defended on 06/07/2024 in front of the Jury:			
HADJI Rihab	**Professor**	**Univ. Ferhat Abbas Sétif 1**	**President**
MERDAS Abdelghani	**Professor**	**Univ. Ferhat Abbas Sétif 1**	**Thesis Supervisor**
BENZAID Riad	**Professor**	**Univ. Jijel**	**Examiner**
HEBBACHE Kamel	**M.C.A.**	**Univ. Ferhat Abbas Sétif 1**	**Examiner**
YAHIAOUI Djarir	**Professor**	**Univ , Batna 2**	**Examiner**

Dedication

To my mother and family for their unwavering love, support, and understanding throughout this academic journey. Their encouragement has been my source of strength during challenging times.

This thesis is the culmination of not just my efforts but also of the support and belief of those around me. Thank you all for making this achievement possible.

Acknowledgments

I would like to express my sincere gratitude to my supervisor, Pr. Abdelghani Merdas., for the untiring help and for the key contributions that allowed the development of this thesis.

I am immensely grateful to the members of my supervisory committee, Pr HADJI Rihab, BENZAID Riad, Dr.HEBBACHE Kamel, and Pr.YAHIAOUI Djarir for generously dedicating their time and expertise to review and evaluate this thesis. Your commitment to ensuring the rigor and quality of my research is deeply appreciated.

My sincere appreciation extends to all the members of the Civil Engineering Department at Setif 1 University for their endless help and support, which greatly facilitated my research.

Special appreciation goes to all the members of the Research Unit Emerging Materials (URME) at Ferhat Abbas University Setif 1 for fostering a supportive and stimulating research environment.

I wish to express my special thanks to Professor Harkti El Hadi and the Members University of Tebessa for their valuable guidance and support throughout my research journey.

Additionally, I am thankful to the members of the L2MGC Laboratory of Civil Engineering at Cergy Pontoise University (France) for their assistance.

I extend my heartfelt thanks to all my friends and colleagues who have supported me along the way.

ملخص

تهدف هذه الأطروحة إلى دراسة استخدام شرائط البوليمر المدعم بألياف الكربون، باستخدام تقنية NSM ، لتحسين مقاومة الانحناء لعوارض الخرسانة المسلحة. تم تطوير نموذج تحليل رقمي غير خطي باستخدام العناصر المحددة لمحاكاة سلوك هذه العوارض، وأظهر النموذج الرقمي نجاحاً في توقع النتائج التجريبية. تم التحقق من دقة سلوك الالتصاق باستخدام اختبارات الشد المأخوذة من الأبحاث السابقة. بعد ذلك، أُجريت دراسات معيارية باستخدام النموذج الرقمي لفحص تأثير مختلف عوامل التدعيم على أداء الانحناء للعوارض، من ضمنها طول الارتباط وعدد أشرطة FRP وشدة الخرسانة ونوع الألياف ونسبة التسليح وطريقة التدعيم. أظهرت النتائج تحسنًا ملحوظًا في مقاومة الانكسار والصلابة عند الانهيار، مع زيادة تصل إلى 126% في المقاومة العظمى عند استخدام تقنية NSM. ولكن لوحظ انخفاض ملحوظ في ليونة العوارض بسبب انفصال شرائط الكربون (FRP) في العوارض المدعمة. وللتخفيف من حدة هذه المشكلة، استعرضت الدراسة تقنيات تدعيم أكثر كفاءة، حيث ركزت على تحسين طول الارتباط ونسبة التسليح ووضعية أشرطة NSM .

الكلمات المفتاحية: البوليمرات المدعمة بالألياف، تدعيم سلوك الانحناء، التسليح القريب من السطح، النمذجة الرقمية ، سلوك الترابط، عوارض الخرسانة المسلحة

Abstract

This thesis explores the use of Near Surface Mounted (NSM) Fiber-Reinforced Polymer (FRP) strips/rods to enhance the flexural strength of reinforced concrete (RC) beams. A nonlinear Finite Element Analysis (FEA) model was developed to simulate the behavior of FRP-strengthened RC beams, successfully predicting experimental outcomes. Validation of bond behavior was conducted using pull-out tests from existing literature. Parametric studies were subsequently performed using the FEA model to investigate the influence of various reinforcement parameters on beam flexural performance, including bond length, number of FRP bars, concrete strength, FRP type, reinforcement ratio, and reinforcement method. Results indicated a significant enhancement in both yield and ultimate strengths, with ultimate strengths improving by up to 126% with CFRP strengthening. However, a notable reduction in ductility was observed due to debonding of CFRP strips in the strengthened beams. To mitigate this issue, the study explored more efficient strengthening techniques, focusing on optimizing the effective bond length, reinforcement ratio, and positioning of NSM bars.

Keywords: Fiber Reinforced polymers, Flexural reinforcement, Near Surface Mounted, Numerical modeling, Bond behavior, Reinforced Concrete Beams

Résumé

Cette thèse explore l'utilisation de barres/tiges en polymère renforcé de fibres (PRF) montées en surface proche (NSM) pour améliorer la résistance à la flexion des poutres en béton armé (BA). Un modèle d'analyse par éléments finis (FEA) non linéaire a été développé pour simuler le comportement des poutres BA renforcées par PRF, prédisant avec succès les résultats expérimentaux. La validation du comportement d'adhésion a été réalisée à l'aide de essais d'arrachement tirés de la littérature existante. Des études paramétriques ont ensuite été effectuées à l'aide du modèle FEA pour examiner l'influence de divers paramètres de renforcement sur les performances de flexion des poutres, incluant la longueur d'adhérence, le nombre de barres PRF, la résistance du béton, le type de PRF, le taux et la méthode de renforcement. Les résultats ont montré une amélioration significative des résistances à la limite d'élasticité et à la rupture, avec des augmentations de jusqu'à 126 % pour la résistance ultime avec le renforcement par PRF. Cependant, une réduction notable de la ductilité a été observée en raison du décollement des bandes PRF dans les poutres renforcées. Pour atténuer ce problème, l'étude a exploré des techniques de renforcement plus efficaces, en se concentrant sur l'optimisation de la longueur d'adhésion effective, du taux de renforcement et du positionnement des barres NSM.

Mots clés : Polymères renforcés de fibres, Renforcement en flexion, Montage près de la surface, Modélisation numérique, Comportement d'adhérence, Poutres en béton armé

Table of Contents

List of Figures

List of Tables

Introduction

Reinforced concrete (RC) stands as a widely utilized construction material due to its favorable strength, affordability, and ease of construction. It finds application in various structures such as buildings, bridges, and heavy constructions. Nonetheless, RC components are subject to deterioration from environmental factors, heavy traffic loads, and seismic activity. Various rehabilitation techniques employing different materials are available to counteract this degradation. One such technique involves the application of high-tensile-strength fiber-reinforced polymer (FRP) materials to the tensile face of the RC beam to improve its flexural performance. [1-4]

FRP composites have emerged as appealing retrofitting materials due to their lightweight nature, high tensile strength, resistance to corrosion, and ease of handling. They are employed to enhance both the flexural and shear performance of RC members. Among the types of FRP materials available, carbon fiber reinforced polymer (CFRP) boasts the highest tensile strength, high modulus of elasticity, and excellent fatigue properties. [5-10]

CFRP materials are accessible in various forms including plates, sheets, and circular rods. Plates offer a large surface area conducive to attachment to the tensile surface of the RC beam using bonding materials like epoxy. Another attachment technique, known as near surface mounted (NSM), has been introduced to mitigate environmental degradation of CFRP plates and further improve their bond to concrete by cutting small grooves into the RC beam.

While experimental testing remains the predominant method to assess the enhancement of RC members strengthened with CFRP plates in flexural response, it can be time-consuming and costly, especially when exploring multiple parameters related to material properties and bonding techniques. Therefore, the finite element method (FEM) can be employed to address these limitations by providing insights into variable changes.

Nonlinear FEMs can effectively model the complex behavior of composite materials such as concrete, including their response to compression, tension, and the behavior of internal steel reinforcement. Several commercial 3D FEM packages like

ABAQUS exist for analyzing complex material behaviors under various circumstances. However, their capabilities in modeling the response of RC beams retrofitted by prestressed CFRP plates may vary, necessitating detailed mechanical property considerations for concrete and CFRP, as well as nonlinear contact surface modeling.

Objectives

The primary aim of this research is to investigate the behavior of RC beams strengthened with CFRP plates and examine how different parameters affect their performance. To validate proposed models for RC beams strengthened with CFRP plates, finite element analysis (FEA) results were compared against experimental data. Developing an FE model representing an RC beam retrofitted by prestressed CFRP plates involves several considerations:

Modeling the RC beam as a composite of nonlinear concrete and elasto-plastic steel reinforcement, alongside elastic materials that fail by maximum tensile strain for CFRP composite material, each exhibiting distinct behaviors under loading.

Modeling the interaction behavior between the RC beam and CFRP plate, crucial for strengthening performance as debonding at the concrete-CFRP interface is a commonly reported failure mode.

Modeling the effect of the CFRP plate and how stresses are transferred to the RC beam.

The validated FE model is used to explore various parameters influencing the behavior of reinforced concrete beams strengthened by NSM FRP.

Firstly, the effect of the bond length and the number of FRP bars is examined, analyzing the impact of the number of strips with a constant CFRP cross-section and different anchorage lengths. The dimensions of the reference strip, groove sizes, and spacing are maintained for comparison purposes.

Next, the effect of concrete strength and FRP type is evaluated. This analysis investigates the influence of concrete strength on NSM bars made from four different FRP materials (CFRP, AFRP, BFRP, and GFRP) with varying concrete strengths.

Lastly, the effect of the FRP reinforcement rate is studied, examining the impact of different reinforcement rates on the performance of NSM FRP bars while maintaining a constant bar length. CFRP cross-sections of different sizes are used to study these effects.

Thesis Outline

In order to achieve the objectives of the current study, the thesis follows a structured approach outlined as follows:

Chapter 1 provides a comprehensive review of the literature to date on techniques for strengthening RC structures for repair and reinforcement purposes. The chapter begins with a thorough examination of FRP composites, including their manufacturing processes, various product categories, and mechanical properties, as well as a discussion of adhesives commonly used in strengthening efforts. The chapter then delves into the specifics of both externally bonded (EB) and near-surface-mounted (NSM) strengthening techniques. This is followed by a detailed analysis of the bond interface between NSM FRP and concrete, including an examination of various bond failure modes and factors influencing bond properties. In addition, existing research on the flexural behavior of RC members strengthened with NSM FRP is reviewed, shedding light on various failure modes. Finally, a comprehensive discussion of the creep behavior of the materials integral to the NSM system, namely concrete, FRP, and adhesive, is presented in this chapter.

In CHAPTER 2, the focus shifts to detailing the experimental parameters used in the research. This includes the specimen test matrix and a comprehensive description of the beam specimen fabrication process, which includes the preparation of RC beams and the application of NSM strengthening techniques. In addition, the instrumentation and test setup are explained, as well as procedures for material characterization.

CHAPTER 3 is dedicated to the numerical simulation of the bond between concrete and CFRP for both EB and NSM techniques. Here, the results of bond pull-out tests are summarized.

Chapter 4 deals with the numerical simulation of RC beams reinforced with NSM-FRP. The validated finite element (FE) model is used to investigate various parameters that influence the behavior of RC beams reinforced with NSM FRP.

Finally, the thesis concludes by summarizing the main findings and providing recommendations for future research efforts.

Chapter I: Literature Review

I.1 Introduction

Fiber Reinforced Polymer (FRP) was introduced in Russia in 1975 as a reinforcing bar that uses synthetic or natural fibers to increase the stiffness and strength of the polymer. It quickly gained recognition for its exceptional strength, being 8 times stronger than conventional steel bars. In Europe, interest in FRPs for structural reinforcement emerged in the 1980s, while in the United States, FRP composites have been used for strengthening projects for more than 25 years. During this time, FRP has become a mainstream construction material. Primarily used as internal or external reinforcement for various structures, FRP bars gained popularity in Japan in the 1990s, particularly in elevated train support structures. Although one-fourth the weight of steel, FRP has higher tensile strength. Japanese researchers published the first design guidelines for FRP in reinforced concrete in 1996, spurring worldwide adoption. High-strength carbon fiber reinforced polymer (CFRP) has since been endorsed for seismic improvements. Interest in repairing and upgrading existing RC bridges has grown, driven by the need to accommodate heavier vehicles and to address deterioration. FRP reinforcements offer a solution by increasing the structural load capacity. The FRP market has experienced rapid growth and is expected to continue to expand. This study aims to provide a comprehensive review of FRP design, materials, and properties, including strength, stiffness, conductivity, and resistance to fatigue, corrosion, and fire. It also examines integrated applications for repair, rehabilitation, retrofit, and strengthening of RC structures in the construction industry. [10-17]

I.2 FRP Materials

Among the various fibers, carbon fiber reinforced polymer (CFRP) stands out for its superior mechanical properties compared to steel and other polymer fibers. CFRP attributes include high tensile strength, stiffness, chemical and corrosion resistance, and low thermal expansion. Despite its higher cost, CFRP is preferred when a high strength-to-weight ratio is critical in construction materials.

CFRPs are widely used in construction to strengthen concrete, steel, and masonry structures, either by retrofitting existing structures to carry additional loads or by addressing weakening over time. They can be wrapped around specific areas or applied as sheets to improve the shear strength of reinforced concrete members.

The advantages of carbon fibers are that they are lightweight, providing strength while requiring less material than metal counterparts. They are also resistant to corrosion and external agents and retain their shape despite temperature changes. However, the main drawback is the complexity and cost of manufacturing, along with the challenges of recycling through thermosetting resins. [18; 19]

Economically, CFRP offers significant advantages despite its higher initial cost compared to steel. Its resistance to corrosion and high temperatures, ease of installation and repair, and eco-efficiency make it a suitable choice for the construction industry. Eco-efficiency considerations, including recycling and reuse of materials and avoidance of heavy structural elements, contribute to its appeal.

A cost comparison between CFRP and steel shows that CFRP reinforcement in concrete can be a more reasonable choice, especially for lightweight and easily transportable structures

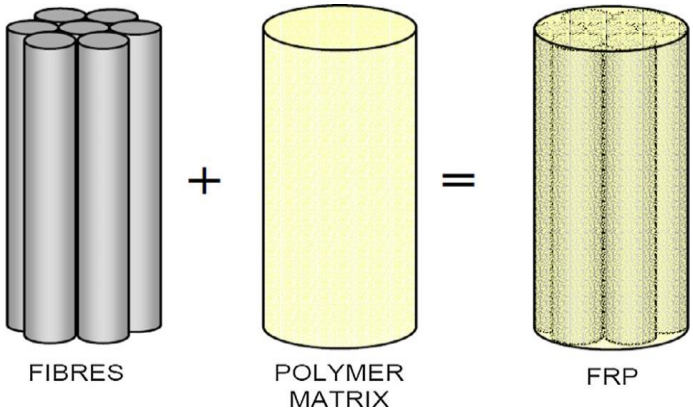

Figure 1.1 FRP constituents [22]

FRP components (figure 1.1) can be manufactured by several techniques, three of which are of particular importance: Pultrusion, Wet Lay-up, and Filament Winding. Pultrusion is used to produce FRP composites with uniform cross-sectional shapes such as bars, rods, tendons, plates, and structural sections. Wet lay-up, on the other hand, is often used in structural repair projects where FRP sheets or fabrics are bonded to the exterior of RC, steel, aluminum, or wood members. Filament winding, an automated

process, involves pulling raw fibers from spools, passing them through a resin bath, and winding them onto a rotating mandrel. In FRP composites, the fibers can be arranged unidirectional or woven in multiple directions. Unidirectional composites are typically preferred for strengthening applications. FRP composites can be formed as reinforcing bars, strips/laminates, plates, and profiles. FRP bars serve as internal reinforcement for RC structures or as near-surface-mounted (NSM) reinforcement for strengthening applications. They are available in various classifications based on fiber type, cross-sectional shape, surface texture and treatment. FRP sheets and strips/laminates are used to strengthen and rehabilitate existing structures. Sheets, typically supplied in roll form, offer high versatility and portability. Strips and laminates provide stiffness due to the polymer matrix, with strips being approximately 1.0-1.5 mm thick and sheets being thinner. FRP profiles, available in a variety of shapes and cross-sections, include strips, the most common reinforcement shape for NSM reinforcement systems due to their resistance to debonding from the concrete substrate. Narrow strips maximize the ratio of surface area to cross-sectional area, minimizing the risk of debonding compared to round bars. Each type of FRP offers unique properties tailored to specific engineering needs. Figure 1.2 shows Types of fibers used in FRP.

Figure 1.2 Types of fibers a)Glass, b)Carbon and c) Aramid [24]

E-GFRP, the most commonly used FRP, is economically viable and widely used due to its affordability. Conversely, BFRP, while more expensive, is characterized by exceptional strength, alkali resistance, and sustainability due to its nearly infinite resource availability.

CFRP, which consists of carbon fibers in a polymer matrix, is used for its ultra-lightweight nature coupled with remarkable tensile strength, making it indispensable in aerospace and infrastructure applications. Despite costing 2 to 10 times more than

traditional materials, CFRP's high strength-to-weight ratio makes it an attractive choice for structural applications. [20-25]

Composed of glass fibers embedded in a plastic matrix, FRP has been a cornerstone of the construction industry since the mid-1930s. Its high strength-to-weight ratio, resistance to salt water and chemicals, and excellent thermal insulation properties make it invaluable in secondary structures such as bridges, domes, and building frames. Figure 1.3 shows Different shapes of FRP used for reinforcement.

AFRP, which uses aramid fibers, has exceptional strength, heat resistance and elasticity, making it suitable for concrete structures. Despite its slightly higher cost compared to GRP, AFRP remains economically viable and offers high resistance to alkaline environments.

BFRP, consisting of basalt fibers, is emerging as a promising technology in construction. Known for its improved stiffness, strength, and resistance to heat and corrosion, BFRP also exhibits high tensile strength and alkali resistance. This makes it ideal for structural reinforcement and the lightweight vehicle industry.

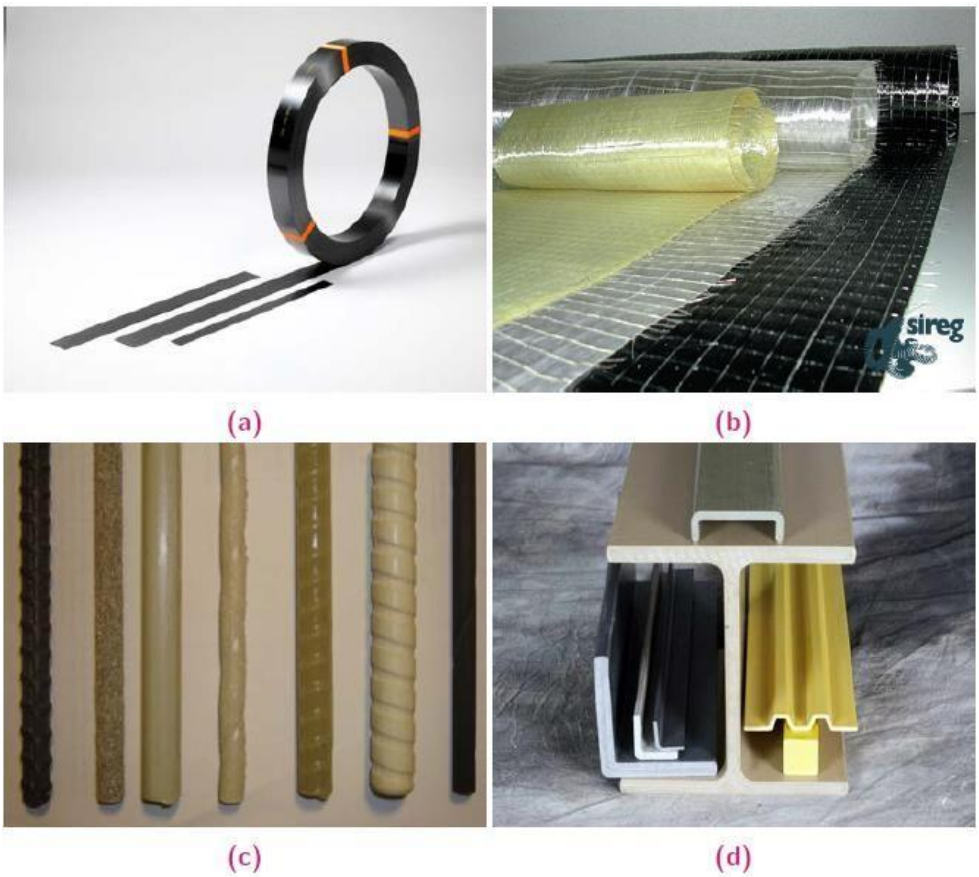

Figure 1.3 Different shapes of FRP composites; (a) Strips/laminates, (b) Sheets, (c) Bars and (d) Profiles [33].

I.3 Mechanical Properties of FRP Materials

Mechanical properties are also utilized to classify and identify materials of FRP bars. The most common properties considered are impact, flexural, shear, and tensile strengths, creep rupture, and modulus of elasticity. FRP composite bars have been widely used in construction in the last few decades. Table 1.1 lists the most commercially available FRP bars and their mechanical properties.[30]

The modulus of elasticity of FRP commercial products is generally lower than that of steel and remains practically constant up to the failure point (elastic brittle behavior) unlike steel bars, for which a ductile behavior is expected and therefore considered in design codes (figure 1.4). Due to the lower values of modulus of elasticity, deformations expected in FRP reinforced concrete structures are larger than that of steel reinforced concrete structures. These two differences in mechanical properties will affect bond behavior and therefore it is important to have them into consideration when developing design codes. Glass fiber reinforced polymer (GFRP) bars (having the lowest value of modulus of elasticity) are cheaper than the other types of FRP bars [31-37].

The tensile strength of FRP bars is higher than that of steel bars. For example, the tensile strength of GFRP bars can be more than twice the tensile strength of steel bars, whereas carbon fiber reinforced polymer (CFRP) and aramid fiber reinforced polymer (AFRP) bars can develop more than threefold, depending on the nature of fibers and matrix.

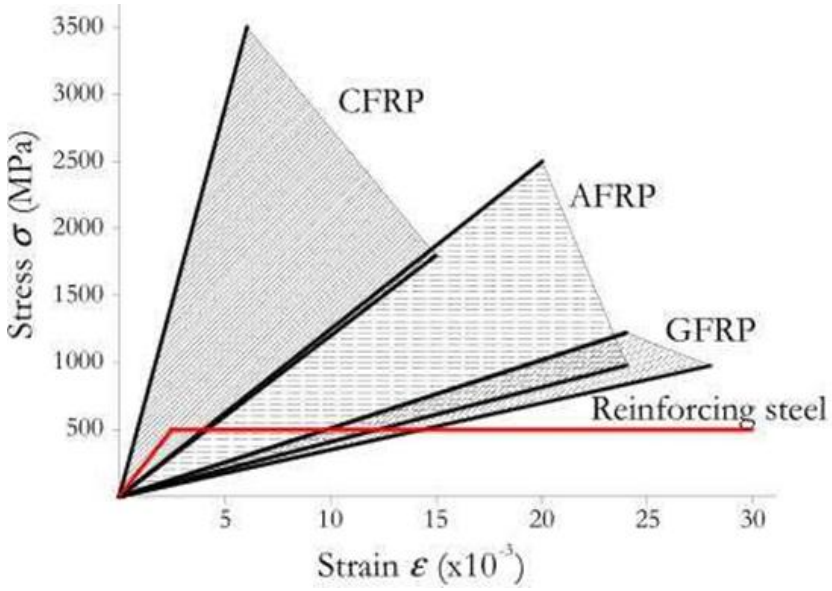

Figure 1.4 Comparison of the tensile properties of FRP and steel bars [34]

Table I.1.Mechanical propreties of FRP

FRP types	Unit	GFRP	CFRP	AFRP	Steel
Tensile modulus	GPa	25-55	120-250	40-125	200
Tensile strength	MPa	400-1800	1200-2250	1000-1800	400

I.4 Adhesives Used With FRP in Strengthening Applications

Adhesives play a pivotal role in a wide variety of industries, serving as indispensable agents for both structural and non-structural applications by securely bonding materials together. Adhesives provide a wide range of benefits, including increased manufacturing efficiency, greater flexibility in combining materials for low-cost production, reduction of localized stress concentrations, and increased fatigue resistance compared to welded structures. Five basic theories explain the mechanisms underlying adhesion:

- Mechanical adhesion theory posits that surfaces adhere by mechanical interlocking, facilitated by adhesive penetration into surface irregularities such as pores and voids.
- Electrostatic adhesion theory suggests that adhesion results from electrostatic effects between the adhesive and the adherent.
- Diffusion adhesion theory explains adhesion by interdiffusion of molecules between the adhesive and the adherent.
- Wetting adhesion theory, or dispersive adhesion, theorizes that molecular contact and van der Waals forces contribute to adhesion.
- Chemical adhesion theory attributes adhesion to the formation of bonds between the adhesive and the adherent, such as hydrogen, covalent, and ionic bonds, which are stronger than dispersion forces.

Adhesive bonds resist various forces, including tension, compression, shear, cleavage, and peel, depending on the design of the bond. [37-40]

Structural adhesives, such as epoxy and cement-based adhesives, are widely used to bond materials such as metals, glass, ceramics, concrete, plastics, and composites, facilitating the creation of load-bearing joints. Epoxy adhesives, introduced in the 1930s, are based on polymeric materials and exhibit a transition from hard to elastic behavior at their glass transition temperature (Tg), which typically ranges from 45°C to 200°C.

I.5 Strengthening Techniques

FRP strengthening techniques for RC structures primarily involve externally bonded reinforcement (EB) and near surface mounted reinforcement (NSM), illustrated in Figure 1.5. These techniques are described as follows:

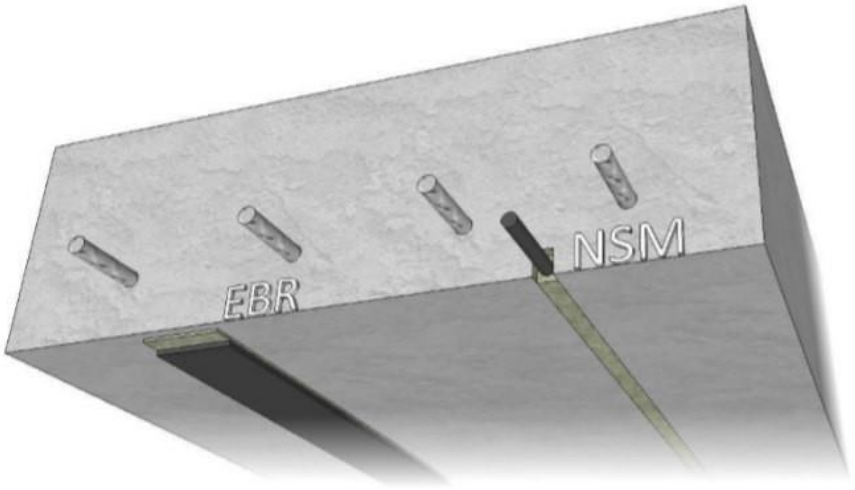

Figure 1.5 NSM And EBR Strengthening Techniques

I.5.1 Externally Bonded Reinforcement (EBR)

The EB technique involves bonding FRP sheets to the tension-side surface of concrete to reinforce existing RC slabs and beams. Historically, externally bonded systems, including bonded steel plates and bars, have effectively strengthened and rehabilitated RC structures. Recently, lightweight, high-strength, and corrosion-resistant FRP laminates have been increasingly used for repair and retrofitting applications.

The use of EB FRP laminates is a highly attractive method for strengthening RC structures, with numerous research and practical projects undertaken. Adhesively bonding FRP CFRP plates to RC structures is a well-established retrofitting approach, supported

by advanced design rules and mathematical models. However, externally bonded plates may experience debonding at low strains, limiting their effectiveness.

Ensuring effective stress transfer at the FRP-to-concrete interface is crucial. Failure modes in FRP-strengthened RC members, such as intermediate crack-induced debonding (IC debonding), often result from interfacial debonding. Research on IC debonding of EB FRP plates has advanced, with fundamental mathematical models established and key parameters identified and quantified.[41-50]

To ensure good bonding between the FRP and concrete, the following steps must be followed:

- Preparation of the concrete surface.
- Stripping and sanding.
- Cleaning, brushing, and dusting of the surface to be repaired.
- Crack repair by resin injection.
- Preparation of the adhesive and bonding.
- Preparation of the reinforcement surface.

The concrete surface must be well-prepared to avoid rupture at the resin/concrete interface. Figure 1.6 shows some examples of reinforcement applications using the EBR technique.

Figure 1.6 Externally Bonded Reinforcement (EBR) [51]

I.5.2 The NSM Technique

The NSM technique has gained widespread use in pioneer countries like the USA and Canada and is recognized as a promising method for increasing the flexural strength of RC members, often considered more convenient than using EBR FRP laminates. Unlike EBR, NSM FRP strengthening doesn't require extensive surface preparation, except for grooving, which can be done in a single step with appropriate tools. High-viscosity bonding agents or fluid products like cementitious pastes can easily fill the grooves during the strengthening process figure 1.7 shows the main stages of the NSM strengthening.

In the positive moment region (M+), NSM technique requires less additional protective cover compared to EBR, making it attractive. Additionally, FRP products used in NSM can be anchored into adjacent members in negative moment regions (M-) without extra protective measures, enhancing the effectiveness of the system.

This technology is now included in some existing codes and guidelines, reflecting its acceptance and recognition in structural engineering practice.

Figure 1.7 Main stages of the NSM strengthening: a) Grooving; b) Adhesive and FRPplacement; c) Strengthened member [30]

I.5.3 Comparison between Strengthening Techniques

In the analysis of strengthening techniques, recent experimental studies by various researchers have shed light on the effectiveness of NSM and EBR strengthening systems. [51-64]

El-Hacha & Rizkalla [65] highlighted the numerous advantages of the NSM technique over EBR. They noted that NSM offers a larger bond surface, enhancing anchorage capacity and resistance against peeling-off. Additionally, NSM requires minimal preparation work, only grooving, and benefits from protection provided by the surrounding concrete against various mechanical influences and environmental factors. NSM also exhibits improved ductility, with ultimate load development less dependent on concrete surface tensile strength. They observed that EBR FRP strips experienced brittle debonding failures at significantly lower load levels compared to beams strengthened with NSM CFRP reinforcing bars or strips and NSM GFRP thermoplastic strips. No slip was observed for the different NSM FRP reinforcing bars and strips strengthening techniques up to ultimate load-carrying capacity.

Similarly, Foret & Limam [66] tested both EBR and NSM CFRP strengthened RC two-way slabs, observing a more pseudo-ductile behavior with NSM compared to EBR. While debonding occurred in both cases, it was more sudden in EBR than NSM. Considering that EBR used a higher amount of carbon for almost the same average bearing capacity, NSM was deemed more economical.

Bilotta et al. [67] Conducted experimental tests on concrete blocks strengthened with different types of EBR and NSM FRP systems. They found that the NSM technique better exploited the tensile strength of FRP materials, achieving much higher utilization factors (36–100%) compared to EBR systems (approximately 15%). NSM also allowed for higher efficiency factors against lower axial stiffness, especially with ribbed reinforcement surfaces. In specimens with low concrete strength, they observed a concrete-adhesive interface failure in most specimens strengthened with both FRP systems.

I.6 Bond Behavior between NSM FRP and Concrete

Bonding characteristics of near-surface mounted FRP to concrete are a focus of research on RC structures strengthened with NSM FRP because they play a critical role in evaluating the effectiveness of this technique. The understanding of the bond behavior is of paramount importance due to the frequent observation of debonding failure modes, such as cohesion failure near the concrete-bond interface, in laboratory tests. To investigate the bond behavior of NSM FRP bonded to concrete, researchers commonly conduct NSM FRP-concrete bond tests. These tests are designed to provide information on bond strength, the local bond-slip relationship, and the effective bond length, which is the limit beyond which the bond strength of the joint cannot increase.

I.6.1 Test Methods for Bonded Joints

Researchers have adopted two primary methods of bonded joint tests to examine the bond behavior of NSM FRP: the beam pull-out test and the direct pull-out test.

The beam pull-out test for NSM FRP originated from the pull-out bending test designed for assessing the bond characteristics of conventional steel bars. Nanni et al. [68] adapted this method for NSM FRP, which has since been widely used by researchers. The schematic of the beam pull-out test, as adopted by De Lorenzis and Nanni [69], is illustrated in Figure. 1.8. This test involves a test beam with a steel hinge at the top and a saw cut at the bottom, both situated at mid-span to regulate internal force distribution. During loading, the saw cut initiates a crack at the beam mid-span, propagating up to the hinge. The beam pull-out test offers advantages such as simplified load alignment and accurate computation of tensile stress in the FRP, yet it requires large specimens and poses challenges in displacement control.

The direct pull-out test entails the direct loading of an NSM FRP bar embedded in a concrete block and comes in three main variations: the traditional one-side direct pull-out test, the two-side direct pull-out test, and the C-shaped block direct pull-out test. The one-side pull-out test, simplest to implement in laboratory settings, features a straightforward loading mechanism. In the two-side direct pull-out test, load application is symmetrical, but controlling loading symmetry becomes challenging as debonding progresses. The single face direct shear pullout test [70], the double face direct shear pullout test [71], and the beam pullout test [72] (shown in Figure 1.8) are the standard tests used to evaluate the bond between NSM FRP and concrete.

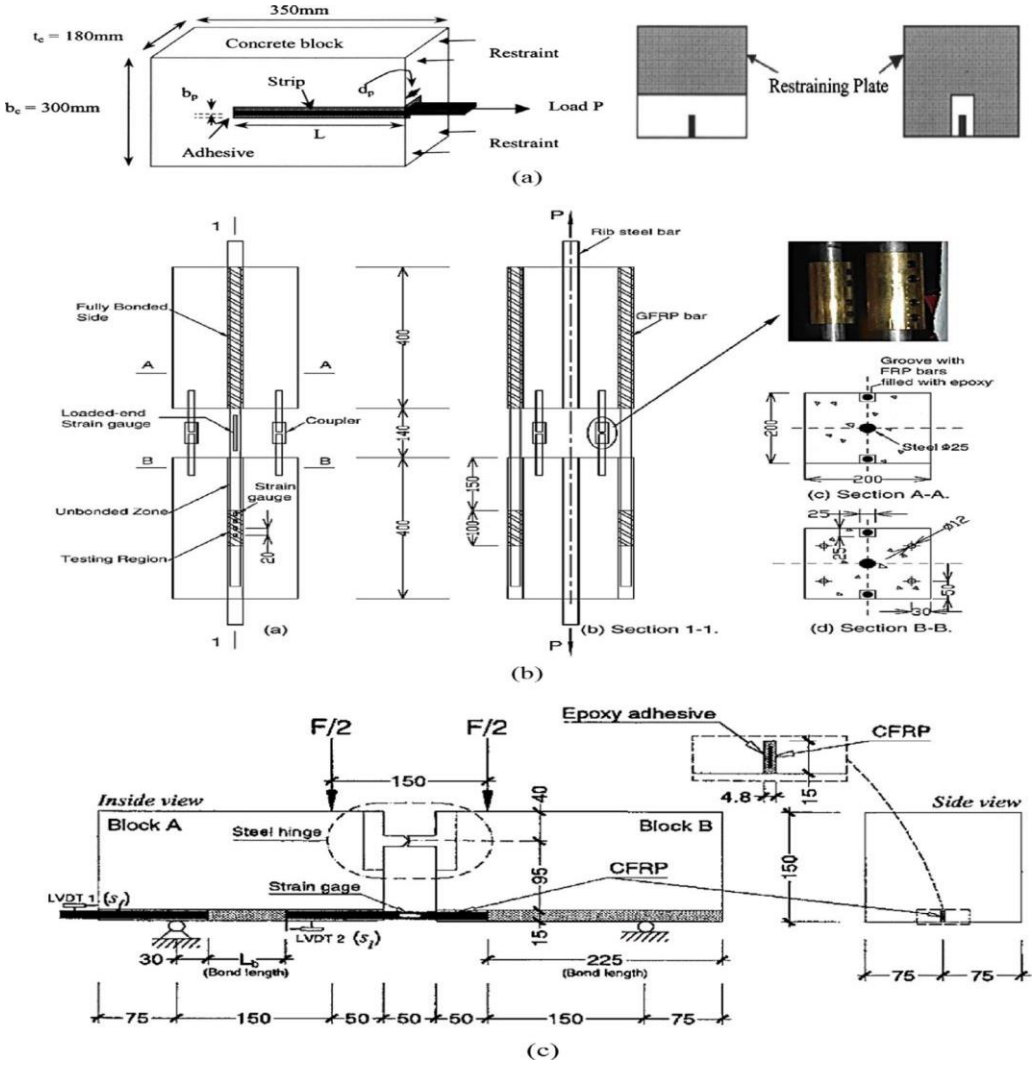

Figure 1.8 Typical test methods; (a) Pull-out direct single-face shear test [70], (b) Pull-out direct double-face shear test [71], (c) Beam pull-out test [72].

Various experiments have been conducted to test the bonding of NSM FRP round bars to concrete.

Blaschko [73] performed tests on NSM CFRP strips bonded to concrete blocks, focusing on variables like bond length, concrete strength, and edge distance using a one-side direct pull-out test setup. Failure modes included concrete edge fracture and adhesion failure at the bar-epoxy interface.

Sena Cruz and Barros [72] conducted bond tests on NSM CFRP strips using a beam pull-out test setup, varying bond length and concrete strength. Failure predominantly

occurred in the adhesive layer, followed by debonding at the bar-epoxy or concrete-epoxy interface.

Shield et al. [74] examined bonded joint tests with different adhesive types, highlighting the impact of adhesive properties on joint strength and failure modes.

Thorenfeldt [75] analyzed NSM CFRP strip bond tests, observing wedge failure near the loaded end, while Seracino et al. [70] investigated NSM CFRP strip bonding under different restraint conditions, identifying cohesion failure in concrete as the primary mode.

Oehlers et al. [76] explored the effect of cover on NSM CFRP strip bond behavior, observing a transition in failure mode with increasing cover thickness. Rashid et al. (2008) studied the influence of groove spacing and concrete edge distance on bond strength, suggesting neglecting their effects under certain conditions.

Perera et al. [77] conducted NSM CFRP bonded joint tests, noting various failure modes and concluding that CFRP strips were the most effective shape due to their perimeter-to-cross-sectional area ratio.

Numerous studies have investigated the bond performance of NSM FRP reinforcement. They consistently show that carbon plates exhibit superior bond performance compared to steel bars. Furthermore, increasing concrete strength significantly enhances pullout forces [108–109]. Additionally, enhancing surface roughness contributes to improved bond performance [110]

I.6.2 Observed Failure in Bonded NSM Systems

In contrast to externally bonded FRP systems, the radial stresses exerted by NSM FRP bars, especially those with rough surfaces like spirally wounded bars or bars with ribs, on the adhesive are significant and cannot be disregarded. These radial stresses transmit through the adhesive to the adjacent concrete, influencing the failure mode of NSM FRP-to-concrete bonded joints. Figure. 1.9 illustrates the Bond failure modes of NSM systems observed in bond tests. The bond behavior relies on two mechanisms: initial chemical adhesion and, subsequently, mechanical interlocking or friction (Hassan and Rizkalla [78]. For NSM CFRP strips, radial stresses from the FRP bar are relatively minor compared to NSM round bars with ribs due to the strip's usually flat surface, though it may be roughened for improved bonding. Following cracking, inclined concrete micro-

columns form, impeding further crack propagation due to surrounding concrete restraint. Chapter 4 will elaborate on the failure process of bonded joints with NSM CFRP strips.

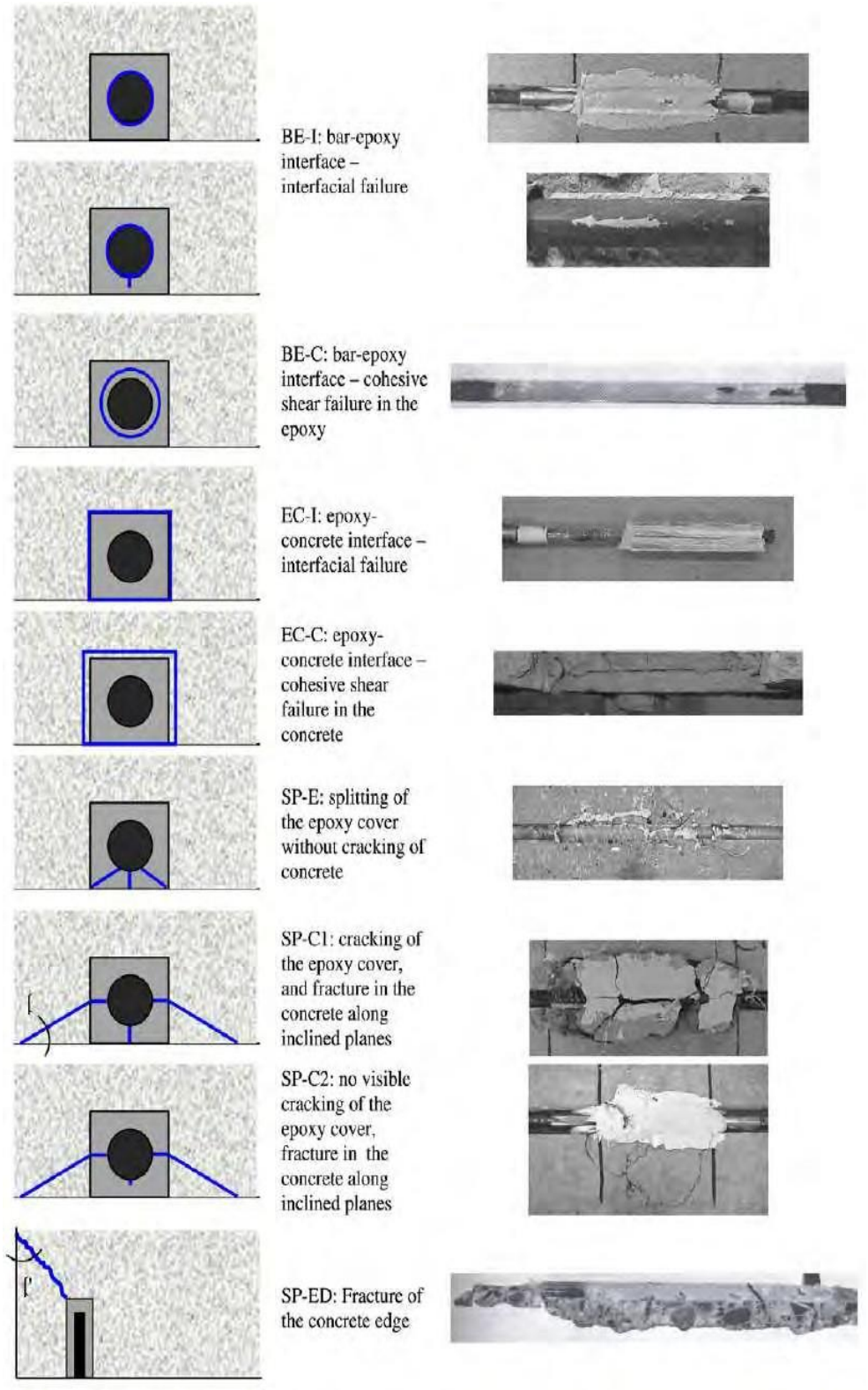

Figure 1.9 Bond failure modes of NSM systems observed in bond tests [69].

Existing test results indicate that NSM FRP strips exhibit higher efficiency than NSM FRP round or square bars.

For NSM round bars, failure mode hinges on the ratio of FRP bar size to groove size, NSM bar surface configuration, groove surface, and tensile strengths of epoxy and concrete. De Lorenzis and Teng [69] offer a comprehensive classification of bond failure modes of NSM round FRP bar-to-concrete bonded joints. For NSM CFRP strips, the following failure modes have been observed in tests

- Adhesion failure at the bar-epoxy interface;often due to poor surface conditions;
- Adhesion failure at the epoxy-concrete interface. critical for specimens with pre-formed grooves;
- Cohesion failure in the adhesive when adhesive strength is exceeded;
- Splitting of the concrete block observed for CFRP strips deeply embedded in concrete blocks.

Existing tests emphasize that cohesion failure in concrete near the epoxy-concrete interface is the most prevalent mode and that with proper surface conditions and a sufficiently strong adhesive, concrete failure governs the behavior and strength of NSM FRP-to-concrete bonded joints.

I.7 Parameters Affecting the Bond Property

The bond performance among NSM system elements (FRP, adhesive, and concrete substrate) is influenced by various factors, outlined as follows:

FRP Dimensions

Increasing the width of the FRP strip enhances NSM strengthening efficiency by providing effective confinement to the concrete. Similarly, augmenting the thickness of the FRP strip increases NSM strengthening efficiency due to the enlarged cross-sectional area. FRP strips with significant aspect ratios (FRP strip width/FRP strip thickness) are particularly effective in enhancing NSM strengthening efficiency.

Concrete Strength

Higher concrete strength correlates with increased NSM FRP strengthening efficiency as the failure load aligns with concrete tensile strength. Conversely, low concrete strength leads to most NSM FRP specimens failing at the concrete-adhesive interface with low ultimate pull-out loads.

Bonded Length

NSM FRP system strengthening efficiency rises with larger bonded FRP lengths, though it doesn't increase substantially beyond a critical bond length.

Adhesive Material Type

NSM specimens utilizing epoxy as adhesive outperform those employing cement paste. The lower mechanical strength of cement adhesive likely contributes to the disparity in performance.

Groove Sizes

The behavior of bond strength is linked to the failure mode. Larger groove sizes can bolster bond strength if failure at the NSM FRP-epoxy interface governs, delaying failure. However, for failures occurring at the epoxy-concrete interface, larger groove sizes can diminish bond strength due to non-uniform stress distribution along the groove's perimeter. For NSM specimens using cement paste as adhesive, larger groove sizes reduce ultimate load capacity compared to smaller groove sizes, attributed to increased shrinkage in the cement adhesive.

Understanding these parameters is crucial for optimizing NSM FRP-to-concrete bonded joint performance and ensuring effective strengthening of structural elements.

I.8 Flexural Strengthening Of RC Beams with NSM FRP

The NSM FRP strengthening method has found widespread use in practical projects globally. Various field applications, including piers, decks, slabs, and silos, have been reported, showcasing the versatility of this technique.

Flexural strengthening of RC beams stands out as one of the key applications of the NSM FRP technique. Compared to the externally bonded FRP method, the NSM FRP method offers several advantages, driving a surge of interest in both research and

application. Numerous experimental studies have been conducted on RC beams strengthened with NSM CFRP strips.

Hassan and Rizkalla [78]. Conducted a series of three-point bending tests on T-beams with a 2.5 m span, strengthened using NSM CFRP strips. While one beam served as a control without FRP strengthening, eight beams were reinforced with NSM CFRP strips, with bond lengths ranging from 150 mm to 1200 mm. Failure modes of the strengthened beams varied, from interfacial debonding to CFRP rupture, depending on the bond length. Notably, an increase in flexural capacity was observed with bond lengths exceeding 250 mm, reaching full CFRP strip capacity at lengths surpassing 850 mm.

El Hacha and Rizkalla [65]. conducted three-point bending tests on RC T-beams with a 2.5 m span, strengthened using NSM FRP round bars. Seven beams were strengthened with different FRP methods, while one served as a control. Results highlighted a significant improvement in stiffness and flexural capacity with NSM FRP bars compared to the control. Additionally, NSM CFRP strips exhibited higher strength capacity than externally bonded CFRP strips of similar stiffness.

Barros and Fortes [79]. tested eight RC beams with a 1.5 m span under four-point bending, dividing them into four series. Each series included one control beam and one beam strengthened with NSM CFRP strips. Observations revealed an average increase in load at the serviceability limit state, yielding of steel reinforcement, and stiffness for strengthened beams. The load at concrete cracking also saw a significant increase, with strains in CFRP laminates nearing ultimate strain levels.

Barros et al. [80].conducted four-point bending tests on RC beams with a 0.9 m span, strengthened using NSM CFRP strips or externally bonded CFRP. The results of these tests provided further insights into the effectiveness of NSM CFRP strips in enhancing the flexural capacity of RC beams.

The comparative efficiency of near-surface mounted (NSM) CFRP strips and externally bonded FRP laminates or sheets in flexural strengthening of RC beams has been extensively studied. In a particular investigation, three beams served as controls without FRP strengthening, three were strengthened with NSM CFRP strips, and six were reinforced with externally bonded FRP. The study evaluated the ultimate load and examined the influence of steel and FRP reinforcement ratios. The failure modes differed

significantly between the two methods, with NSM CFRP strips primarily experiencing concrete cover separation, while externally bonded FRP exhibited interfacial debonding, CFRP rupture, or concrete cover separation. Results demonstrated that the NSM FRP method outperformed externally bonded FRP, with percentage increases in ultimate load ranging from 35% to 118% for NSM FRP and 5% to 72% for externally bonded FRP. Moreover, as the FRP reinforcement ratio increased, the difference in strengthening efficiency between the two methods diminished.

Teng et al. [81]. Reported on a series of four-point bending tests on rectangular RC beams strengthened with NSM CFRP strips. The study varied the embedment length of the NSM strip and monitored its bond behavior extensively. Except for the shortest embedment length, all others notably increased the load-carrying capacity and post-cracking stiffness of the beams. Primary failure modes included bar-end cover separation, except for the beam with the longest embedment length, which failed due to interfacial debonding in the pure bending zone. The study also conducted preliminary bond tests to characterize local bond-slip behavior, offering insights into debonding failures and contributing valuable data for future numerical and analytical models.

Aidoo et al. [82]. conducted three-point bending tests on RC bridge girders retrofitted with various FRP systems, including externally bonded CFRP laminate, NSM CFRP strip, and hybrid FRP laminate with mechanical fasteners. Failure modes varied, with concrete cover separation for externally bonded and NSM CFRP, and mechanical fastener failure for the hybrid FRP laminate. While the capacity enhancement of the NSM CFRP strip was similar to the externally bonded laminate, it was significantly lower than that achieved with the hybrid FRP laminate, although initial conditions of the NSM CFRP girder were noted to be worse.

Yost et al. [83]. presented experimental results of 12 RC beams under four-point bending, discussing yield and ultimate loads, failure modes, and ductility. The beams were divided into three series, with one un-strengthened control beam and two beams strengthened with NSM CFRP strips for each series. Experimental variables included different ratios of steel bars and CFRP strips.

Castro et al. [84]. presented results of four-point bending tests on T-shaped RC beams of 4.0 m in span strengthened with either FRP and steel bars with the axial stiffness of the two types of reinforcement being the same. The FRP was either NSM round bars

and strips or externally bonded sheets. Two beams without strengthening were treated as the control beams with their concrete strengths being different, and the 10 strengthened beams were divided into 5 series. Each series contained two strengthened beams with the same configuration and parameters except for the concrete strength. The control beams and the beams strengthened with NSM steel bars failed by conventional flexural failure; the beams strengthened with externally bonded CFRP laminates failed by interfacial debonding of the CFRP near the support after extensive cracking of the concrete cover below the load points; and the beams strengthened with NSM CFRP failed by concrete cover separation or by the rupture of the CFRP. The NSM CFRP system showed a higher ultimate load increase than the externally bonded CFRP system and the NSM steel system.

Kotynia et al. [85] conducted four-point bending tests on RC beams of 4.2 m in span strengthened with NSM CFRP strips. A total of 7 strengthened beams were tested, and no un-strengthened beam was tested as the control beam. The varied parameters included the steel reinforcement ratio, the concrete strength, the cover thickness (with the depth of the longitudinal steel being kept the same) and the axial stiffness of the CFRP strips. One beam with the highest steel ratio failed due to concrete crushing, and the other beams failed by intermediate crack (IC) induced cover separation. A variation of the tension concrete cover thickness did not influence the load-bearing capacity because the depth of the longitudinal steel reinforcement was the same for all beams. The increases in the ultimate load were 221% and 137% respectively for beams with the higher CFRP ratio and beams with the lower CFRP ratio. Moreover, an increase in the cracking load, steel yielding load and stiffness of the beam was also observed. Novidis and Pantazopoulo [86]. Conducted four-point bending tests on RC beams of 1.0 m in span strengthened with externally bonded or NSM CFRP strips. Two beams were tested as control beams, and seven beams were strengthened with FRP in different ways. With the total amount of reinforcement being the same for all specimens, the most interesting aspects of this research included: different groove dimensions, presence or absence of a U-shaped FRP jacket at each end of the CFRP. Bar-end concrete cover separation, bar-end interfacial debonding and IC interfacial debonding were the main failure modes of the strengthened RC beams. The results showed that the increase in the load capacity of the beams with NSM CFRP strips was much more obvious than that for beams with externally bonded CFRP strips. Optimal results were obtained when the NSM CFRP strip was placed with

the thickness direction being horizontal. For the cases where the NSM CFRP strip was placed with the thickness direction being vertical, a deeper position of the NSM CFRP strip gave a higher enhancement. The placement of CFRP jackets in the anchorage regions of the CFRP strips contributed to the attainment of a higher deflection and a higher flexural strength of the beam

Thorenfeldt [87]. Conducted four-point bending tests on RC beams of 2.5 m in span strengthened with NSM CFRP strips. Two beams were treated as control beams, and four beams with two CFRP strip ratios were tested in room temperature while two beams with two CFRP strip ratios were tested under fire. Compared with the control beams, the beams strengthened with NSM CFRP strips tested in room temperature showed an increase in the cracking load, steel yielding load, ultimate load, and stiffness after cracking. However, it is surprising that the results of the two beams tested under fire were not mentioned. The control beams failed by crushing of the concrete after yielding of the steel. Except for the beams strengthened with the smallest CFRP strip ratio that failed by FRP rupture, all strengthened beams failed by bar-end cover separation.

Kalayci et al. [88]. Conducted three-point bending tests on T-shaped RC beams of 2.0 m in span strengthened with NSM CFRP strips or round CFRP bars. Two groups were tested to study the effect of construction tolerances (tolerances of the groove size) on the behaviour of the strengthened beam. In the first group, the RC beams were strengthened with NSM CFRP strips; two identical beams with a groove size of 25mm in depth and 14 mm in width were tested as control beams, two identical beams with a groove size of 25mm in depth and 11 mm in width were tested as “under-sized groove” beams, and two identical beams with a groove size of 25mm in depth and 17 mm in width were tested as “over-sized groove” beams. In the second group, the RC beams were strengthened with NSM CFRP round bars. Similar to the first group, two identical beams with a 14mm x 14 mm groove was tested as “normal groove” beams, two identical beams with a 11mm x 11 mm groove were tested as “under-sized groove” beams, and two identical beams with a 17mm x 17 mm groove were tested as “over-sized groove” beams. Although it was concluded that within the studied range (a tolerance of up to ±22%), the groove size tolerance did not affect the overall response of the beam, the plotted load-displacement curves showed some differences between the “over-sized groove” beams, the “normal-groove” beam and the “under-sized groove” beam; furthermore, two failure modes were

observed for beams with different groove sizes: epoxy failure for beams with the smallest groove and concrete cover separation for beams with the larger grooves

Tanarslan et al. [89]. Conducted an experimental test to explore the impact of varying the ratio of internal steel reinforcement and the FRP superficial reinforcement on the flexural behavior of RC beams strengthened with NSM bar reinforcement. The results affirmed that NSM FRP rods significantly augmented the flexural capacity of RC elements. The beams tested exhibited an increase in the ultimate load ranging from 21.3% to 60.6%. The failure mode varied, with some beams experiencing concrete crushing after steel longitudinal reinforcement yielding, while others faced splitting of the concrete cover accompanied by NSM rod debonding.

Hassan and Rizkalla [90]. Delved into the bond mechanism of NSM FRP bars for flexural strengthening of concrete structures. Their findings indicated that the development length of NSM CFRP bars should not be less than 80 times the diameter of the bars. Moreover, altering the type of epoxy adhesive had minimal impact on the ultimate load capacity of the strengthened beams.

Further experimental tests by Rizzo et al [91]. Illustrated that the ultimate load increased with the bond length of the rod and resistance to splitting grew with the size of the groove. Other investigations focused on flexural behavior with NSM AFRP rods, studying axial stiffness variation by changing the FRP bar size.

Al-Mahmoud et al. [92] conducted experimental and analytical studies on the strengthening of RC members with NSM CFRP rods, considering factors like CFRP length, filling type, CFRP section, and concrete compressive strength. Their findings emphasized the negligible effect of concrete strength on the load-carrying capacity of the strengthened beam under NSM system failure.

The behavior of RC beams strengthened using high-performance CFRP bars with a trapezoidal cross-section was studied, with load-carrying capacity increasing between 14.2% and 55.1% depending on the strengthening methodology. Concrete peel-off or CFRP rod pullout were identified as failure modes depending on the strengthening length.

Wahab et al. [93] investigated the bond behavior of concrete beams strengthened with NSM non-prestressed and prestressed CFRP rods, noting failure modes such as CFRP rod pullout or concrete peel-off depending on the type of rod used.

Kalayci et al. [94] conducted an experimental program to examine the impact of groove size tolerance on NSM FRP systems. The results showed that within the studied range, groove size tolerances did not affect the response of strengthened beams with NSM strips or bars. Failure modes varied, with epoxy splitting and concrete splitting observed for specimens with small and large grooves, respectively.

A study by Barros and Fortes [95] explored the flexural strengthening of concrete beams with CFRP laminates bonded into slits. The strengthening technique, termed NSM, resulted in an average increase of 91% in the ultimate load of the tested RC beams. The main failure mode observed was characterized by the detachment of a layer of concrete at the bottom of the beam.

Other studies focused on the flexural behavior of strengthened beams with NSM FRP strips or laminates. Choi et al. explored the behavior of RC beams with partially bonded strengthening reinforcement using NSM CFRP bars to improve deformability. Stiffness decreased as the unbounded length increased, while deformability increased after yielding.

Soliman et al. [96] investigated the effect of internal steel reinforcement ratio, type of NSM FRP bars, FRP bar diameter, bond length, and groove size on the flexural behavior of concrete beams strengthened with NSM FRP bars.

Sharaky et al. [97] conducted experimental and numerical studies on the behavior of bottom and side NSM strengthened RC beams using GFRP bars, with and without end anchorage. They observed that the load-carrying capacity of the strengthened RC beams with bottom NSM bars was higher than those with side NSM bars due to the internal arm effect. The highest improvement ratio in load-carrying capacity compared to the control beam was 201% for beams with bottom NSM bars and end anchorage inclined by 45˚, while the lowest ratio was 142% for the same configuration with side NSM bars.

In another study, Sharaky et al. [98] investigated the effectiveness of axial stiffness and the type of confinement of NSM FRP reinforcement on the bearing capacities and failure modes of strengthened beams. They found that the yield load ratio of the strengthened beams relative to the control beams was proportional to the axial stiffness ratio of NSM FRP reinforcement. Concrete cover separation became the failure mode when the axial stiffness ratio reached a critical value, beyond which the ultimate load of

strengthened beams was not affected. This critical stiffness ratio was experimentally determined to be about 1.25. Confinement significantly enhanced the load-carrying capacity of RC beams with only a small increase in their steel reinforcement yielding load.

To address concrete cover separation and enhance bond strength, they investigated the use of mechanical interlocking with shear connectors or transverse wrapping. This method increased the load-carrying capacity of strengthened beams by up to 23.3% and the ultimate load of conventionally strengthened beams by 33%.

Furthermore, Sharaky et al. [99] studied the interaction between FRP strips and internal reinforcement on the flexural behavior of NSM strengthened RC beams. They found that NSM GFRP strips installed side by side had lower interfacial stress than those installed separately, particularly when installed near the internal reinforcement. NSM strips in deeper grooves experienced higher load-carrying capacity than those in shallow grooves, potentially delaying or preventing peeling/debonding failure.

Hebah et al. [111] investigated the flexural strengthening of reinforced concrete beams using near-surface mounted carbon-fiber-reinforced polymer (NSM-CFRP) strips, demonstrating significant capacity enhancement and effective mitigation of CFRP debonding failures

Pour et al. [112] measured the efficiency of different strengthening techniques to advance the flexural characteristics of reinforced concrete (RC) beams using glass fiber-reinforced polymer (GFRP) laminates,

In conclusion, the studies mentioned demonstrated a significant effect of FRP and steel reinforcement ratios, as well as CFRP elasticity modulus, on ultimate loads and CFRP strain utilization. Increasing CFRP stiffness led to an increase in ultimate load but a decrease in CFRP debonding strain.

I.9 Observed Failure Modes

The observed failure modes in beams strengthened with NSM CFRP strips can be classified into the following types:

Flexural Failure by Crushing of Compressive Concrete: This is a conventional failure mode of RC beams following yielding of steel or before the yielding of steel when the amount of tension steel is high. It occurs when the compressive concrete crushes. (Figure 1.10)

Figure. 1.10 Flexural Failure by Crushing of Compressive Concrete [83]

Flexural Failure by Rupture of FRP: This happens in beams in which the length of the FRP reinforcement is sufficient to avoid the debonding of the FRP and the amount of the FRP is small. It can be predicted by section analysis based on the plane section assumption. . (Figure 1.11)

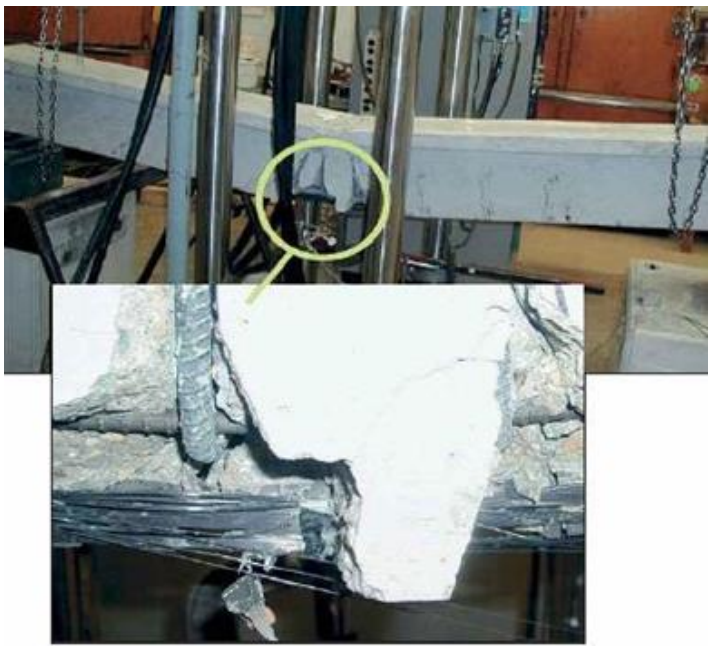

Figure. 1.11 FRP rupture failure mode [78]

Bar-End Failure: This failure mode can be divided into:

- **Bar-End Interfacial Debonding**: The CFRP strip debonds from the beam starting from the bar-end, mainly due to high interfacial shear and normal stresses.(Figure 1.12)

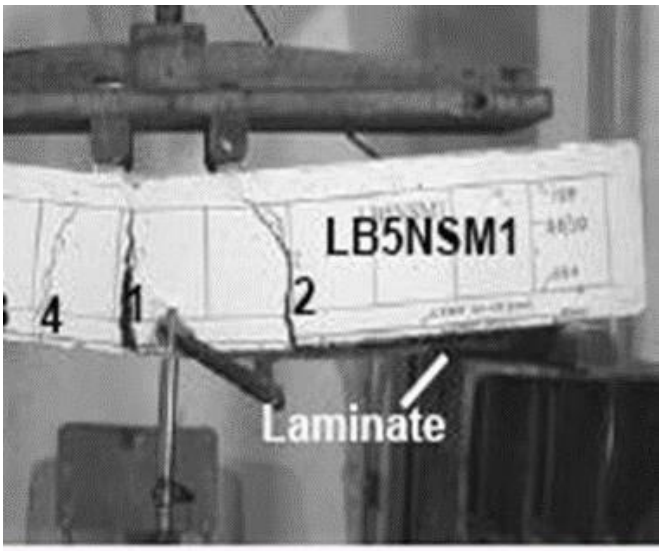

Figure. 1.12 Bar-end interfacial debonding failure mode [86]

- **Bar-End Cover Separation**: The CFRP strip, together with the concrete cover, is detached from the beam starting from the bar-end, with a major crack traveling on the plane of the steel tension reinforcement.(Figure 1.13)

Figure. 1.13 Bar-end cover separation failure mode [79]

Intermediate Crack (IC) Induced Failure: This mode can be divided into:

- **IC Interfacial Debonding**: Similar to the intermediate crack-induced interfacial debonding failure mode observed in RC beams strengthened with an externally bonded FRP plate. . (Figure 2.14)

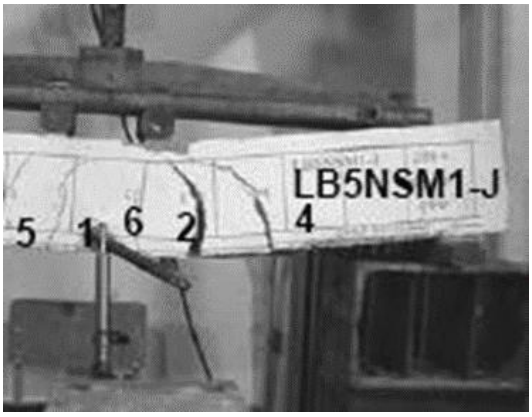

Figure. 1.14 IC interfacial debonding failure mode [86]

- **IC Cover Separation**: The detachment of the FRP with the concrete cover from the beam starts from the maximum moment region and propagates to one of the FRP bar ends. Some researchers only indicated that failure of the beam was due to concrete cover separation but did not mention where the failure initiated. (Figure 2.15)

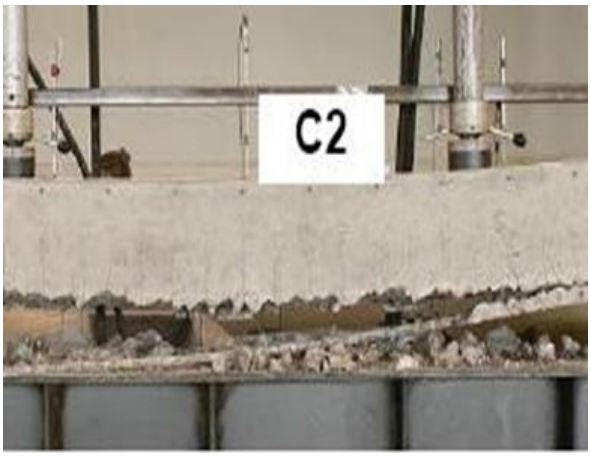

Figure. 1.15 IC cover separation failure mode[65]

As can be seen from the above review of failure modes, for RC beams strengthened with NSM CFRP strips, although interfacial debonding failures were also observed in RC beams strengthened with NSM CFRP strips, concrete cover separation failure was the dominant failure mode.

It should be noted that, in this thesis, the term “debonding” is used as a generic term to refer to both interfacial debonding failure and cover separation failure; that is, it refers to all failure modes where the composite action between the FRP and the concrete beam is not maintained.

I.10 Shear Strengthening

For shear reinforcement, numerous resources detail the design procedures for RC structures using externally bonded FRP [100-102]. In the case of shear reinforcement, FRP bars are affixed to the outer surface of beams in a vertical U-shape configuration, akin to exterior stirrups. In the realm of wall shear reinforcement, which includes under-RC walls and unreinforced masonry walls, FRPs can be applied in vertical, horizontal, or X patterns (45°) to one or both sides of the wall [103]. Shear reinforcement can be accomplished with very thin sheets, often only 0.5–1.0 mm thick, yielding significant seismic enhancements, especially for in-plane shear walls [104]. Despite the strength of existing epoxy resins, surface failures frequently occur in concrete, particularly at weak joints in RC members requiring shear reinforcement. The EBR method is employed as continuous jacketing or strips, with three primary configurations of FRP reinforcement: U-wrapping, complete wrapping, and side bonding. Complete wrapping of structural RC elements is regarded as the most effective method for FRP shear reinforcement due to its adaptability in the presence of geometric constraints [105].

Various methods have been employed to reinforce RC beams in shear, including exterior prestressed reinforcement, bonded steel plate, and fiber materials. Externally applied FRP, including aramid, carbon, and glass fibers, are widely used for shear and flexural reinforcement of RC beams/columns. Studies have reported that using CFRP for shear reinforcement of RC beams increased shear strength by 19%–122% due to the orientation of the FRP at 45° and CFRP sheets, compared to control beams. The shear strength of FRP-reinforced beams is typically calculated by adding individual elements of shear resistance from concrete, FRP, and steel stirrups. For instance, the use of U-wrap CFRP shear reinforcement increased shear capacity by 50% for one CFRP layer and 92% for two CFRP layers , with the limitation that the shear-span-to-depth ratio be equal to 3 or greater than 2. For RC beams with a ratio of 1.5, CFRP shear reinforcement did not increase shear strength. Another study examined bridge deck slabs reinforced with CFRP bars with ratios higher than the balanced reinforcement ratio, resulting in an 81% to 111%

increase in shear strength compared to control slabs. However, a study on the influence of bucky paper interleaves formed from carbon nanofibers on the interlaminar strength of CFRP exhibited a 31% and 104% enhancement in interlaminar shear strength. Liu et al. [106] investigated the permissible level of BFRP composites submerged in saltwater for 240 days. The findings showed no reduction in shear strength of the BFRP composites even after 199 days, but an unexpected decrease in shear strength occurred after immersion in hot saltwater at 40°C. Abdel-Kareem et al. [107] investigated the shear enhancement of reinforced concrete (RC) beams using steel stirrups, Fiber Reinforced Polymers (FRP) rods, and FRP strips applied with the (NSM) technique. Thirteen half-scale RC beams were tested, including specimens strengthened with steel stirrups, various configurations of Glass Fiber Reinforced Polymer (GFRP) rods, and externally bonded GFRP strips. Results showed significant capacity improvements: GFRP rod-strengthened beams enhanced capacity by 14% to 85%, while GFRP strip-strengthened beams improved by 7% to 22%, compared to the reference beam.

I.11 Numerical Modelling

Numerical analysis proves to be a valid and efficient method for examining the behavior of RC beams reinforced with NSM FRP. Unlike RC beams strengthened with externally bonded FRP, there is notably less experimental data available for those reinforced with NSM FRP. This disparity is even more pronounced in the realm of finite element studies. This section provides a review of the existing FE studies concerning RC beams strengthened with NSM FRP.

2.4.1 FE Analysis of Bonded Joints

De Lorenzis et al. [115] devised a 3-D FE model focusing on the bonded joints of NSM FRP round bars using DIANA. They employed eight-node continuum elements to model both concrete and FRP round bars. Concrete behavior was simulated using the rotating smeared crack model. For modeling the bond between steel bars and concrete, they adopted a pre-existing model, while the epoxy-concrete interface was represented using a Coulomb frictional model. Both interfaces were depicted using interface elements illustrates a typical mesh for a bonded joint specimen. The findings from the FE analysis aligned well with experimental results, although further research is necessary to validate the proposed model with a broader experimental database.

Sena Cruz and Barros [116] conducted FE analysis on beam pull-out tests employing the FEMIX computer code. Their model utilized four-node plane stress elements to simulate concrete and steel hinges, while CFRP strips were simulated using beam elements. They employed interface elements with a two-point Lobatto integration rule to represent the connection between CFRP strips and concrete.

Lundqvist et al. [117] performed a linear elastic 3-D FE analysis on direct pull-out tests using ABAQUS. Their model employed eight-node continuum elements to represent concrete, adhesive, and CFRP, assuming perfect bonding at all interfaces.

2.4.2 FE Analysis of RC Beams

Lundqvist et al. [118] investigated the anchorage length of NSM FRP square bars used for flexural strengthening of RC beams. They conducted a 3-D nonlinear FE analysis using ABAQUS. The model employed eight-node linear brick elements for concrete, steel, NSM FRP bars, and adhesive, assuming perfect bonding between CFRP and adhesive, adhesive and concrete, as well as steel bars and concrete. They used a damaged plasticity model for concrete modeling and a bi-linear curve to define tensile softening, minimizing mesh sensitivity.

Hassan and Rizkalla. [119] modeled RC beams strengthened with NSM CFRP strips using a 3-D FE model developed using the ANACAP program. They used twenty-node brick elements with a 2x2x2 reduced Gauss integration scheme for concrete, FRP, and adhesive, simulating concrete with the smeared crack model.

Vasquez and Seracino .[120] investigated stress distributions near one of the two ends of CFRP strips in RC beams strengthened with NSM CFRP strips using a 3-D FE model developed with the commercial FE program ANASYS. Their model employed eight-node brick elements for concrete and epoxy, and assumed a perfect bond without interfacial elements.

Kalayci et al. [121] established a 3-D FE model using the commercial FE program ANASYS to study the effect of construction tolerances on the behavior of RC beams strengthened with NSM CFRP strips. The concrete was modelled using the 8-node brick element (“Solid-65”) with a 2 × 2× 2 Gauss integration scheme and the smeared crack model. The adhesive and the FRP were modelled using the same 8-node brick element with a 2× 2× 2 Gauss integration scheme and simulated as linear elastic materials. A

perfected bond was assumed for the two interfaces. The constitutive law of cracked concrete was not examined in detail and the shear retention factor was simply treated as a constant for cracked concrete. The adopted element size might have been too large to properly reflect the effects of groove size tolerance. As a result, a big difference in the load-deflection curve before yielding of the tension steel was observed between the FE predictions and the test results, with the predicted stiffness being much larger than that from the test.

Soliman et al. [122] developed a 3-D FE model of RC beams strengthened with NSM FRP round bars using ADINA. The 8-node brick element was used to model the concrete, the adhesive and the FRP while the 2-node truss element was used to model the steel. Interfacial elements were used to simulate the behaviour of the epoxy-concrete interface while a perfect bond was assumed for the bar-epoxy interface. The smeared crack model was used for the simulation of concrete, but details of the post-cracking behaviour of concrete such as strain softening and shear retention were not mentioned in describing the FE model. The adhesive was modelled as a linear elastic material. The FRP was modelled as an orthogonal material with brittle cracking. The bond-slip relationship used to determine the properties of the interfacial elements was from the bonded joint tests conducted by the same research group. However, since the RC beams failed by concrete cover separation, the use of a bond-slip relationship between the FRP and the concrete plays a limited role in ensuring the accurate prediction of cover separation failure.

Barros et al. [123] used the FEA program FEMIX to simulate the behavior of NSM CFRP strengthened columns. However, these studies used a perfect bond-slip model which may not be accurate to predict the debonding failure mode.In contrast,

Obaidat et al. [124] used the cohesive zone approach to model externally bonded CFRP retrofitted beams, which can provide a more accurate prediction of debonding.

Hawileh[125] developed a model using the FE program ANSYS to study the effect of different NSM material bar types and diameters.

Rezazadeh et al[126]. simulated the combined effect of both EBR and NSM systems using a 3D FE model developed with the FE program ABAQUS.

Stephen et al[127]. created fnite element models to calculate the gradient of defection of RC beamsunder fexural load when strengthened by EB-basalt reinforcement. They found that the fexural capacity of basaltreinforced beams was higher than those reinforced withsteel

I.12 Concluding Remarks

An analysis of the existing literature on the use of NSM FRP rods/strips for the reinforcement of RC beams leads to several important conclusions. First, the effectiveness of this technique depends on numerous factors such as bar dimensions, concrete properties, bond characteristics, reinforcement configurations, and groove width. In addition, the bond properties play a critical role in determining the performance of the NSM technique.

Second, increasing the amount of NSM reinforcement doesn't always result in a significant increase in load-bearing capacity, especially in cases where failure is due to problems within the NSM system itself rather than concrete strength. In addition, it's been observed that high-strength concrete increases resistance to certain failure modes.

Third, there is a direct correlation between increasing the bond length and increasing the load capacity of reinforced RC beams, although there is a notable threshold beyond which further increases in bond length don't significantly increase the load capacity

Fourth, the type of loading doesn't have a discernible effect on CFRP rod reinforced beams with similar failure modes, although partially bonded beams show slight differences in deflection and capacity compared to fully bonded beams. In addition, while NSM FRP has advantages over EB FRP in terms of bonding, protection, and aesthetics, it may result in lower strength efficiency in certain failure scenarios.

Finally, the limited amount of experimental research on the NSM technique compared to the EB technique underscores the need for further investigation to develop comprehensive predictive models for NSM connections. This review serves as a fundamental exploration of NSM FRP, encompassing bond behavior and flexural strengthening, and sets the stage for future advancements in the field through additional research efforts.

Chapter II:

Experimental Parameters

II.1 Introduction

The numerical model developed in this study has been calibrated using a series of tests conducted on beams reinforced with Near-Surface Mounted (NSM) FRP, which were carried out by Pr.Merdas [113] conducted in the L2MGC Laboratory of Civil Engineering Department, Cergy Pontoise University (France). Polymer and epoxy materials. This chapter is dedicated to elucidating the experimental methodology employed in conducting these tests. By providing a detailed overview of the experimental procedures, materials, and parameters utilized in the testing phase, this chapter aims to establish a comprehensive foundation for understanding the data obtained and its subsequent integration into the numerical modelling process.

II.2 Materials

II.2.1 Concrete

The concrete specimens were prepared using a mixture of Ordinary Portland Cement, fine sand (0-4 mm), crushed gravel (4-10 mm), and (6–20 mm) aggregates according to the mix proportion presented in Table 2.1.

Table 2.1 Mix proportion of concrete

Water l/m3	Cement kg/m3	Sand kg/m3	Gravel 4/10 kg/m3	Gravel 6.3/20 kg/m3	W/C	G/C
209	336	419	471	834	0.62	2.48

To characterize the compressive strength and modulus of elasticity of the concrete used, uniaxial compression tests were conducted at 28 days on cylindrical specimens measuring 16x32 in accordance with the NF P 18-406 standard [128] (Figure 2.2).

Figure 2.1 Concrete specimens coated with sulfur. [113]

The specimens were coated with sulfur, heated to its liquefaction temperature beforehand. Once coated (Figure 2.1), a waiting period of at least 2 hours was required before conducting the mechanical test. This delay allowed the sulfur to harden. After these two hours, the tests could proceed. They were conducted on a computer-assisted hydraulic press with a maximum capacity of 3200 kN .The compressive strength of the concrete was determined by averaging the values obtained from the 16x32 cm cylindrical specimens.

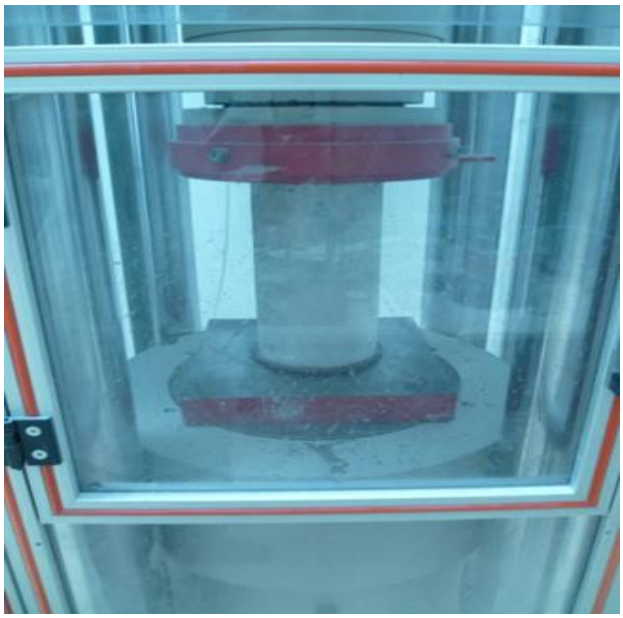

Figure 2.2. Concrete compression test. [113]

The measurement of the modulus of elasticity was then performed on the 16x32 cm specimens (Figure 2.3). The test comprised 3 cycles of loading unloading between 0.5 MPa and one-third of the compressive strength of the concrete determined beforehand. The loading and unloading rates were set at 0.5 MPa/s.

During the test, the specimen was equipped with a ring extensometer consisting of two disjointed rings fixed by six-screw pegs positioned 120° apart. These rings, spaced 167 mm apart, allowed the relative displacement to be measured during the test using three LVDT displacement sensors located on generators spaced 120° apart. The sensors had a stroke of 2 mm and an accuracy of one µm. They were connected to a conditioner delivering an electrical voltage of 10 volts, which was in turn connected to a computer for data recording. For tests conducted on the three types of concrete, the modulus resulted from an average of three specimens.

Figure 2.3 Measurement of the Young's modulus. [113]

Figure 3.4 depicts the average trend of displacements recorded by the displacement sensors for the concrete specimen. The modulus of elasticity is determined by averaging the secant moduli obtained from the loading curves of the last 2 cycles.

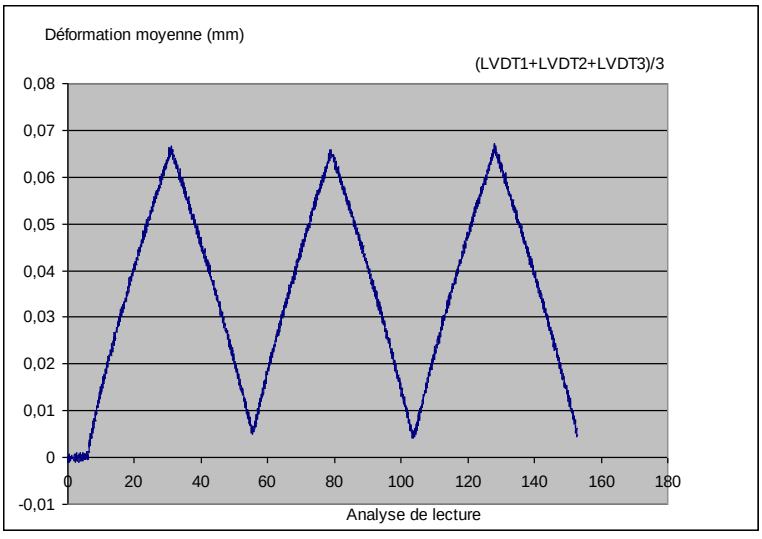

Figure 2.4. Cyclic loading and unloading to determine Young's modulus of concrete. [113]

The tensile strength at 28 days, f_{t28}, was obtained from tensile splitting tests in accordance with the NF P 18-406 standard [129]. This test involved crushing a concrete cylinder along two opposing generators between the plates of a press (Figure 2.5).

Figure 2.5. Splitting tensile test of concrete. [113]

F_{max}being the maximum compressive load causing the cylinder to split due to tension along the vertical diameter, the tensile strength is determined as follows:

$$f_{tj} = \frac{2F_{\max}}{\pi \phi L_R} \qquad (3.1)$$

Where: j = age of the concrete (in days) at the time of the test; ϕ = diameter; and L_R = length of the cylinder. Table 2.2 and Table 2.3 display the mechanical properties of the concrete used for the experiment.

Table 2.2 compressive Stress of concrete

Specimen	compressive Stress (MPa)	Average Stress (MPa)	Standard Deviation (MPa)	Coefficient of Variation (%)
1	32.57	33,76	1,33	3,94
2	33,51			
3	35,2			

Table 2.3 compressive Stress of concrete

Specimen	Tensile Stress (MPa)	Average Stress (MPa)	Standard Deviation (MPa)	Coefficient of Variation (%)
1	2,83	3,18	0,36	11,35
2	3,15			
3	3,55			

The average values of the three characterization cylinders tested were considered to determine the properties of concrete.The results revealed that the average compressive strength of the concrete was 33.76 MPa, while the average tensile strength and modulus of elasticity were 3.11 MPa and 33.55 GPa, respectively.

II.2.2 CFRP and Steel Reinforcements

The carbon reinforcements utilized in this study were manufactured using the pultrusion process. This manufacturing process enables the production of significant quantities at a moderate cost. In this case, rods and flat profiles measuring 8 mm in diameter for the rods and 20x2.5 mm² in cross-section for the flats were utilized. These reinforcements are composed of carbon fibers bound together in an epoxy resin matrix, presenting smooth outer surfaces. The modulus of elasticity and tensile strength will be determined through laboratory tests discussed subsequently Participants.

The main longitudinal reinforcements consisted of high-grade steel bars, 8 mm in diameter, while transverse stirrups were formed using mild steel bars, 6 mm in diameter. Experimental methods, in accordance with Euro-Norm EN10002 [130], were employed to determine the characteristics of the steel reinforcement, with average values obtained from testing three specimens.

In order to better understand the microstructure of carbon reinforcement, samples were observed using a scanning electron microscope. The objective was to characterize the cross-sectional and longitudinal aspects of the carbon reinforcement: fiber percentage and perimeter developed per unit length. Examples of backscattered electron images are presented in Figure 2.6.

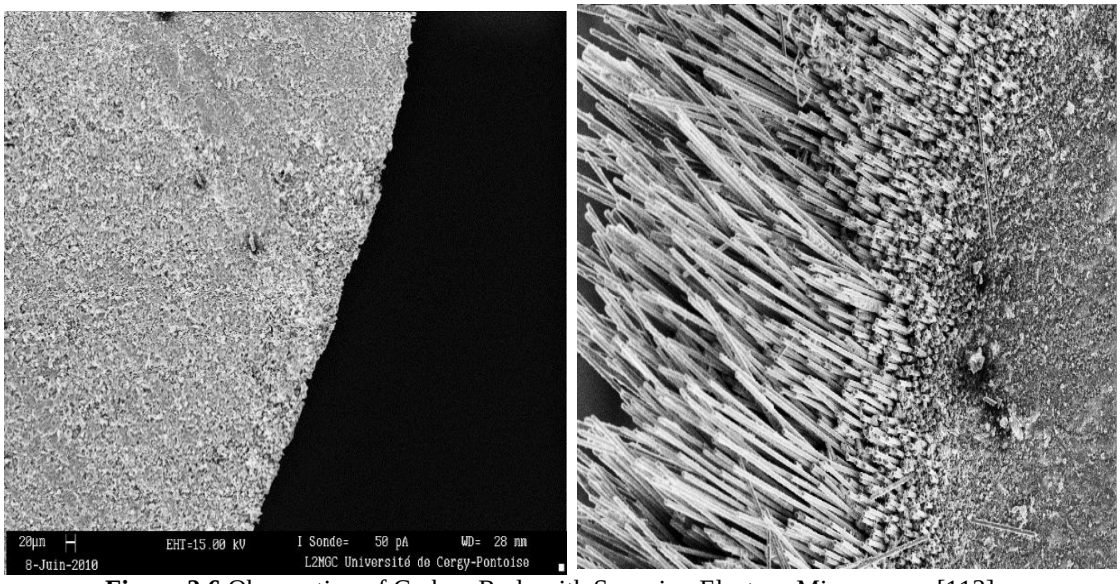

Figure 2.6 Observation of Carbon Rods with Scanning Electron Microscope. [113]

Tensile Strength and Modulus of Elasticity of Reinforcements

The carbon strips and rods are supplied by SOFICAR France®, consisting of CFRP (Carbon Fiber Reinforced Polymer) comprising unidirectional carbon fibers bonded with an epoxy adhesive matrix. As per the manufacturer's specifications, the primary mechanical properties include a tensile modulus of 160 GPa, a tensile strength of 3000 MPa, and an elongation at rupture of 2.0%. All these reinforcements possess a section of 50 mm².

To assess the tensile strength and Young's modulus of the reinforcements, uniaxial tensile tests were conducted. Three smooth carbon rods measuring 70 cm in length and 8 mm in diameter, along with three carbon strips measuring 44 cm in length and having a section of 20x2.5 mm², were subjected to testing. The carbon rod was anchored at both ends within 25 cm long steel tubes with a 12mm diameter, pre-filled with epoxy resin. The flats were reinforced with materials affixed to the ends to prevent premature failure due to stress concentrations resulting from the machine's clamping. (Figure 2.7).

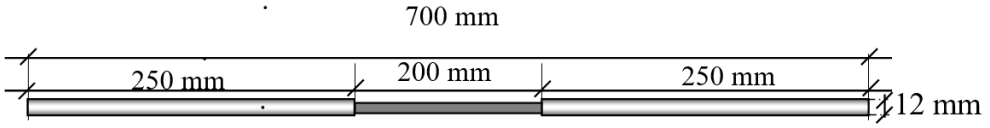

Figure 2.7 CFRP specimens clamped at the ends. [113]

During testing, the tensile load applied to the reinforcement ends was recorded, and deformations were measured using an extensometer. A hydraulic traction machine applied the load with a maximum capacity of 200 kN and a precision of 1.3 ‰, with a constant loading rate of 0.1 kN/s until the reinforcement ruptured (Figure 2.8).

Figure 2.8 Tensile test of the reinforcements. [113]

The rupture of the carbon specimens was abrupt. At approximately 70% of the ultimate tensile strength, the fibers began to separate transversely, culminating in a brittle rupture. In some specimens, the rupture region did not occur at the central part of the specimen, possibly due to challenges in ensuring perfect symmetry and homogeneity in fiber distribution and alignment during manufacturing. The rupture mode of the carbon reinforcements is depicted in (Figure 2.9).

Figure 2.9 Failure mode of carbon reinforcements. [113]

In contrast, for steel reinforcement, rupture occurred in the middle of the specimens and in a ductile manner, likely due to the properties and homogeneity of steel compared to carbon fiber composite reinforcements.

The stress-strain curve for carbon reinforcements (Figure 3.10) displayed a linear relationship until the rupture point, without a noticeable plastic plateau as observed in steel bars.

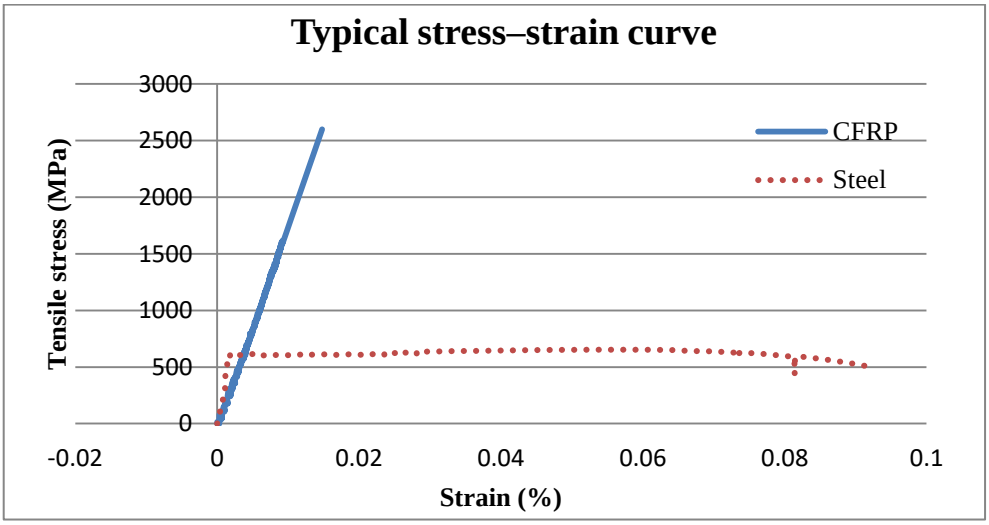

Figure 2.10. Stress-strain curves for reinforcement materials. [113]

Table 2.4 summarizes the observed values for maximum tensile stress and modulus of elasticity obtained from three specimens for each reinforcement type. It is noteworthy that the Poisson's ratio, defined as the transverse unit stress divided by the axial unit elongation, is equal to 0.2

II.2.3 Epoxy Adhesive

Grooves were filled using EPONAL 371; an epoxy adhesive manufactured by BOSTIK France, this epoxy adhesive is characterized by its fluid consistency, designed primarily for sealing composite bars to reinforce structures internally. Comprising two parts, hardener (A) and resin (B), the mechanical properties were evaluated using an Instron Series 5565 testing machine, following ISO 527 1 to 5 standards for tensile tests and ISO 604 for compression tests. The specimen geometries adhered to ISO 178 standards. [131; 132]

Table 2.4 Material properties

Material	Property		Standard deviation	CV %
Compression and tension steel reinforcement	Diameter (mm)	8	/	/
	Tensile strength (MPa)	666.20	10.71	1.60
	Yield stress (MPa)	598.1	8.25	1.37
	Modulus of elasticity (GPa)	200	/	/
Sear steel stirrup	Diameter (mm)	6	/	/
	Tensile strength (MPa)	558.91	26.58	2.25
	Yield stress (MPa)	456.19	12.16	2.66
	Modulus of elasticity (GPa)	200	/	/
CFRP rod	Diameter (mm)	8	/	/
	Tensile strength (MPa)	2561.23	36.98	1.44
	Modulus of elasticity (GPa)	179.46	1.52	0.84
CFRP strip	Thickness x width (mm)	2.5 x 20	/	/
	Tensile strength (MPa)	2538.15	157.79	6.2
	Modulus of elasticity (GPa)	179.85	0.78	0.44
	Ultimate strain (%)	1.2	0.1	8.33

The epoxy components were mixed in specified weight ratios (37.5% hardener and 62.5% resin), using a mixer (800 rpm) for 3 minutes. After uniform mixing, the resin was poured into standardized plastic molds, compacted, and surfaced for uniform thickness and smoothness. Samples were demolded after 24 hours and tested after 7 and 10 days of curing at laboratory conditions (approx. 20°C, 50% relative humidity). (Figure 2.11).

Figure 2.11 Tensile specimens for adhesive testing. [113]

Mechanical properties including maximum tensile stress (σ_{max}), elongation at rupture (ε_u), and Young's modulus (E) were measured.

Tables 2.5 summarizes the experimental results at 7 and 10 days the adhesive.

Compression tests revealed a single rupture mode for The adhesive, characterized by longitudinal fissures indicating tensile stress concentration. (Figure 2.12).

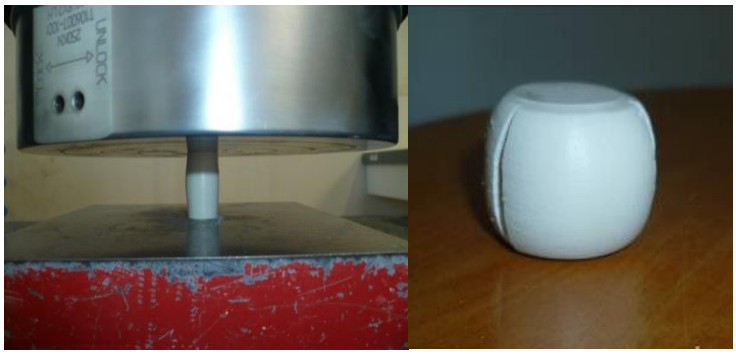

Figure 2.12 Failure mechanism in compressive adhesive testing. [113]

Table 2.5 Mechanical properties of the adhesive

Epoxy-Adhesive Type	E 371
Tension	
- Tensile Strength (MPa)	31.7 ± 3.2
- Elongation at Rupture (%)	1.2 ± 0.3
- Young's Modulus E (MPa)	3800 ± 130
Compression	
- Compression Strength (MPa)	76.8 ± 0.8
- Compression Shortening (%)	4.2 ± 0.2
- Young's Modulus E (MPa)	3400 ± 250

II.3 Specimen Configuration

The experimental investigation consisted of twelve concrete beam specimens, reinforced with steel bars to increase their flexural strength. A CFRP-NSM strengthening approach was used to enhance their flexural capacity. Each of the twelve beams was 1000 mm long and had a rectangular shape, with dimensions of 150 mm in height and 100 mm in width. To reinforce the beams against flexural stresses, two 8 mm diameter bars served as both tension and compression reinforcement, ensuring a steel ratio of 0.0067. To mitigate shear failure prior to flexural failure, 6 mm diameter rectangular stirrups were installed at 120 mm intervals within the shear zone. reinforcement specifications of the typical beam specimen prior to strengthening are shown in (Figure 2.13).

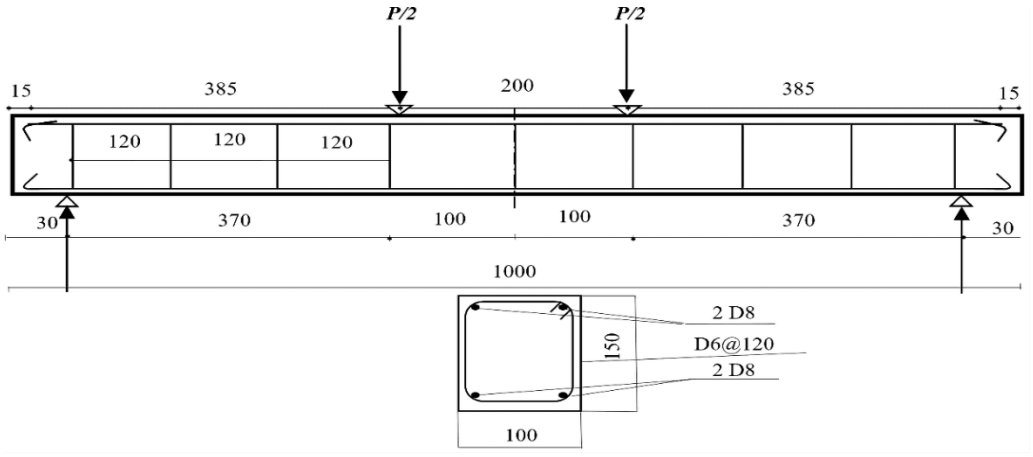

Figure 2.13 Details and cross section of the specimen (mm)

II.4 Test Parameters

Table 2.6 presents the experimental parameters explored in the research. Alongside the tested beams, control specimens were fabricated to establish a comparative framework. The variables under investigation encompassed the reinforcement type (bar or strip), concrete cover depth (10 mm or 30 mm), CFRP strip insertion method (full or partial), and shear stirrups condition (unaltered or partially cut at the bottom), as depicted in (Figure 2.14). Maintaining a consistent CFRP reinforcement ratio ensured uniformity across all strengthened beams. Specimen nomenclature reflected specific attributes: (C) for control beams and (B) for strengthened beams. Concrete cover depth was denoted by (10 or 30), and CFRP reinforcement type was indicated by (R for rod, S for strip). Moreover, CFRP strip embedment was identified by (F for full or P for partial), while shear stirrups condition was labeled as (1) for unchanged or (2) for partially cut.

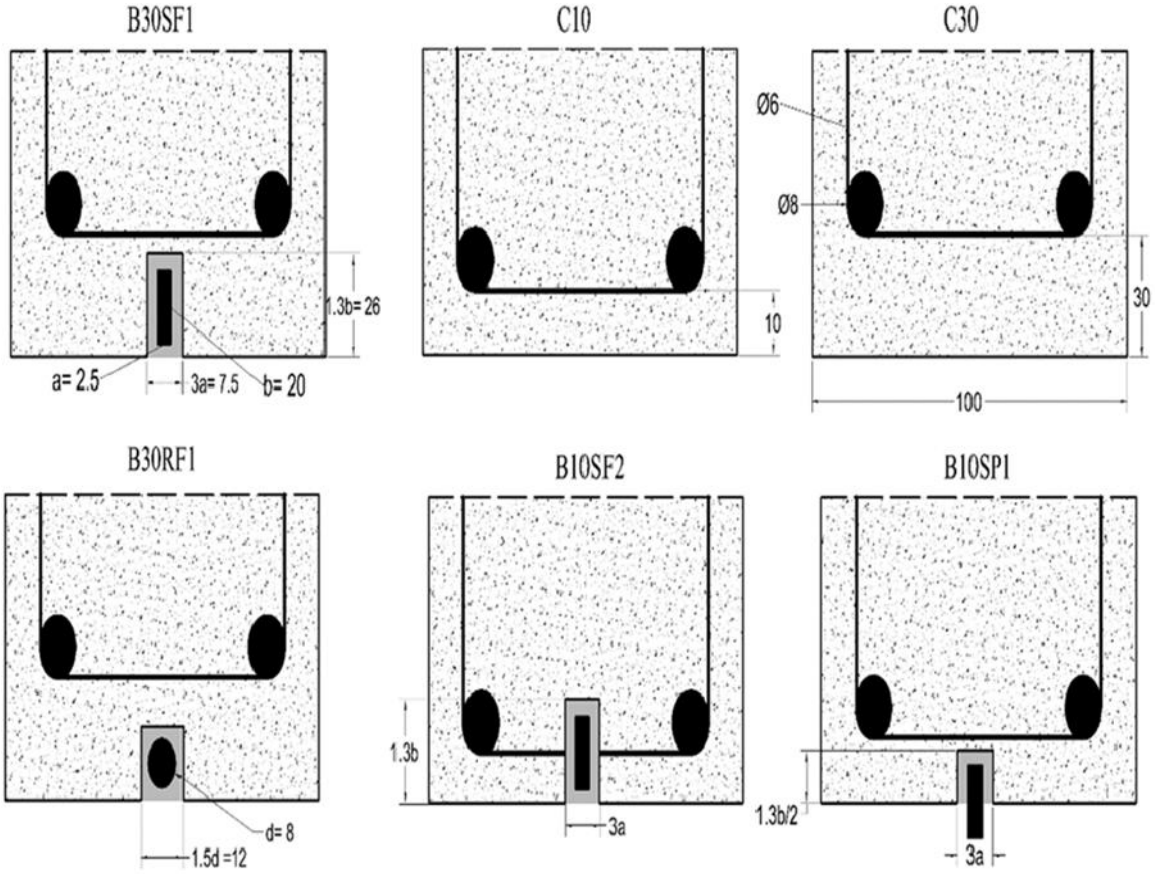

Figure 2.14 Test variables

Table 2.6 Experimental parameters

Designation of specimens	Number of specimens	CFRP Reinforcement	Concrete cover (mm)
C10	2	Without	10
C30	2	Without	30
B30RF1	2	CFRP rods fully embedded	30
B30SF1	2	CFRP strip fully embedded	30
B10SP1	2	CFRP strip partially embedded	10
B10SF2	2	CFRP strip fuly embedded with cutting off steel stirrups at bottom	10

Following 28 days of curing, the beams underwent longitudinal grooving using a specialized saw equipped with a 4 mm diamond blade. The grooving process targeted the tensile side, with each groove incised two or three times, depending on its width: 12 mm for an 8 mm diameter rod and 7.5 mm for a 2.5 mm thick plate. High-pressure air jets cleared debris from the grooves, ensuring optimal adhesion between the sealant and the existing concrete.

The grooves were filled halfway with sealant before positioning the carbon reinforcement at the center and lightly compressing it to facilitate sealant flow. Additional sealant was then applied to completely fill the grooves, and the surface was leveled. The beams were left to cure for a week to ensure the sealant's strength. (Figure 2.15)

a) Steel reinforcements assembling

b) Concrete mixture pouring

c) groove cutting, placing of CFRP bars and epoxy filling

Figure 2.15 Strengthening procedure [113]

The experimental setup involved positioning the beams on a suitable frame designed for four-point bending. An INSTRON 250 kN load cell machine with controlled displacement (1.0 mm/min) was used. This machine had a movable upper crosshead and a lower crosshead for specimen placement, along with a computer for load application and data acquisition. The load was applied monotonically until failure. Carbon reinforcements were instrumented with strain gauges positioned on plates or carbon rods in the center section,. Surface treatment by grinding preceded gauge application, followed by coating with paint and protective putty to mitigate degradation. In addition, a displacement sensor (LVDT) measured the deflection of the center section. Two systems were used for data acquisition: the INSTRON computer running Blue hill software recorded real-time displacement and force values using built-in sensors, while a separate computer equipped with VISHAY acquisition hardware and Workshop software measured deformations in the carbon reinforcements. To attach strain gauges and soldering wires, carbon elements were cut to a length of 75 cm to accommodate the semi-integrated plates during testing without contacting the supports. Gauges were attached to the plates and rods after cleaning with acetone to remove contaminants, marking for centering, taping with special circuit-side tape, and applying adhesive. After a weekend of drying, wires connecting the meter to the measurement software were soldered at both ends, followed by the application of mastic (approximately 1 to 2 mm) for protection. Voltmeter checks were performed after mastic application. Epoxy adhesive facilitated the bonding of the carbon reinforcements in the RC beams, prepared by mixing 100 grams of E371 resin with 60 grams of E371 hardener. Marks on the beams aided in centering the carbon rods, with grooves cleaned for optimum resin-concrete beam adhesion. This was followed by resin application, carbon rod placement, and resin filling of the grooves,

II.5 Conclution

In conclusion, this chapter has provided a comprehensive overview of the experimental methodology used in conducting the tests. Through detailed descriptions of the procedures, materials, and parameters, it has laid out a clear framework for understanding the data collected and its integration into numerical modeling.

Chapter III:

Numerical Simulation Of The Bond Between Concrete And FRP

III.1 Introduction

Understanding the bond between fiber reinforced polymer (FRP) and concrete is critical to improving the strength and durability of reinforced concrete structures. This chapter presents a numerical study focused on evaluating the bond behavior of CFP to concrete using Finite Element Analysis (FEA). The investigation includes two primary methods: Near-Surface Mounted (NSM) reinforcement and Externally Bonded Reinforcement (EBR), with particular emphasis on modeling pullout tests to elucidate bond performance under varying conditions.

Pullout tests are widely recognized as a reliable experimental technique for quantifying the bond strength between FRP and concrete. By integrating these tests into our FEA simulations, we can closely mimic the behavior of the bonded interface under varying loading conditions, providing invaluable insight into the mechanisms governing bond performance.

III.2 Bond-Slip Relationship

The bond strength of an FRP-to-concrete bonded joint is the maximum/ultimate load that the bonded joint can resist. The bond strength is influenced by many parameters such as the bonded length, groove size and configuration, groove filling material and bar surface configuration. In general, with other parameters being the same, a larger bond length gives a higher bond strength.

III.2.1 Bond models for Externally Bonded Reinforcement (EBR)

An important step toward understanding bond behavior is to have characterization of the local bond stress–slip behavior, whichis the most important thing to describe the interface performance between the concrete and the FRP. It further characterizes bond

aspects, such as for example the effective bond transfer length and the strain distribution along the bond length. Despite the difficulties in obtaining local bond stress–slip curves from pull tests directly, models have been developed based on strain measurements or load–slip curves .

The models discussed by Lu et al. [133], which draw from Neubauer and Rostasy [134], as well as Brosens, [135] adopt a bilinear framework to characterize the bond behavior between FRP and concrete. These models seek to capture the relationship between the maximum bond stress (τ_m), concrete tensile strength (f_t), fracture energy (G_f), and width ratio factor (βw) that accounts for the size effect of the bonded width of the FRP (b_f) relative to the width of the concrete (b_c). Eq 3.1

$$
\begin{aligned}
&s \le s_\tau \qquad \tau = \tau_m \left(\frac{s}{s_\tau} \right) \\
&s \ge s_\tau \qquad \tau = \tau_m \left(\frac{s_f - s}{s_f - s_\tau} \right) \\
&\tau_m = \alpha_1 \beta_w f_t \\
&s_\tau = 0.0195 \beta_w f_t \\
&s_f = 2G_f / \tau_m \\
&\beta_W = \sqrt{\frac{2 - b_f / b_c}{1 + b_f / b_c}}
\end{aligned}
\qquad (3.1)
$$

The model developed by Dai et al. [136], introduces additional considerations for the maximum bond stress between Fiber-Reinforced Polymer (FRP) and concrete. In this mode the maximum bond stress (τ_m) is influenced by interfacial fracture energy (G_f) and an interfacial parameter denoted as B. The value of B depends on the characteristics of the FRP material and the adhesive used for bonding. Eq 3.2

$$
\begin{aligned}
&\tau = 2BG_f(\exp(-Bs) - \exp(-2Bs)) \\
&\tau_m = 0.5BG_f \\
&S_\tau = 0.693B \\
&B = 6.846(E_f t_f)^{0.108}(G_a/t_a)^{0.833} \\
&G_f = 0.446(E_f t_f)^{0.023}(G_a/t_a)^{-0.352} f_c^{0.236}
\end{aligned}
\qquad (3.2)
$$

Where E_f, t_f young modulus and thickness of the FRP strip respectively and, G_a t_a ,shear modulus and thickness of the adhesive respectively .

The Popovics type model, developed by Nakaba et al. [137], is rooted in Popovics numerical approach, which focuses on establishing a comprehensive stress–strain relationship for concrete. In contrast to other models, this model simplifies the determination of the maximum bond stress by considering only the concrete compressive strength (f_c) as a parameter. Additionally, the slip (s) at maximum bond stress (τ_{sm}) is determined through a specific value obtained via least square minimization between theoretical predictions and experimental data. Eq 3.3

$$\tau = \tau_m \left(\frac{s}{s_\tau}\right)\left[3/\left(2+\left(\frac{s}{s_\tau}\right)^3\right)\right]$$
$$\tau_m = 3.5 f_c^{0.19} \qquad (3.3)$$
$$S_\tau = 0.065$$

III.2.2 Bond Models for NSM Reinforcement

For NSM CFRP strips, Sena Cruz and Barros [138] adopted the bond-slip model given by Eq 4.4, which was originally proposed by Focacci et al. [139] for steel bar-to-concrete interfaces, for NSM CFRP strip-to-concrete interfaces and calibrated the unknown parameters based on the test results presented in Sena Cruz and Barros [138] This bond-slip relationship was also adopted by De Lorenzis et al. [140] for NSM round bars.

$$\tau(s) = \tau_{\max}\left(\frac{s}{s_0}\right)^{a_1} = C.s^{\alpha_1} \quad for\ s \le s_0$$
$$\tau(s) = \tau_{\max}\left(\frac{s}{s_0}\right)^{a_2} = C.s^{\alpha_2} \quad for\ s \le s_0 \qquad (3.4)$$

α_1 and α_2 are the constants to be determined by best fitting the test data.

Borchert and Zilch [141] proposed the use of the bond-slip relationship adopted by CEB-FIP [143] for steel bar–to-concrete interfaces for NSM CFRP strip-to- concrete interfaces. This model is defined by Eq 3.5.

$$\begin{aligned}
&\tau(S) = \tau_{\max}\left(\frac{S}{S_1}\right)^{\alpha} && for \quad 0 \le S \le S_1 \\
&\tau(S) = \tau_{\max} && for \quad S_1 \le S \le S_2 \\
&\tau(S) = \tau_{\max} - \frac{\tau_{\max} - \tau_f}{S_3 - S_2}(S - S_2) && for \quad S_2 \le S \le S_3 \\
&\tau(S) = \tau_f && for \quad S > S_3
\end{aligned} \tag{3.5}$$

zhang et al.[142] believed that it was not unreasonable to use the bilinear bond-slip relationship which was originally proposed for externally bonded FRP systems to describe the bond-slip behaviour of NSM strips bonded to concrete. Eq 3.6

$$\begin{aligned}
&G_f = 0.4\gamma^{0.422} f_c^{\,0.619} \\
&\tau_{\max} = 1.15\gamma^{0.138} f_c^{\,0.613}
\end{aligned} \tag{3.6}$$

Where τ_{max} is the maximum shear stress, γ is the ratio of height to width for the grooves, f_c is the concrete compressive strength and G_f is the fracture energy.

III.3 Description of the FEA Model

To numerically simulate the bond behavior of the experimental pullout tests, the ABAQUS finite element (FE) software is used. The bond strength in the considered pullout tests is mainly controlled by occurring failure modes of pullout debonding, concrete cover splitting and combination of these two failure modes Accordingly, in order to consider these failure modes in the FE simulation, a 3D FE model, capable of simulating the nonlinear behavior of concrete and the CFRP bar-concrete interface, was developed to predict the bond behavior. The support and loading conditions were simulated according to the characteristics of the test setup in the laboratory as shown in figure 3.1

Eight-node 3D solid hexahedral elements (C3D8R element) were used to model the concrete and GFRP bars, while eight-node 3D cohesive elements (COH3D8 element) were adopted to model the bond zone. In order to assess the mesh dependency of the FE model a mesh sensitivity study was conducted.

The bond behavior of the CFRP bar-concrete interface was simulated using the cohesive elements by defining the relevant bond properties. These properties were built based on the bond-slip law derived from the experimental data, and assigned to the cohesive element with a thickness close to zero.

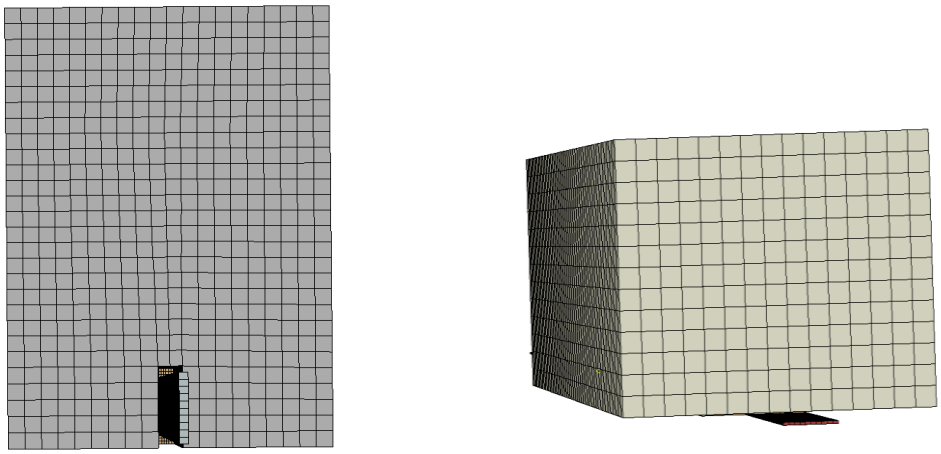

Figure 3.1 FEA mesh a) NSM, b) EBR

III.4 Materials Modeling

III.4.1 Concrete

In this study, the concrete damaged plasticity (CDP) model was selected among various concrete modeling approaches to capture the nonlinear behavior of concrete. The CDP model incorporates two primary failure mechanisms: cracking propagation under tension and concrete crushing under compression (Figure 3.2). Through sensitivity analyses, calibrated CDP parameters essential for defining in Abaqus were determined: dilation angle (ψ=38°), eccentricity (ξ=0.1), the ratio of initial equibiaxial compressive yield stress to initial uniaxial compressive yield stress (σ_{b0}/σ_{c0}) =1.16, and the ratio of the second stress invariant on the tensile meridian to that on the compressive meridian (K=0.667).

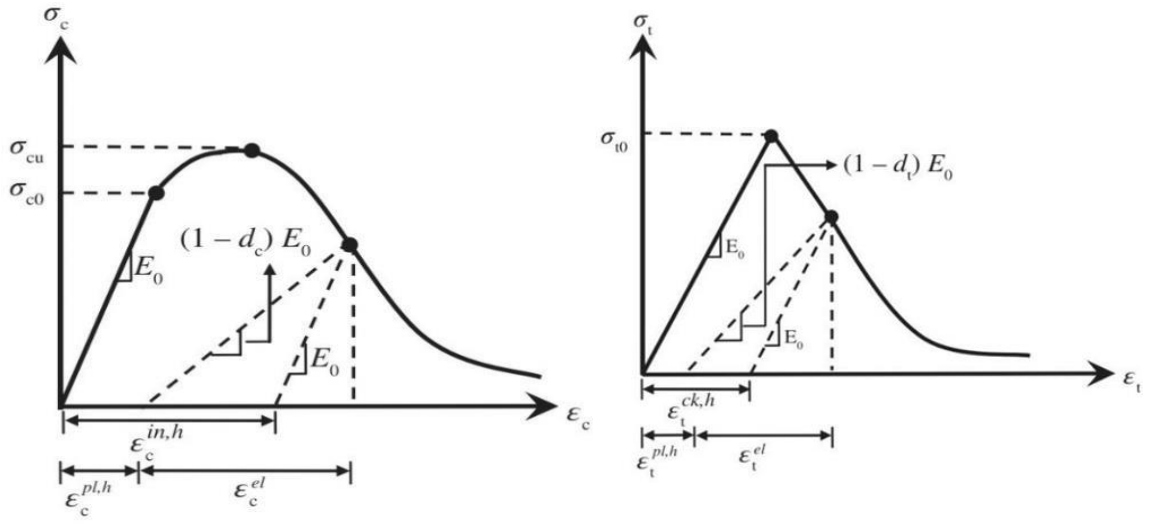

Figure 3.2 Concrete behavior a) compression, b) Tension [144]

The CDP data, encompassing compressive crushing and tensile cracking, were computed based on the mechanical properties of the tested specimens as follows: The stress-strain relationship employed for modeling the nonlinear behavior of concrete under uniaxial compression was proposed by Carreira and Chu [145] and is described by Eq. (3.7) and Eq. (3.8).

$$\frac{\sigma}{f_{cm}} = \frac{\beta_c(\varepsilon/\varepsilon_c)}{\beta_c - 1 + (\varepsilon/\varepsilon_c)^{\beta_c}} \qquad (3.7)$$

$$\beta_c = \left(\frac{f_{cm}}{32.4}\right)^3 + 1.55 \quad \text{(MPa)} \qquad (3.8)$$

In the equation, σ represents the section's normal stress, $f$cm denotes the mean compressive concrete strength, βc is the form factor of concrete, ε represents the strain, and εc is the compressive strain.

To characterize the post-cracking behavior of concrete concerning its tensile properties, the fracture energy cracking criterion GFI was applied. This criterion necessitates inputting the mean tensile strength f_{ctm} and fracture energy G_f, following the guidelines outlined in the CEB-FIP model code. [143] (Eq.3.9).

$$G_f = G_{f0}\left(\frac{f_{cm}}{10}\right)^{0.7} \qquad (3.9)$$

Where f_{cm} is the mean compressive concrete strength and G_{f0} is the base value of fracture energy, which depends on the size of the maximum aggregate in the concrete.

III.4.2 FRP Reinforcement

The CFRP laminate was modeled as a linear elastic behavior up to the brittle failure,where the CFRP composite is mainly stressed in the fiber direction. The elastic behavior was modeled as a lamina type in ABAQUS.

III.5 Epoxy Adehsive

The epoxy resin material was characterized by an elastic perfectly plastic stress-strain relationship. The values for the tensile resistance and modulus of elasticity of the resin were determined experimentally

III.6 Results

III.6.1 Externally Bonded Reinforcement (EBR)

This section is devoted to the assessment of the accuracy of simulations in predicting the bond behavior of fiber-reinforced polymer (FRP) strips. Table 4.1 presents the results of thirty-five tests conducted with varying strip and concrete properties. These results are employed to assess the simulations based on the ultimate load results presented in Table 4.1. The ultimate load is defined here as the initial load observed at the onset of the plateau. The experimental loads exhibited a considerable range, spanning from 14.36 to 57.6 kN. This encompasses a diverse array of width ratios , concrete compressive strengths (35-45 MPa), axial stiffness (24-150 GPa·mm), and bond lengths (250-330 mm). There is a close agreement between the simulated and experimental values, which validates the proposed computational model and illustrates its reliability in predicting the ultimate loads of FRP strips.

The load versus slip relations generated by simulations and corresponding tests are depicted in Figure. 3.3. The corresponding tests were selected at random from the database listed in Table 4.1. All simulations reveal three distinct stages. The elastic stage is characterized by a nearly uniform slope across the curves, with slip increasing almost linearly with applied load. Subsequently, the softening stage emerges, distinguished by a slower load increase, indicating the initiation of debonding at the FRP-concrete interface. Finally, the plateau stage is marked by a rapid increase in slip without a significant load increase, which signifies the propagation of debonding along the load direction until complete strip detachment. Notable differences emerge in the post-elastic stage,

suggesting that the model accurately predicts the load-slip relationship of FRP strips bonded to concrete substrates.

Table 4.1 Bond strength comparison between numerical and test experimental (EBR)

Test		L (mm)	B_c	t_f	B_f	f_c	E_f (GPa)	Pu exp (kN)	Pu Num (kN)
CR1L1		330	400	0.11	100	35	230	23.4	24.12
CR1L1		330	400	0.11	100	35	230	23.1	24.22
CR1L1		330	400	0.11	100	35	230	24.9	25.61
CR1L2		330	400	0.22	100	35	230	33.5	36.36
CR1L2		330	400	0.22	100	35	230	39.3	41.51
CR1L2		330	400	0.22	100	35	230	39.3	41.11
CR1L3		330	400	0.33	100	35	230	42.9	43.10
CR1L3	[47]	330	400	0.33	100	35	230	38.4	38.61
CR1L3		330	400	0.33	100	35	230	38.4	38.64
CR1L3		330	400	0.33	100	35	230	36.9	39.12
CR2L1		330	400	0.11	100	35	230	28.1	30.02
CR2L2		330	400	0.22	100	35	230	43.2	46.12
CR2L3		330	400	0.33	100	35	230	47.4	47.12
CR3L2		330	400	0.22	100	35	230	47.7	47.23
CR3L3		330	400	0.33	100	35	230	57.6	58.74
CNW-50-1		250	250	0.393	50	43.5	227	15.73	16.86
CNW-50-2		250	250	0.393	50	43.5	227	16.03	18.02
CNW-75-1		250	200	0.393	75	43.5	224	24.27	26.23
CNW-75-2		250	200	0.393	75	43.5	224	25.66	27.02
CNW-100-1		250	200	0.393	100	43.5	224	33.48	34.95
CNW-100-2	[48]	250	200	0.393	100	43.5	224	32.38	33.65
CNW-125-1		250	200	0.393	125	43.5	227	41.28	43.03
CNW-125-2		250	200	0.393	125	43.5	227	39.54	41.23
CNW-150-1		250	200	0.393	150	43.5	227	51.65	53.65
CNW-150-2		250	200	0.393	150	43.5	227	52.49	53.12
CNT-2-1		250	200	0.262	50	38.9	227	14.36	15.54
CNT-2-2		250	200	0.262	50	38.9	227	14.36	16.01
CNT-3-1		250	200	0.393	50	38.9	227	16.49	17.85
CNT-3-2	[48]	250	200	0.393	50	38.9	227	16.81	18.12
CNT-4-1		250	200	0.524	50	38.9	227	19.45	20.71
CNT-4-2		250	200	0.524	50	38.9	227	18.37	19.77
CNT-5-1		250	200	0.655	50	38.9	227	19.57	21.17
CNT-5-2		250	200	0.655	50	38.9	227	20.34	21.74
CNE-94-1		250	200	0.51	50	38.9	94	13.03	14.38
CNE-94-2		250	200	0.51	50	38.9	94	13.80	15.10

$B_{c=}$ height of concrete ,L = bond length of CFRP strip; t_f = thickness of CFRP strip; b_f = height of CFRP strip; E_f = elastic modulus of CFRP; f_c = cylinder compressive strength of concrete

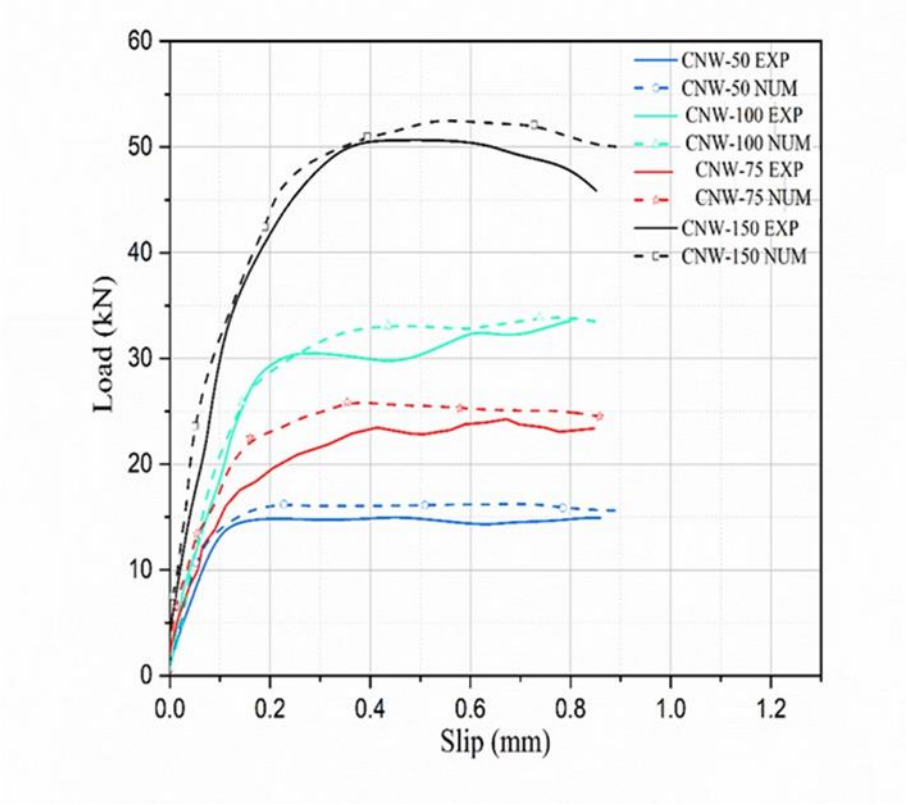

Figure 3.3 Load slip curves from EBR reinforcement.

III.6.2 NSM Reinforcement

To evaluate the accuracy of simulations in predicting the bond behavior of NSM (Near Surface Mounted) reinforcement systems, a series of tests were conducted and compared with simulation results. Table 4.1 presents the findings from thirty-three tests conducted with varying NSM reinforcement and concrete properties. These tests covered a wide range of parameters, including NSM bar diameters, concrete compressive strengths (ranging from 23 to 65 MPa), and embedment lengths (30-350 mm). The ultimate loads observed in the experiments varied considerably, ranging from 14.82 to 130.6 kN. Comparing simulated and experimental ultimate loads, as presented in Table 4.2, shows a close agreement. This consistency validates the proposed computational model and underscores its reliability in predicting the ultimate loads of NSM reinforcement systems. The load-slip relations generated by simulations and corresponding tests are depicted in Figure.3.4. Tests selected randomly from the dataset listed in Table 4.2 were used for comparison. Across all simulations, three distinct stages were observed. The elastic stage is characterized by a nearly uniform slope in the load-slip curves, with slip increasing almost linearly with applied load, representing the initial

loading phase. The softening stage follows, marked by a slower increase in load, indicating the onset of debonding at the NSM reinforcement-concrete interface and signifying the initiation of bond deterioration. Finally, the plateau stage is recognized by a rapid increase in slip without a significant increase in load, indicating the propagation of debonding until complete detachment of the reinforcement, representing bond failure. Small differences were observed in the post-elastic stage between simulations and experiments, suggesting that the model accurately predicts the load-slip relationship of NSM reinforcement systems bonded to concrete substrates. This alignment further supports the reliability and efficacy of the computational model in simulating the behavior of NSM reinforcement systems.

Table 4.2 Bond strength comparison between numerical and test experimental (NSM)

Test		L (mm)	t_f	b_f	b_g	h_g	E_f (GPa)	f_t (MPa	Pu exp (kN)	Pu FEA (kN)
CS2-30		30	4	16	8	20	131,000	23.2	14.82	15.05
CS2-100	[50]	100	4	16	8	20	131,000	23.2	36.28	31.28
CS2-150		150	4	16	8	20	131,000	23.2	46.07	47.07
TS1-3.6-C0		350	3.6	10	5.6	11	150,000	38.8	40.00	41.22
TS1-3.6-C0R		350	3.6	10	5.6	11	160,000	38.8	39.20	40.51
TS1-3.6-C10		350	3.6	10	5.6	21	165,000	38.8	61.80	62.96
TS1-3.6-C20		350	3.6	`10	5.6	21	166,000	38.8	79.60	80.56
TS1-3.6-C30		350	3,6	10	5.6	21	157,000	38.8	101,80	102.45
TS2-6.0-C0		350	6	10	8	11	166,000	38.8	54.80	55.94
TS2-6.0-C10		350	6	10	8	21	165,000	38.8	86.10	87.12
TS2-6.0-C20	[52]	350	6	10	8	31	169,000	38.8	136.00	137.13
TS3-6.0-C15		350	6	10	8	26	160,000	38.8	89.80	91.04
TS3-6.0-C25		350	6	10	8	36	161,000	38.8	117.00	118.21
TS3-6.0-C30		350	6	10	8	41	160,000	38.8	129.90	131.11
TS3-6.0-C40		350	6	10	8	51	154,000	38.8	130.60	133.01
30-MPa-100-10		100	1.2	10	3.2	11	161,8	30	22.60	22.74
30-MPa-100-10		100	1.2	10	3.2	11	161,8	30	20.40	21.88
30-MPa-150-10		150	1.2	10	3.2	11	161,8	30	23.20	24.58
30-MPa-200-10		200	1.2	10	3.2	11	161,8	30	27.90	29.01
30-MPa-250-10		250	1.2	10	3.2	11	161,8	30	26.60	28.10
30-MPa-300-10		300	1.2	10	3.2	11	161,8	30	26.00	27.12
30-MPa-350-10		350	1.2	10	3.2	11	161,8	30	23.00	24.02
42-MPa-200-10		200	1.2	10	3.2	11	161,8	41.8	30.60	32.04
30-MPa-100-20		100	1.2	20	3.2	21	161,8	30	51.40	53.10
30-MPa-200-20		200	1.2	20	3.2	21	161,8	30	57.80	58.19
30-MPa-300-20	[51]	300	1.2	20	3.2	21	161,8	30	66.70	67.20
65-MPa-200-10		200	2.9	10	4.9	11	161,8	64.8	45.00	46.18
65-MPa-200-20		200	2.9	20	4.9	21	161,8	64.8	108.1	110.1
53-MPa-200-10		200	1.24	10	3.2	11	161,8	52.8	31.90	33.12
53-MPa-200-10		200	1.3	10	3.3	11	161,8	53	34.00	35.26
53-MPa-100-20		100	1.25	20	3.2	21	161,8	53	63.80	64.50
33-MPa-200-15		200	1.26	15	3.2	17	161,8	33.4	47.50	48.42
33-MPa-300-15		300	1.26	15	3.2	16	161,8	33.4	51.60	53.12
65-MPa-200-10		200	2.9	10	4.9	11	161,8	64.8	45.10	46.63
33-MPa-200-20		200	1.2	20	3.2	21	161,8	33.4	60.70	61.90

L = bond length of CFRP strip; tf = thickness of CFRP strip; hf = height of CFRP strip; bg = width of groove; hg = height of groove; Ef = elastic modulus of CFRP; fc = cylinder compressive strength of concrete;

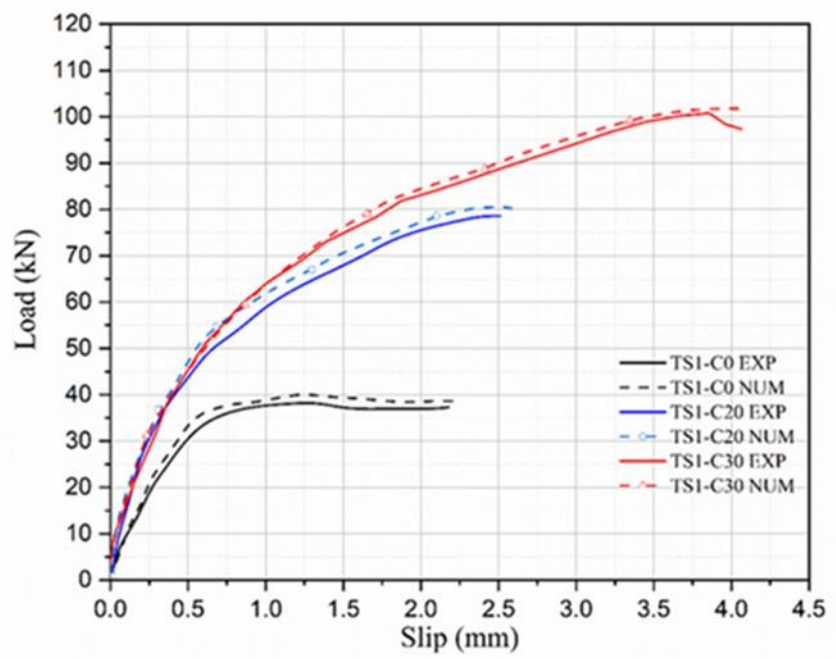

Figure 3.4 Load slip curves from NSM reinforcement.

III.7 Conclution

In conclusion, this chapter provides a thorough assessment of simulation accuracy in predicting the bond behavior of both externally bonded reinforcement (EBR) and Near Surface Mounted (NSM) reinforcement systems. Thirty-five tests were conducted for EBR systems, while thirty-three tests were conducted for NSM systems. These tests covered a wide range of parameters including bar diameters, concrete compressive strengths, embedment lengths, axial stiffness, and bond lengths .The simulations closely matched for both FRP and NSM systems, with minor differences in the post-elastic stage.

Chapter IV:

Numerical Simulation Of RC Beams Reinforecd By NSM FRP

IV.1 Introduction

A numerical simulation of the behavior of the NSM CFRP-reinforced beams was performed by three-dimensional finite element modeling using ABQSUS FEA software. The numerical results, including load-deflection curves, strain distributions, and crack patterns, were carefully compared with the experimental observations. [114]

IV.2 Description of the Finite Element Model

To expedite computations and enable finer meshing, only one quadrant of the beam was modeled, leveraging geometry, loading, and boundary condition symmetries. The simulation utilized 3D solid deformable elements (C3D8R) for concrete, CFRP strips, and epoxy adhesive. Meanwhile, 3D concrete-embedded truss elements (T3D2) represented the steel rebars and stirrups. The adhesive/CFRP/concrete interface was simulated using cohesive elements (COH3D8).

A sensitivity analysis was conducted to validate mesh dimensions and assess their impact on accuracy and computation time. Optimal results were achieved with a 10 mm mesh size for the concrete beam. Critical areas and regions with anticipated high strain gradients were assigned a finer mesh. Epoxy and CFRP reinforcement were assigned a 4 mm mesh size. Support and loading conditions were simulated in line with the experimental setup depicted in Figure 4.1.

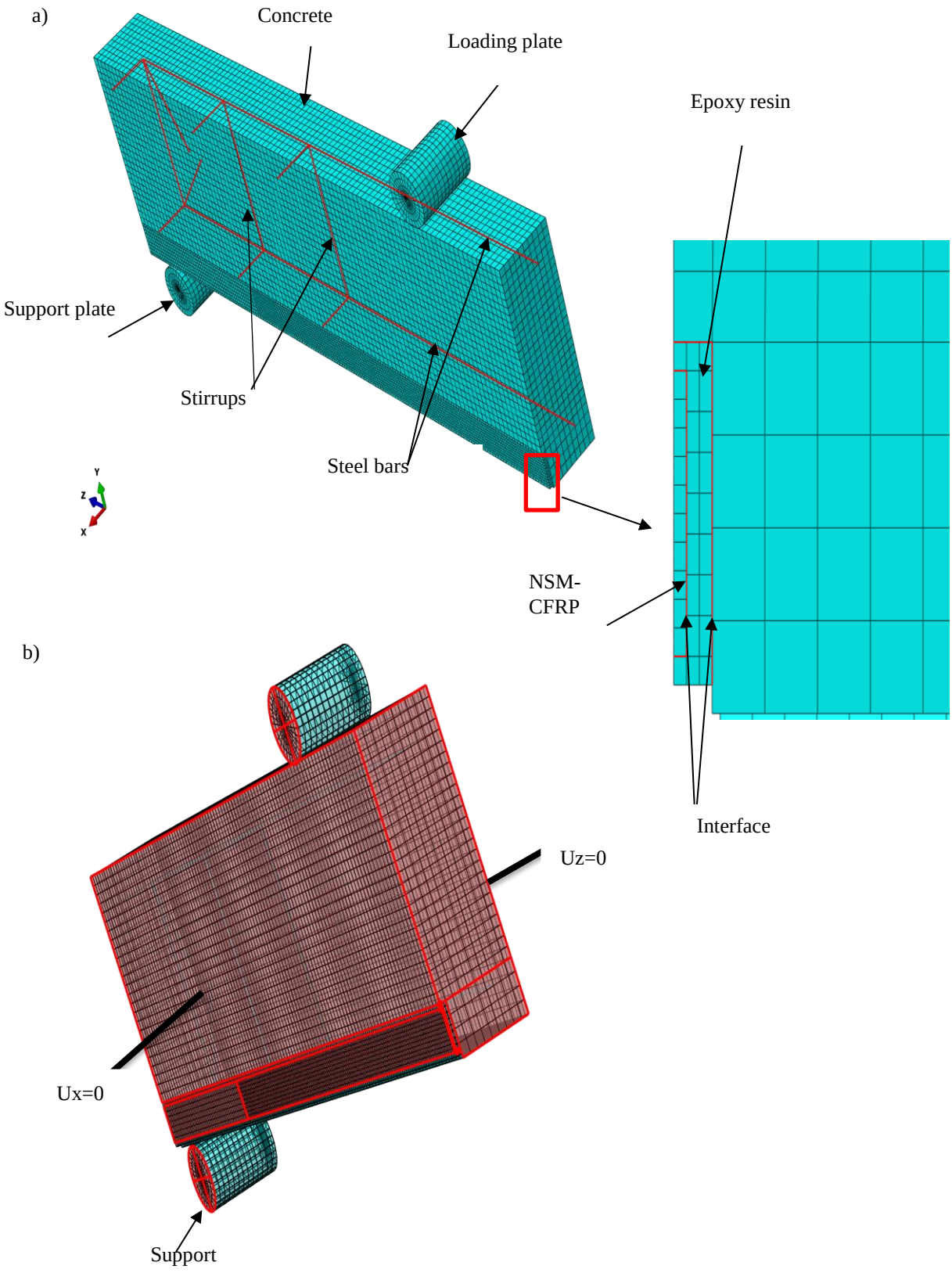

Figure 4.1 a) Meshed FE model, b) boundary conditions

IV.3 Materials Modeling

IV.3.1 Concrete

In this study, the concrete damaged plasticity (CDP) model was selected among various concrete modeling approaches to capture the nonlinear behavior of concrete. The CDP model incorporates two primary failure mechanisms: cracking propagation under tension and concrete crushing under compression as discussed in chapter 4

IV.3.2 Cfrp Reinforcement

The CFRP strips and rods were represented in the model as elastic isotropic brittle materials until reaching the ultimate tensile stress, at which point brittle damage ensues (Figure 4.2). This modeling strategy was chosen because of the unidirectional characteristics of the composite material, with the main stress applied in the fiber direction. The elastic modulus and ultimate strength of the CFRP bars utilized in the analysis are detailed in Table 3.4. Moreover, a Poisson's ratio of 0.3 was assumed for the CFRP material.

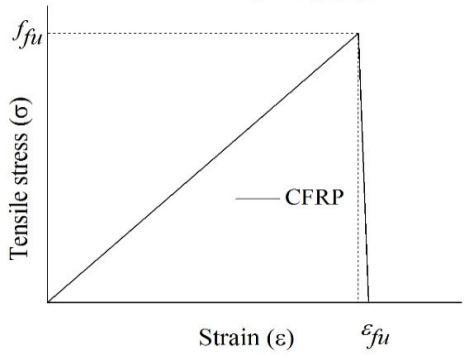

Figure 4.2 Uniaxial constitutive laws of CFRP reinforcement

IV.3.3 Steel Reinforcement

The steel reinforcement was modeled using the elastic-plastic approach. The elastic modulus, yielding strength, and ultimate strength of the steel bars were determined through experimental testing, as discussed in section 3. A Poisson's ratio of 0.3 was applied to the steel reinforcement in the analysis

IV.3.4 Epoxy Adehsive

The epoxy-resin material was characterized by an elastic perfectly plastic stress-strain relationship (Figure 4.3). The values for the tensile resistance and modulus of elasticity of the resin can be found in Table 2.5. Additionally, a Poisson's ratio of 0.35 was adopted

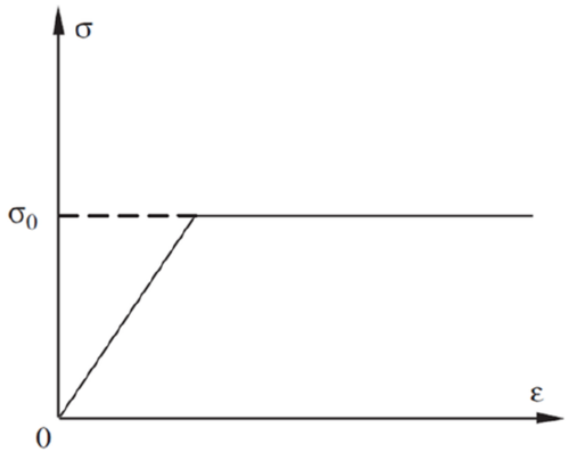

Figure 4.3 Uniaxial constitutive law of epoxy adhesive

IV.4 Interactions Modeling

IV.4.1 Interface Between Concrete and Steel Rebars

Accurately representing the bond-slip behavior between the concrete and the embedded steel reinforcement is crucial to achieve distinct discrete crack patterns in the simulated beam model and realistic flexural responses beyond the cracking stage. In the current FE analyses, the bond between the longitudinal reinforcement and the concrete was simulated using 0-length SPRING2 elements, (nonlinear springs). These elements connect the concrete and steel elements at shared nodes, and the bond-slip relationship specified in the fib Model Code [144] was applied as follows eq (4.1)

$$\tau_b = \begin{cases} \tau_{b\max}\left(s/s_1\right)^{\alpha} & for\ \ s \le s_1 \\ \tau_{b\max} & for\ \ s_1 \le s \le s_2 \\ \tau_{b\max} - \dfrac{\left(\tau_{b\max} - \tau_{bf}\right)\left(s - s_2\right)}{\left(s_3 - s_2\right)} & for\ \ s_2 \le s \le s_3 \\ \tau_{bf} & for\ \ s < s_3 \end{cases} \qquad (4.1)$$

Where, $\tau_{b\max} = 2.5\sqrt{f_{cm}}$ $\tau_{bf} = 0.4$, $\tau_{b\max}$ $s_1 = 1.0$ mm, $s_2 = 2.0$ mm, s_3= distance between rebar ribs, and τ_b is the bond stress. (Figure 4.4).

The discrete node-to-node connections used to simulate the bond-slip behavior necessitate the derivation of the bond force F instead of the bond stress τ_b, this relationship is expressed by Eq (4.2).

$$F = \tau_b c_r l_b \qquad (4.2)$$

Where C_r is the circumference of the steel rebar, and l_b represents the bond length.

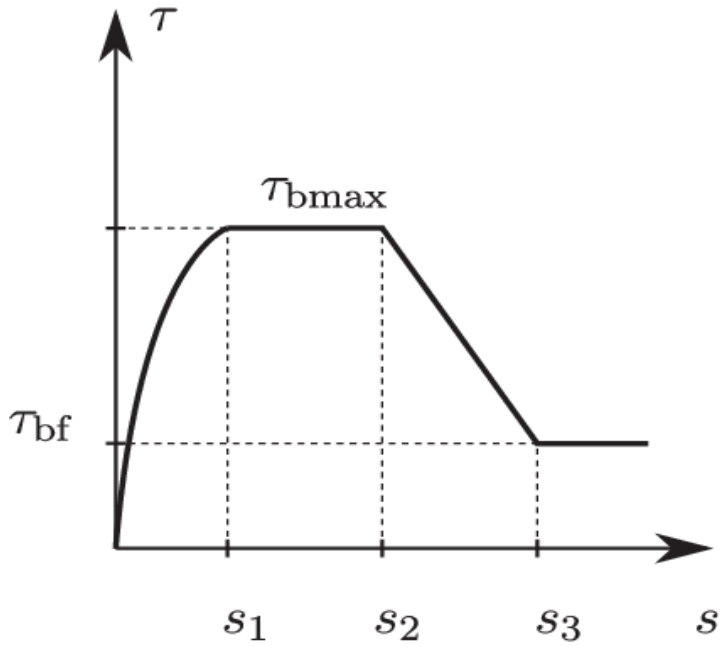

Figure 4.4 Stress-slip relationship of the Steel-Concrete interface [144]

IV.4.2 Interface Between Concrete and FRP

To simulate the bond behavior of the CFRP-adhesive-concrete connections, two layers of cohesive elements with a traction-separation model were used, one for the concrete/adhesive interface and the other for the CFRP-adhesive interface these elements behave in a linear elastic way until a damage initiation criterion is reached, followed by the propagation of damage which eventually leads to the degradation of the elements and failure of the bonded interface. (Figure 4.5)

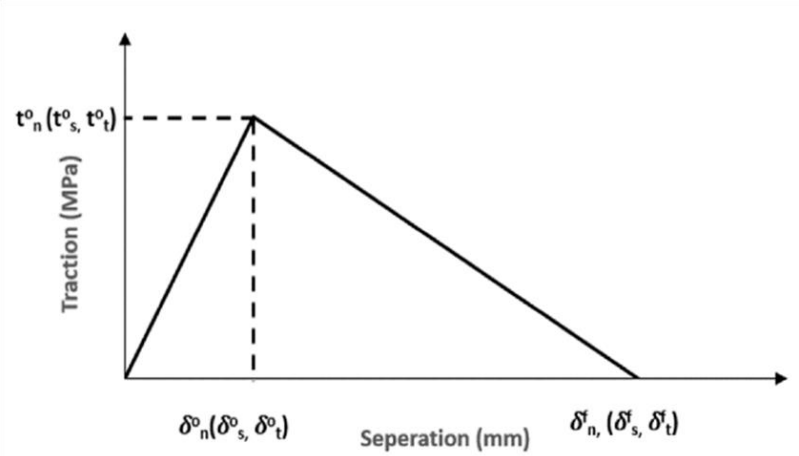

Figure 4.5 Stress-slip relationship of the interface

The Quadratic Delamination criterion was adopted for the damage imitation with normal tress equal to the concrete tensile strength (Figure 4.6). The slip model developed by Zhang. [143], was adopted to calculate the maximum shear stress and the damage evolution in terms of fracture energy is given by the following equations:

$$G_f = 0.4\gamma^{0.422} f_c^{0.619} \tag{4.3}$$

$$\tau_{\max} = 1.15\gamma^{0.138} f_c^{0.613} \tag{4.4}$$

Where τ_{max} is the maximum shear stress, γ is the ratio of height to width for the grooves, f_c is the concrete compressive strength and G_f is the fracture energy.

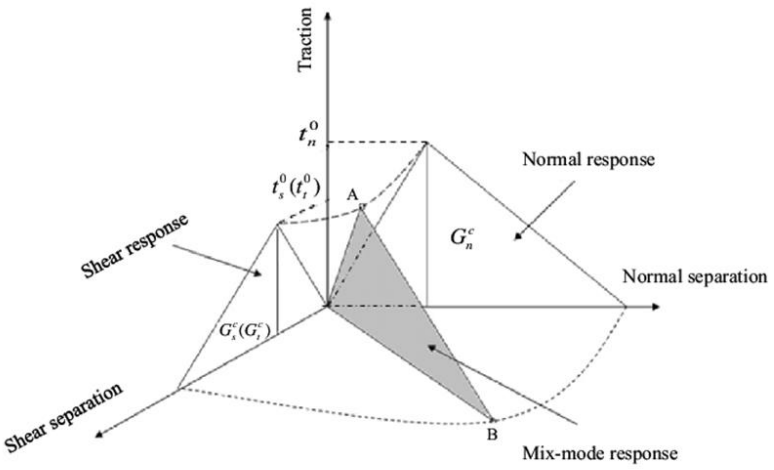

Figure 4.6 Mixed mode response of the interface

IV.5 Results and Discussion

A comparison between experimental and numerical results is presented in (Table 4.1), which summarizes the cracking load (P_{cr}), yield load (P_y), ultimate load (P_u), yield deflection (Δ_y), maximum deflection (Δ_u), and failure modes for the tested beams. The numerical results were obtained by simulating the tested beams using a finite element model as described in the previous section. The comparison shows good agreement between the experimental and numerical results, validating the accuracy of the proposed numerical model. The load-carrying capacity results indicate that the numerical values are slightly higher than the experimental ones, but the overall difference between the two sets of results is within an acceptable range.

Both control samples (c10 and c30) exhibited similar behavior, with beam c10 showing a higher peak load and deflection of approximately 27.26% and 10%, respectively, compared to beam c30 due to the lower concrete cover depth. A negligible increase in the cracking load of about 12%, 11%, 6.3%, and 1.2% for beams B30RF1, B10SF2, B30SF1, and B10SP1, respectively, was observed in comparison with the control beams. The yield load increased by 61%, 58%, 27.5%, and 21% respectively, for beams B30RF1, B30SF1, B10SF2, and B10SP1, due to the increased flexural stiffness during the second phase of the beam's behavior.

The use of NSM CFRP laminates significantly increased the ultimate load-carrying capacity of the RC beams. An increase of 69%, 70%, 39%, and 17% was obtained in terms of maximum load for B30SF1, B30RF1, B10SF2, and B10SP1, respectively, compared to the maximum load of the reference beam. Specimen B10SF2 had the highest peak load of 48.79 kN, indicating that cutting the bottom arm of the steel stirrups had negligible influence on the load-carrying capacity of the beams. However, beams strengthened with partly inserted strips had the lowest increase in load-bearing capacity due to the reduced contacting surface and groove size. It should be noted that beams with higher concrete cover depth saw greater improvement from reinforcement, as the steel reinforcement is further away from the region of highest stress concentration, which is at the bottom of the beam. In such cases, NSM bars can be particularly advantageous, as they are inserted precisely in this region of high-stress concentration, providing additional reinforcement and increasing the load-carrying capacity of the beam. However, the overall maximum load did not increase as much after the yielding load due to the onset

of premature debonding failure modes that occurred in the strengthened beams, caused by the detachment of the concrete cover, resulting in a brittle failure mode. This ultimately limited the maximum load that the beam could support. A noticeable reduction in deflection at maximum load was observed in the NSM strengthened beams by 70.24%, 64.18%, 64.1%, and 61.6%, for specimens B10SP1, B10SF2, B30SF1, and B30RF1, respectively. This reduction can be explained by the observed failure mode of the CFRP bars, which was confirmed by the decrease in the ductility of the NSM strengthened beams defined as the ratio of ultimate deflection to yield deflection by 65%, 56.3%, 52.25%, and 48.5%, for beam B10SP1, B10SF2, B30SF1, and B30RF1, respectively. These results indicate that the use of NSM CFRP laminates can significantly increase the load carrying capacity of RC beams, but the design and installation should be carefully considered to prevent premature failure and ensure the long-term effectiveness of the reinforcement.

Table 4.1 Test results

Beam ID	Ultimate loads P_u (kN)		Ultimate displacement Δ_u (mm)		CFRP Strain at ultimate load (%)		μ	FM
	EXP	FEA	EXP	FEA	EXP	FEA		
C10	35.01	35.90	15.15	19.15	-	-	3.34	FF
C30	27.51	26.86	16.5	15.50	-	-	2.66	FF
B30RF1	46.46	47.18	6.34	6.45	0.35	0.35	1.37	ED+CDC
B30SF1	46.86	46.51	5.80	5.94	0.26	0.27	1.27	ED+CDC
B10SP1	40.41	40.95	5.40	5.68	0.38	0.38	1.17	ED+CDC
B10SF2	48.55	48.79	6.50	6.20	0.24	0.25	1.46	ED+CDC

Note : P_{cr} : cracking load , P_y and Δ_y : yielding and deflection load , P_u and Δ_u : ultimate load and deflection , μ (ductility index) : Δ_y/Δ_u , FM : Failure mode (FF: Flexural failure, ED: End debonding of the CFRP reinforcement , CDC: Critical diagonal crack)

Beam ID	Cracking load P_{cr} (kN)		Yield load P_y (kN)		Yield dispclament Δ_y (mm)	
	EXP	FEA	EXP	FEA	EXP	FEA
C10	9.12	9.35	31.50	33.60	5.44	5.81
C30	8.98	9.06	24.36	26.20	6.20	5.89
B30RF1	10.08	10.21	39.37	38.39	4.60	4.72
B30SF1	9.55	9.82	38.65	37.16	4.55	4.06
B10SP1	9.25	9.67	34.78	36.45	4.61	4.52
B10SF2	10.12	10.39	39.78	40.71	4.44	4.23

IV.5.1 Load–Deflection Curves

Figure 4.7 illustrates both the experimental and numerical load-deflection curves, serving as a robust validation of the established predictive model. The behavior of CFRP strengthened beams is characterized by a brittle failure mode, in contrast to the more ductile behavior observed in the control beam. The curves delineate a three-phase response, marked by concrete cracking, steel yielding, and post-yielding stages.

Prior to cracking, the strengthened beams exhibit linear elastic behavior akin to the control beam during the initial stage. The influence of NSM bars on the stiffness of the load-deflection curves is minimal, with their effect on cracking behavior being slight. This is attributed to the high flexural rigidity of beams and the fact that the bonding between the filling material and concrete remains largely unaffected at this stage.

Transitioning to the second stage, spanning from cracking to steel yielding, the NSM bars notably augment the stiffness of the specimen and the yielding load compared to the control beam. Concrete cracking initiates in the beam cross-sections situated in the maximum moment zone. Initially, the cracks refrain from crossing the resin due to its low elastic modulus. However, as the load intensifies, the cracks widen, and fresh flexural cracks emerge.

Cracking progresses uniformly across the beam length in response to the applied bending moment. Once the moment surpasses a threshold causing the steel bars to yield, concrete cracking stabilizes. In the final stage, with increasing load, the deflection rate accelerates more rapidly than in the preceding stage. Throughout this phase, the width of the cracks is governed by the FRP bars until the point of failure is reached.

While the control beam succumbs to flexural failure, the CFRP bar-strengthened beams experience premature debonding, significantly impacting their reinforcement potential. Subsequent analysis delves into the parameters dictating the behavior of NSM FRP systems, as detailed in the ensuing section.

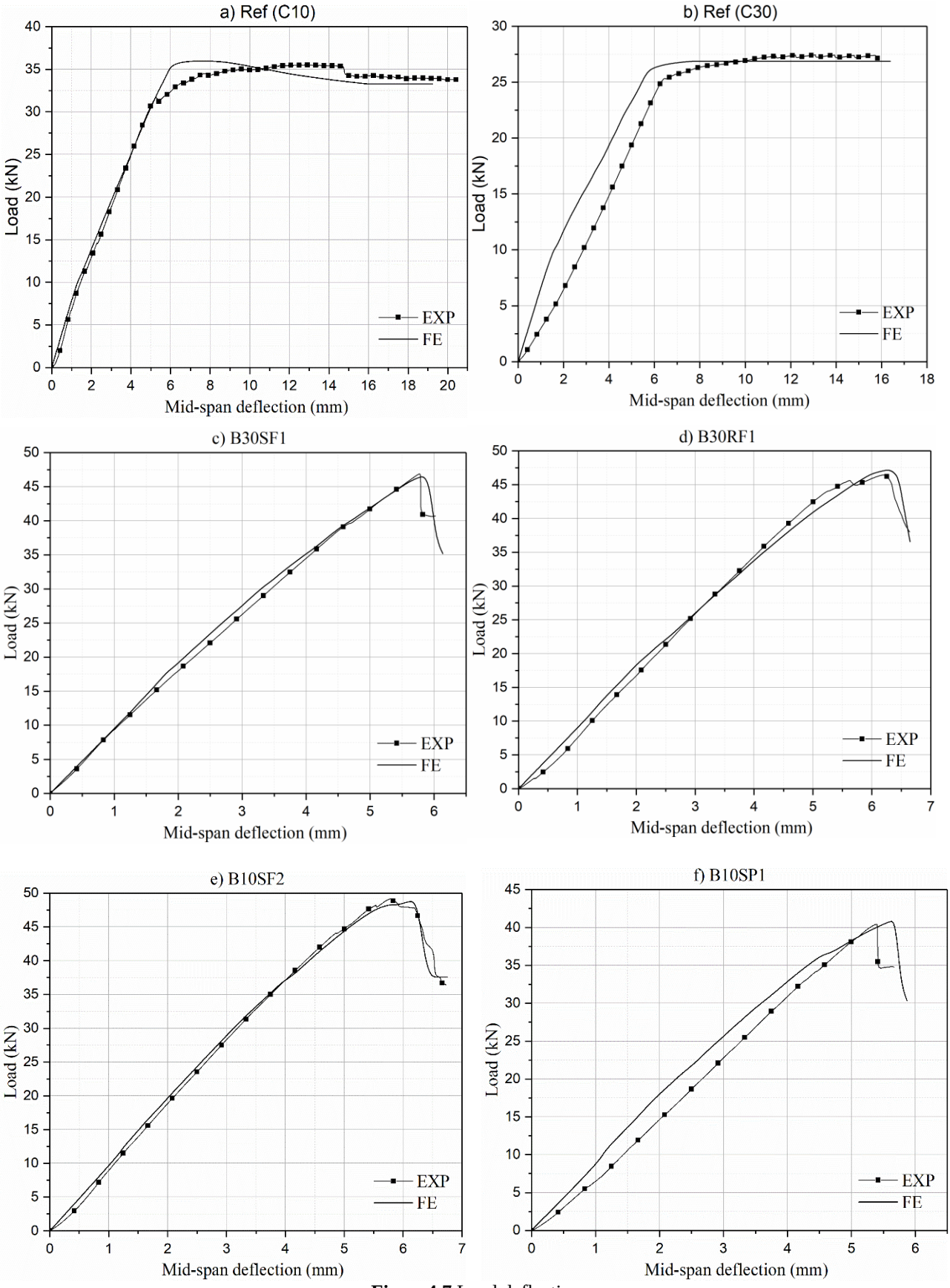

Figure4.7 Load deflection curves

4.2 Load–strain Curves

Figure 4.8 shows good predictive accuracy of the variation in tensile strains in the CFRP reinforcement

The behavior observed in the tensile strains of the CFRP reinforcement demonstrates a remarkable predictive accuracy in the context of the variation. Initially, during the onset of the cracking stage, the CFRP bars exhibited minimal load-carrying capacity, with strains registering nearly zero. Consequently, their contribution to augmenting the cracking load of the NSM-CFRP strengthened beams remained marginal. However, with the progressive increase in applied load, the CFRP strain curves exhibited discernible inclinations, signifying that the additional bars commenced bearing significant loads. This phenomenon led to a notable enhancement in the yielding and ultimate loads of the beams.

Analyzing the CFRP strain curves, it is evident that they followed nearly linear trajectories up to the point of tension steel yielding. This indicates that the CFRP bars adeptly resisted the tensile stresses induced by the applied loads. Subsequent to the yielding of the tension steel, the CFRP strains experienced gradual increments until reaching the point of failure. Such behavior underscores the potential of CFRP bars in augmenting the structural performance of reinforced concrete beams.

Nevertheless, it is imperative to note that the maximum strain attained by the CFRP bars only reached approximately 28% of their ultimate strain. This suggests an underutilization of the reinforcement potential. Primarily, this underutilization stemmed from the premature detachment of the reinforcement, which curtailed its effectiveness in bolstering the load-carrying capacity of the beams. Consequently, further enhancements in the bonding between the CFRP bars and the concrete substrate are warranted to fully realize the potential of NSM-CFRP reinforcement.

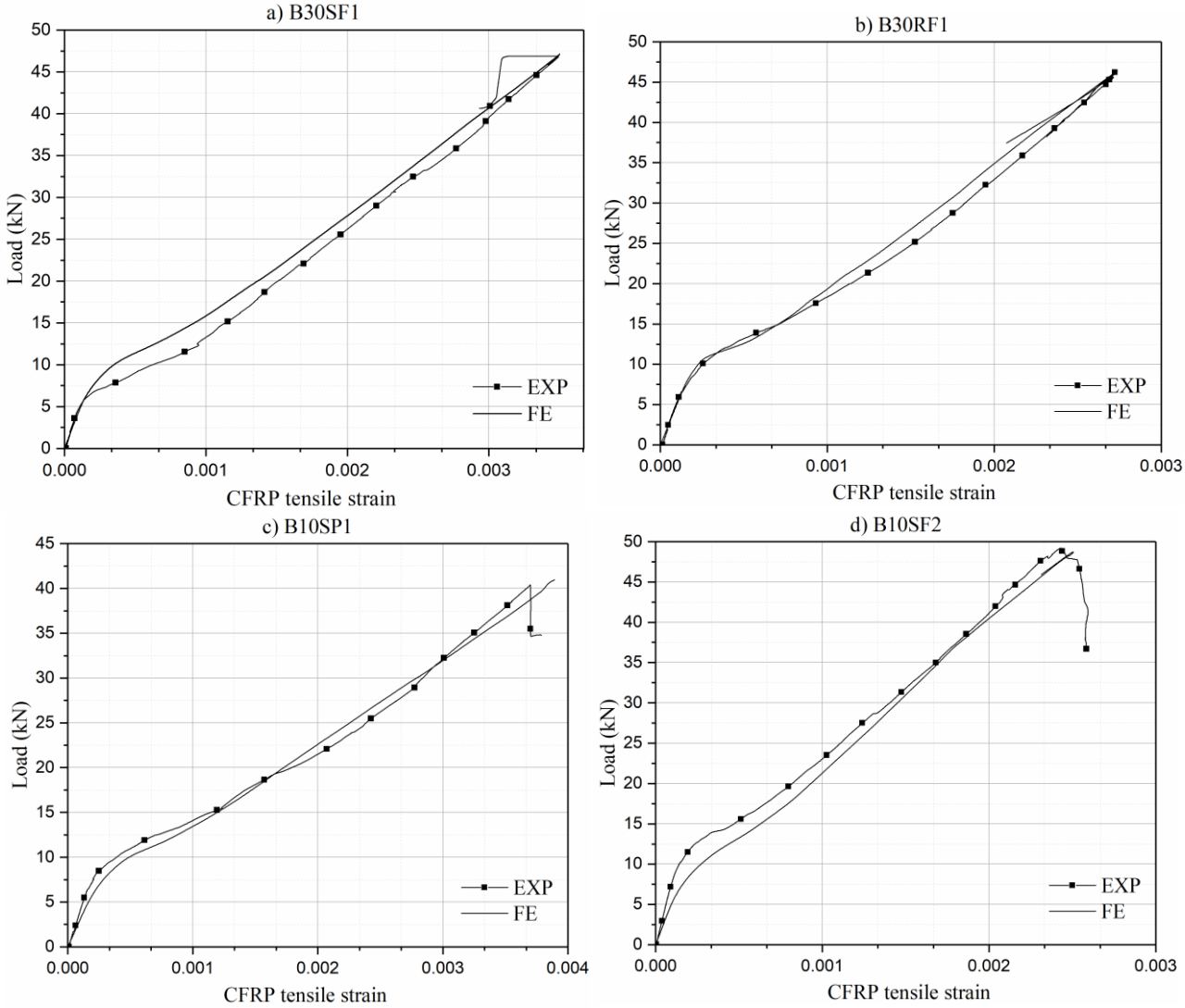

Figure 4.8.Load strain curves

4.3 Failure modes

The crack pattern on the reference beam is illustrated in Figure 4.9, which consisted of flexural cracks. The first cracks started from the mid-span on the tension side of the beam and propagated towards the neutral axis. Concrete crushing in the compression zone near the loading plates after the yielding of the tensile steel followed this. These observations indicate a flexural failure, which was accurately captured by the numerical model.

Figure 4.10 presents the experimental recorded and numerically predicted failure modes and crack patterns of the beam strengthened with NSM CFRP strips. It was observed that the failure initiated with the end debonding of the CFRP strip from the

bottom of the concrete beam sample, followed by a critical diagonal crack that started exactly from the end of the plate. This confirms the interaction between different failure phenomena close to the end of the FRP plate. The debonding failure mechanism of this set of beams was particularly influenced by the length of CFRP bars. The debonding failure was sudden and complete, occurring immediately after the yielding of the tension steel followed by a subsequent beam failure

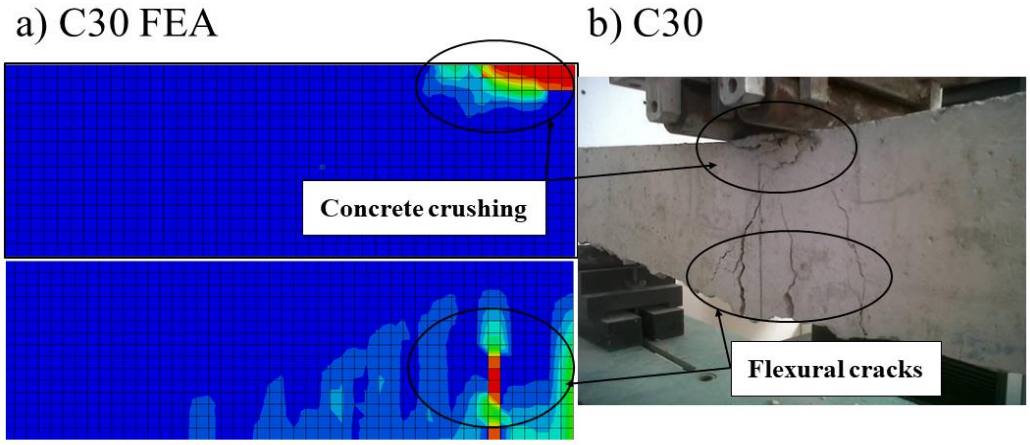

Figure 4.9 Crack patterns and Failure modes of the reference beam: a) FEA, b) EXP

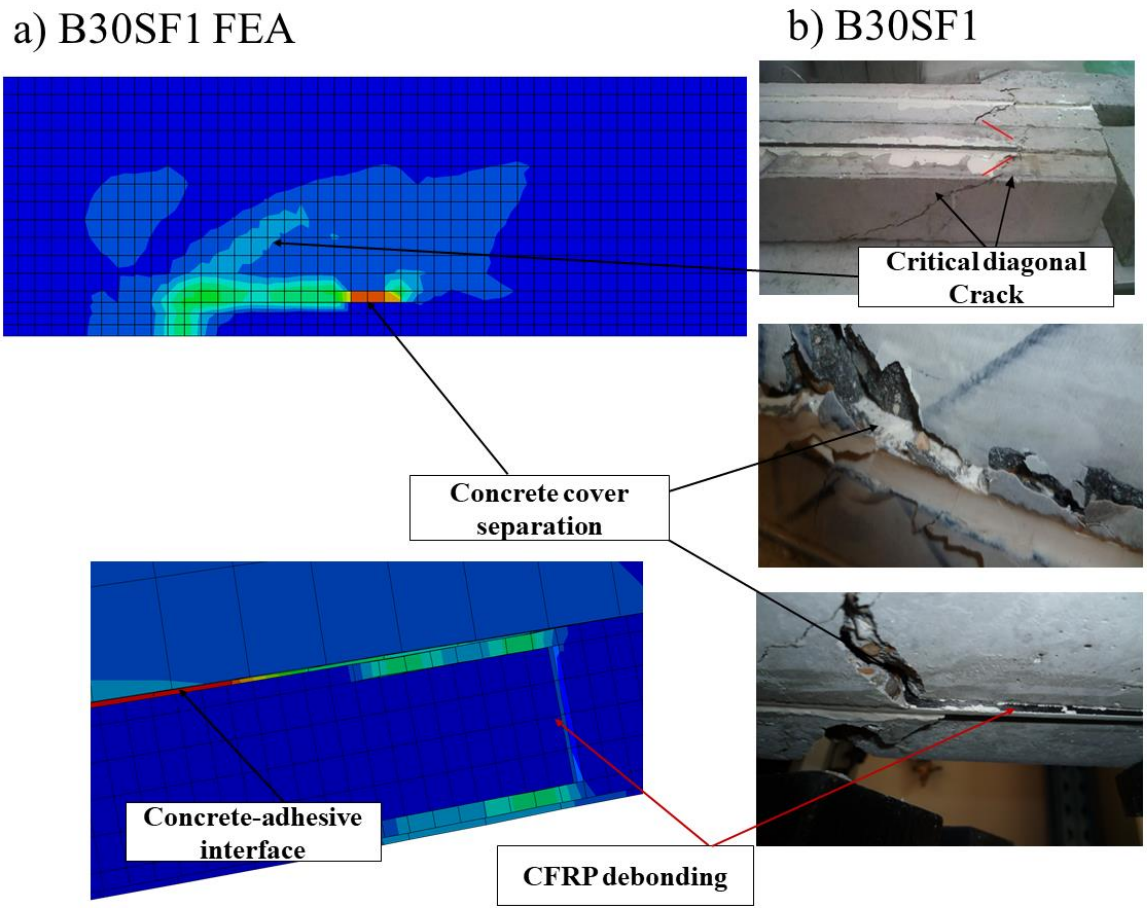

Figure 4.10 Crack patterns and Failure modes of the NSM reinforced beams

IV.6 Parametric Studies

The validated FE model is used in this section to conduct a parametric study into the effects of key variables affecting the behaviour of S-NSM FRP strengthened RC beams.

IV.6.1 Effect of the Bond Length and FRP Bar Number

This section explores the impact of the number of strips on a constant CFRP cross-sectional area and different embedment lengths. The reference strip dimensions, groove sizes, and spacing were the same as the experimental ones for comparison purposes. Two concrete cover values (10 mm and 30 mm) were used, and the effect of 1, 2, 3, and 4 strips inserted within four different bond lengths (25%, 50%, 75%, and 100% of the beam span) was considered. Load-deflection curves were produced for the different cases, and their mechanical characteristics in terms of cracking load, yield load, ultimate load, yield displacement, ultimate displacement, ductility, and failure modes were evaluated and summarized in Table 4.2, showing a detailed illustration of the effect of the number of strips in conjunction with the effect of bond length on different mechanical characteristics. An overall increase in cracking and yielding load was observed when the number of strips increased for all tested bond lengths, which can be attributed to the increased stiffness of the beams.

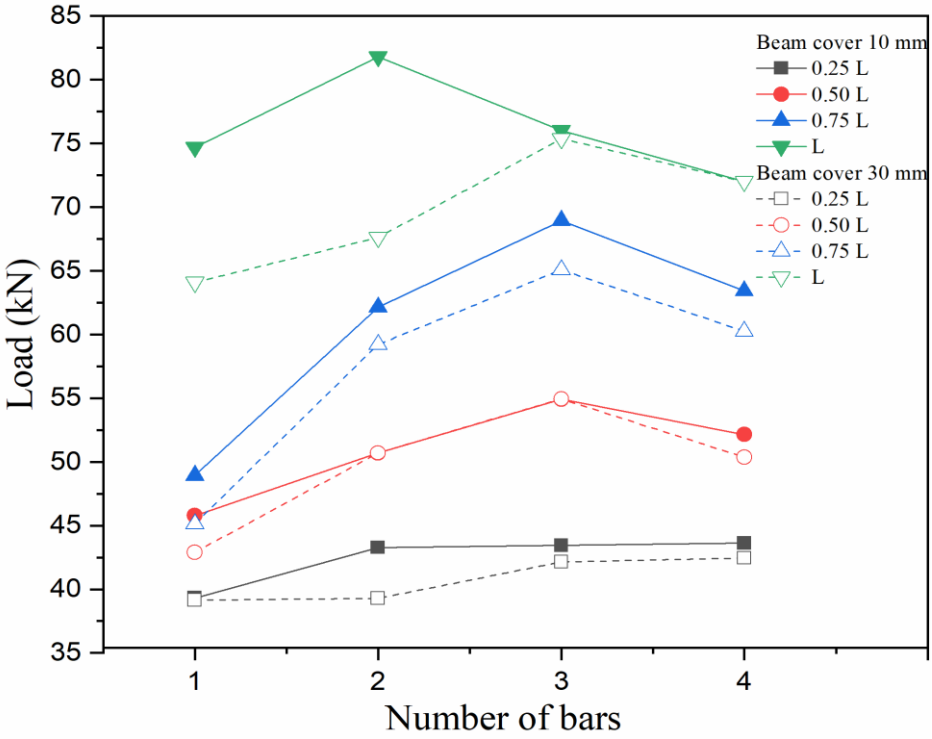

Figure 4.11 The effect of NSM bar length and number.

Figure 4.11 shows the effect of varying the NSM bar number for different reinforcement lengths. It is clear that for a bond length of 25% L, the influence of NSM bars on the load capacity was marginal, regardless of bar number and concrete cover. Increasing the bond length to 50% L resulted in an increase of (27.52%, 41.20%, 52.95%, 45.26%) and (59.72%, 79.37%, 104.54%, 87.53%) for a bar number equal to 1, 2, 3, and 4 and concrete cover of 10 mm and 30 mm, respectively, compared with the control beam. In the case of a bond length of 75% L, an increase of (36.3%, 73.06%, 86.99%, 69.83%) and (68.02%, 120.44%, 142.29%, 124.35%) for a bar number equal to 1, 2, 3, and 4 and concrete cover of 10 mm and 30 mm, respectively, was recorded, comparing with the control beam. The highest increase was recorded when using a bond length of 100%, resulting in (107.99%, 109.89%, 112.34%, 101.45%) and (138.61%, 151.71%, 180.53%, 174.01%) for bar number 1, 2, 3, and 4 and concrete cover of 10 mm and 30 mm, respectively, in comparison with the concrete beam. It should be noted that this increase was not proportional to the increase in the number of bars. For a bond length of 100%, using two NSM bars resulted in a negligible increase of 1% and 5% for concrete covers of 30 mm and 10 mm, respectively. Increasing the number of bars to four resulted in a reduction of the load capacity of the beams, which can be explained by the weakened concrete cover because of the larger grooves area and the interference between the NSM bars. In this case, the failure mode changed from a ductile to shear failure, significantly compromising the strength of the beam.

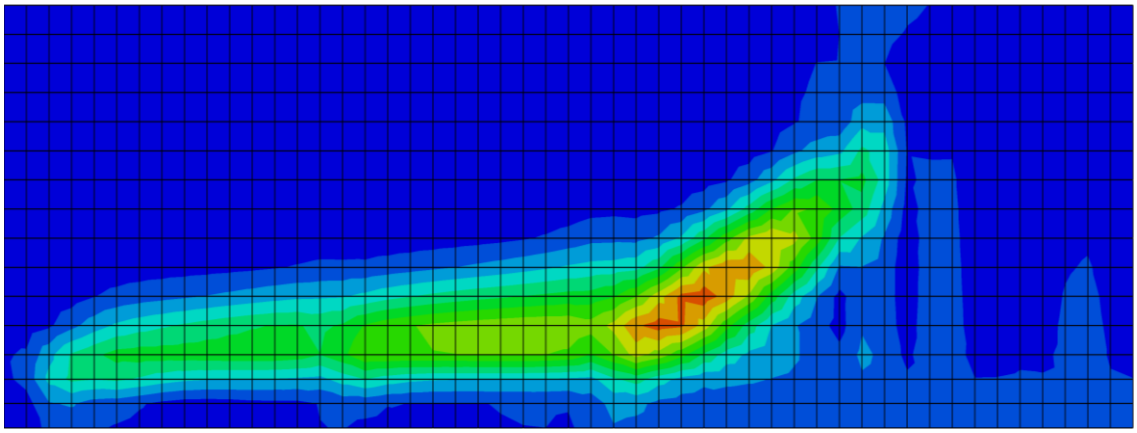

Figure 4.12 Shear failure of the beam B10N4L100-CS1

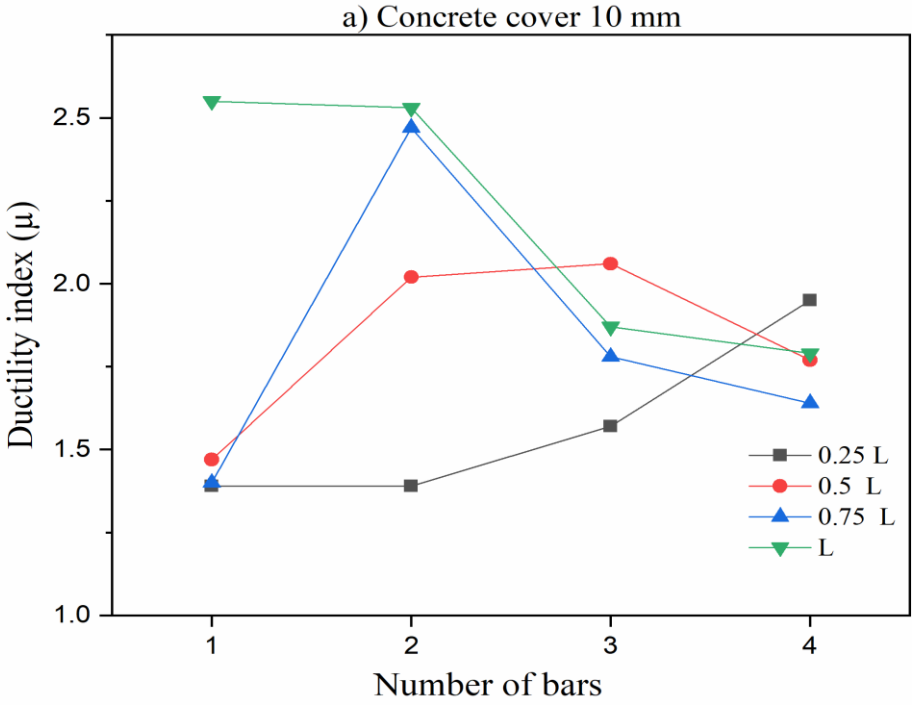

Figure 4.13 The effect of NSM bar length and number for concrete cover 10 mm

Figure.4.13 and 4.14 depicts the ductility index variation concerning different NSM bar numbers and lengths. The same trend was observed for beams with concrete cover of 10 and 30 mm. The results showed that bond length had the most significant impact on ductility. For a single NSM bar, increasing the CFRP bar length from 75% L to 100% L led to a ductility increase of approximately 82% and 65% for beams with concrete covers of 30 mm and 10 mm, respectively. This change also altered the beam's failure mode from a premature debonding to a more ductile flexural and intermediate crack debonding failure.In the case of two NSM bars, an 8% increase in ductility was noted for the concrete cover of 30 mm, while it had a negligible effect on the lower concrete cover. However, increasing the bar number from 2 to 4 resulted in a significant decrease in ductility of approximately 29% for both concrete cover lengths and changed the failure mode to brittle shear failure.

Moreover, it was observed that using two NSM bars with lengths of 50% and 75% resulted in a significant increase in ductility of approximately 43% and 76% for concrete covers of 10 mm and 30 mm, respectively, compared to using one bar. However, this increase was nullified when the number of bars was increased further.

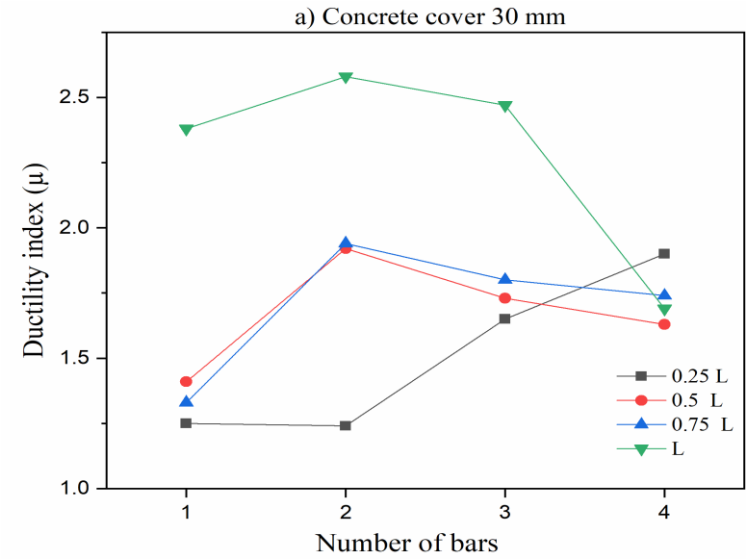

Figure 4.14 The effect of NSM bar length and number for concrete cover 30 mm

Table 4.2 FE analysis results for various NSM bar number and lengths

Beam ID	Concrete COVER	CFRP length	N	P_{cr} (kN)	P_y (kN)	Δ_y (mm)	P_u (kN)	Δ_u (mm)	P_u (%)	μ	FM
C10 (CB)	10	/	/	9.35	33.60	5.81	35.90	19.10	/	3.29	FF
B10N1L25			1	9.39	40.67	4.38	39.32	6.10	9.53	1.39	ED
B10N2L25	10	0.25 L	2	9.41	37.11	4.07	43.26	5.65	20.50	1.39	ED
B10N3L25			3	9.60	38.04	4.03	43.43	6.31	20.97	1.57	ED
B10N4L25			4	10.21	39.63	4.23	43.61	8.25	21.48	1.95	ED
B10N1L50			1	9.77	41.70	4.60	45.78	6.51	27.52	1.41	ED
B10N2L50	10	0.50 L	2	9.90	41.58	4.05	50.69	8.20	41.20	2.02	ED
B10N3L50			3	10.21	49.20	4.40	54.91	9.05	52.95	2.06	ED+CDC
B10N4L50			4	10.95	42.16	4.72	52.15	8.36	45.26	1.77	ED+CDC
B10N1L75			1	10.39	39.78	4.23	48.93	5.91	36.30	1.40	ED+CDC
B10N2L75	10	0.75 L	2	10.61	51.72	4.35	62.13	9.59	73.06	2.47	ED+CDC
B10N3L75			3	10.71	57.54	4.77	67.13	8.58	86.99	1.78	CCS
B10N4L75			4	11.01	52.64	4.87	60.97	7.97	69.83	1.64	CCS
B10N1L100			1	10.85	55.80	5.11	74.67	13.08	107.99	2.55	FF+ICD
B10N2L100	10	L	2	11.41	64.09	4.60	75.35	11.64	109.89	2.53	FF+ICD
B10N3L100			3	12.48	71.13	4.45	76.29	8.32	112.34	1.87	SF
B10N4L100			4	12.68	70.34	4.22	72.35	7.54	101.45	1.79	SF
C30 (CB)	30	/	/	9.06	26.20	5.89	26.86	16.39	/	2.78	FF
B30N1L25			1	9.15	35.71	4.64	39.14	5.80	45.72	1.25	ED
B30N2L25	30	0.25 L	2	9.35	37.03	4.26	39.29	5.29	46.28	1.24	ED
B30N3L25			3	9.71	38.06	4.91	42.15	8.08	56.92	1.65	ED
B30N4L25			4	10.11	32.07	4.27	42.45	8.10	58.04	1.90	ED
B30N1L50			1	9.27	38.93	4.41	42.90	6.22	59.72	1.41	ED
B30N2L50	30	0.50 L	2	9.82	44.10	4.79	48.18	9.21	79.37	1.92	ED
B30N3L50			3	10.31	49.01	4.86	54.94	8.41	104.54	1.73	ED+CDC
B30N4L50			4	10.92	58.42	4.60	50.37	7.51	87.53	1.63	ED+CDC
B30N1L75			1	9.82	37.16	4.06	45.13	5.85	68.02	1.44	ED
B30N2L75	30	0.75 L	2	10.51	49.88	4.53	59.21	8.80	120.44	1.94	ED
B30N3L75			3	10.81	54.11	4.22	65.08	7.61	142.29	1.80	CCS
B30N4L75			4	11.38	54.04	4.19	60.26	7.32	124.35	1.74	CCS
B30N1L100			1	10.09	50.57	5.23	64.09	12.45	138.61	2.38	FF+ICD
B30N2L100	30	L	2	11.12	57.02	4.79	67.61	12.37	151.71	2.58	FF+ICD
B30N3L100			3	12.08	61.65	4.35	75.37	10.75	180.53	2.47	SF
B30N4L100			4	13.35	70.35	4.50	73.60	7.61	174.01	1.69	SF

Note : L : Beam span, N: Number of CFRP bars , P_{cr} : cracking load , P_y and Δ_y : yielding and deflection load , P_u and Δ_u : ultimate load and deflection , P_u% is the percentage increase in the load carrying capacity in comparison with the control beam, μ (ductility index) : Δ_y/Δ_u , FM is the failure mode (FF: Flexural failure , ED :FRP end debonding , CDC : Critical diagonal crack , CCS : Concrete cover separation , ICD : Intermediate crack debonding , SF : Shear failure)

IV.6.2 Effect of the Concrete Strength and FRP Type

The influence of concrete strength on NSM bars made of four different FRP materials (CFRP, AFRP, BFRP and GFRP) was investigated. Four different concrete grades (25 MPa, 35 MPa, 45 MPa, and 65 MPa) were explored. A single NSM bar with a bond length of 100% L was used. Results are summarized in Table 4.4.

Table 4.3 Material properties of FRP materials

	AFRP	BFRP	GFRP
Tensile strength (MPa)	1300	1100	900
Modulus of elasticity (GPa)	59	55	48
Ultimate strain (%)	1.93	1.45	1.69

The properties of CFRP strips were provided in the experimental study and typical mechanical properties found in the literature [146] were used for the AFRP, BFRP, and GFRP strips and are listed in Table 4.3.Control beams were tested for each concrete grade, and bond-slip model parameters were calculated using Eq. (4.3) and Eq. (4.4). The results indicated an overall increase in beam characteristics as the concrete strength increased. The load-deflection curves for the tested specimens showed trilinear behavior, with all strengthened beams exhibiting an almost similar trend at all loading stages and increased load capacity compared to the non-strengthened beam. The curves showed an approximate trilinear response, characterized by concrete cracking, steel yielding, and post-yielding stages as shown in figure 4.15. All the composites showed similar performance, with CFRP reinforced beams exhibiting superiority as the concrete strength increased. For beams strengthened with AFRP, GFRP, and BFRP, greater displacement was observed in lower concrete strengths due to their higher elongation. As the concrete grade increased to 45 MPa, the failure mode of the beams strengthened with GFRP bars changed to FRP rupture, with the strains in the composites reaching the ultimate value, resulting in beam failure. This failure mode was also observed for beams reinforced with BFRP and AFRP bars when the concrete was 65 MPa. In contrast, no FRP rupture occurred in beams strengthened with CFRP bars due to its higher mechanical characteristics. The ultimate load and ductility index for the various materials and concretes was presented in Figure 4.16. The increase in concrete strength resulted in an increase in the ultimate load of beams strengthened with all the composites used. CFRP reinforced beams had a higher percentage increase in ultimate load compared to the other

composites, but this came at the expense of ductility for lower concrete strengths due to concrete brittle failure. AFRP strengthened beams had the highest ductility for high concrete grade, while GFRP bars performed best at lower grade concrete.

In summary, AFRP, GFRP, and BFRP are more cost-effective and better suited for low-strength concrete, while CFRP is more suitable for high-strength concrete grades.

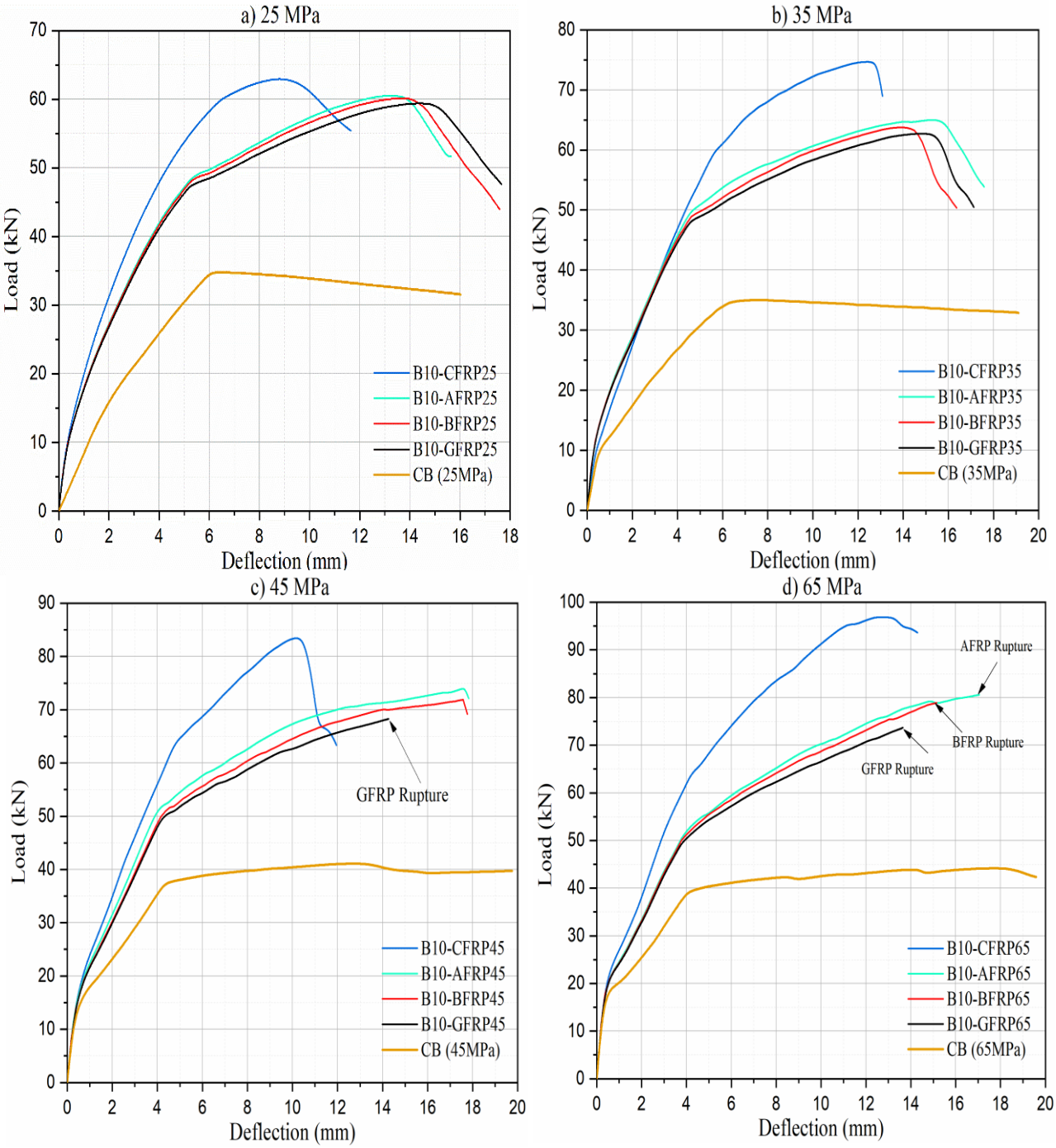

Figure 4.15 load-deflection curve for various materials

Table 4.4 FE analysis results for various concrete grades and FRP material types

Beam ID	f_c	Material type	P_{cr} (kN)	P_y (kN)	Δ_y (mm)	P_u (kN)	Δ_u (mm)	P_u%	μ	FM
C10-25 (CB)	25	/	9.05	33.73	5.79	34.07	15.87	/	2.74	FF
B10-CFRP25		CFRP	10.32	54.41	5.13	62.93	11.64	84.71	2.27	ICD
B10-AFRP25		AFRP	9.88	47.79	5.12	60.51	15.64	77.60	3.05	ICD
B10-BFRP25		BFRP	9.45	47.46	5.13	60.12	16.55	76.46	3.23	ICD
B10-GFRP25		GFRP	9.37	46.96	5.14	59.38	16.97	74.29	3.3	ICD
C10-35 (CB)	35	/	9.35	33.60	5.85	35.90	19.10	/	3.26	FF
B10-CFRP35		CFRP	10.85	55.80	5.11	74.67	13.08	107.99	2.55	ICD
B10-AFRP35		AFRP	10.27	49.64	4.58	64.99	17.39	82.20	3.8	ICD
B10-BFRP35		BFRP	9.48	49.38	4.80	63.72	16.36	78.64	3.41	ICD
B10-GFRP35		GFRP	9.44	47.42	4.45	62.70	17.12	75.78	3.85	ICD
C10-45 (CB)	45	/	15.60	37.46	4.43	39.74	19.74	/	4.46	FF
B10-CFRP45		CFRP	17.36	63.54	4.79	83.44	11.95	111.40	2.49	ICD
B10-AFRP45		AFRP	16.92	52.10	4.26	73.87	17.64	87.15	4.14	ICD
B10-BFRP45		BFRP	16.87	51.61	4.53	71.58	17.57	81.35	3.88	ICD
B10-GFRP45		GFRP	16.79	50.68	4.54	68.27	14.26	72.97	3.14	FR
C10-65 (CB)	65	/	18.91	39.40	4.22	44.16	19.59	/	4.64	FF
B10-CFRP65		CFRP	22.02	63.38	4.15	96.88	14.30	119.38	3.45	FF
B10-AFRP65		AFRP	20.88	51.79	3.97	80.57	17.05	82.45	4.29	FR
B10-BFRP65		BFRP	20.84	51.13	3.98	78.92	15.14	78.71	3.8	FR
B10-GFRP65		GFRP	20.75	50.33	3.99	73.66	13.64	66.80	3.42	FR

Note :f_c : concrete strength , P_{cr} : cracking load , P_y and Δ_y : yielding and deflection load , P_u and Δ_u : ultimate load and deflection , P_u% is the percentage increase in the load carrying capacity in comparison with the control beam, μ (ductility index) : Δ_y/Δ_u , FM is the failure mode (FF: Flexural failure , ICD : Intermediate crack debonding , FR: FRP rupture)

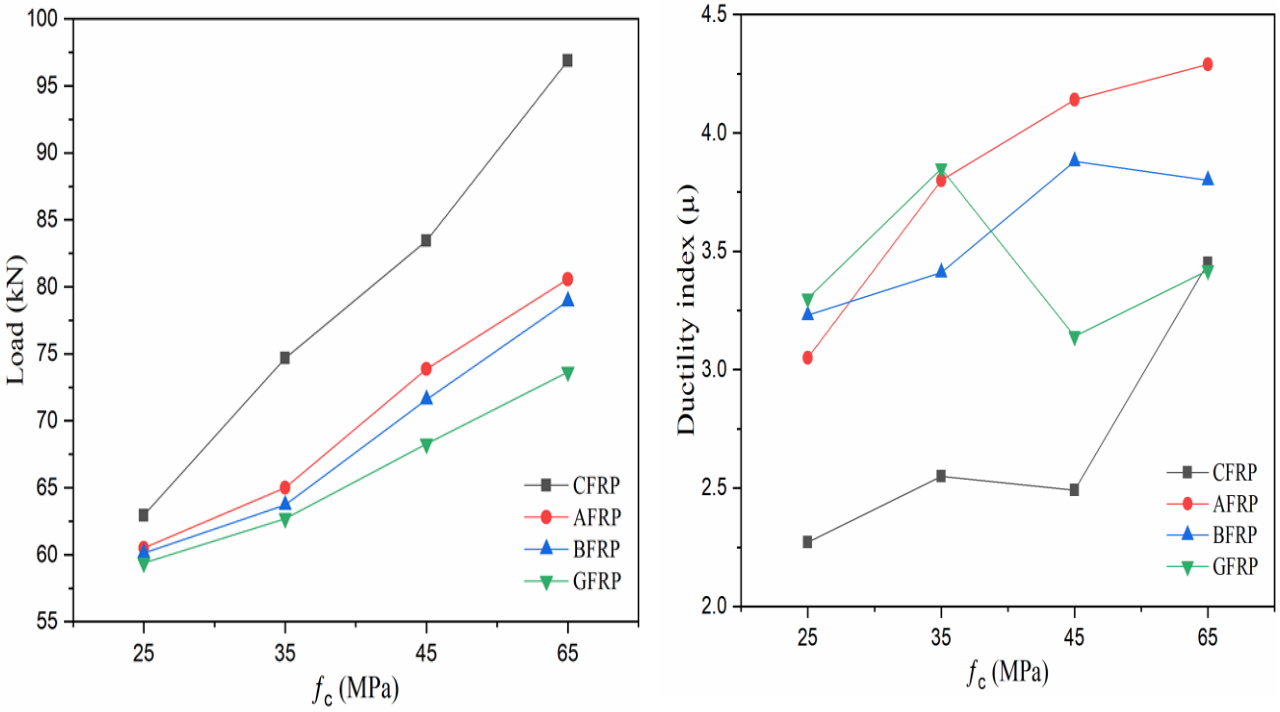

Figure 4.16 Effect of the concrete strength for different FRP materials.

IV.6.3 Effect of FRP Reinforcement Ratio

This section aimed to investigate the effect of different reinforcement ratios on the performance of NSM FRP bars using a constant bar length of 100% L. In addition to the original CFRP cross-sectional area of 50 mm^2 used in the previous sections, two values of 25 mm^2 and 12.5 mm^2 were examined in this section for a different number of bars, and the results are summarized in Table 4.5. Given that the previous sections had already covered specimens with a cross-sectional area of 50 mm^2, which resulted in a change of the failure mode to shear due to over-reinforcing, as illustrated in Figure 4.12., they were not further discussed in this section. Figure 4.17 depicts the load-deflection curves of the tested beams, showing that the curves generally exhibit similar behavior with increased ductility when the cross-section of the bar decreased. In general, beams strengthened with distributed smaller cross-sectional area NSM bars performed better than beams strengthened with higher ones for similar reinforcement ratios, indicating the importance of determining the optimal positioning for maximum efficacy and stress distribution. Figure 4.18 demonstrates the effect of the CFRP cross-sectional area for different numbers of NSM bars, showing that increasing the number of bars while using smaller cross-sectional area leads to a higher ultimate load. Figure 4.19 shows the influence of the reinforcement cross-section on the ductility of the beams, with a significant increase in ductility of about 63% observed in the case of using 2 bars of 12.5 mm2 sectional area instead of one bar at 25 mm2, even though they had the same reinforcement ratio of 0.167%.

Table 4.5 FE analysis results for various reinforcement ratios

ID	CS (mm^2)	N	ρ_{cf} (%)	P_{cr} (kN)	P_y (kN)	Δ_y (mm)	P_u (kN)	Δ_u (mm)	P_u %	μ	FM
B10N1L100-CS1	50	1	0.33	10.85	55.80	5.11	74.67	13.08	107.99	2.55	FF+ICD
B10N2L100-CS1		2	0.67	11.41	64.09	4.60	75.35	11.64	109.89	2.53	FF+ICD
B10N3L100-CS1		3	1	12.48	71.13	4.45	76.29	8.32	112.34	1.87	SF
B10N4L100-CS1		4	1.33	12.68	70.34	4.22	72.35	7.54	101.45	1.79	SF
B10N1L100-CS2	25	1	0.167	10.54	50.22	5.03	66.80	13.21	86.07	2.63	FF+ICD
B10N2L100-CS2		2	0.33	11.21	57.54	5.22	77.58	16.48	116.10	3.16	FF+ICD
B10N3L100-CS2		3	0.50	11.68	65.38	5.25	81.52	13.99	127.08	2.66	ICD
B10N4L100-CS2		4	0.67	14.11	70.43	5.45	80.91	13.70	125.38	2.51	ICD
B10N1L100-CS3	12.5	1	0.083	9.94	45.06	4.74	60.50	14.08	68.52	2.97	ED
B10N2L100-CS3		2	0.167	10.61	48.30	4.83	73.32	20.78	104.23	4.30	FF+ICD
B10N3L100-CS3		3	0.25	12.77	53.67	4.85	81.15	19.06	126.04	3.93	FF+ICD
B10N4L100-CS3		4	0.33	13.34	57.88	5.06	79.71	18.66	122.03	3.69	FF

Note : CS is cross-sectional area of the CFRP bars, N is the number of CFRP bars , ρ_{cf} is the percentage of (cross-sectional area of the CFRP reinforcements / cross-sectional area of the beam), P_{cr} : cracking load , P_y and Δ_y : yielding and deflection load , P_u and Δ_u : ultimate load and deflection , P_u% is the percentage increase in the load carrying capacity in comparison with the control beam, μ (ductility index) : Δ_y/Δ_u , FM is the failure mode (FF: flexural failure ED: end debonding , ICD : Intermediate crack debonding , SF : Shear failure)

This is because the use of smaller section bars results in a uniform distribution of loads and a more gradual failure mode compared to using one large area bar, which can lead to a sudden failure mode. This is especially evident for beams having low concrete cover.

It is worth noting that increasing the number of bars may enhance the performance of the strengthened beams, but it also increases the complexity of installation and the cost of reinforcement. Hence, a balance between the cost and benefits of using a larger number of smaller bars versus using fewer larger bars is crucial for an optimal reinforcement strategy. This can be achieved by taking into account factors such as the required strength, ductility, and the expected durability of the reinforced beam.

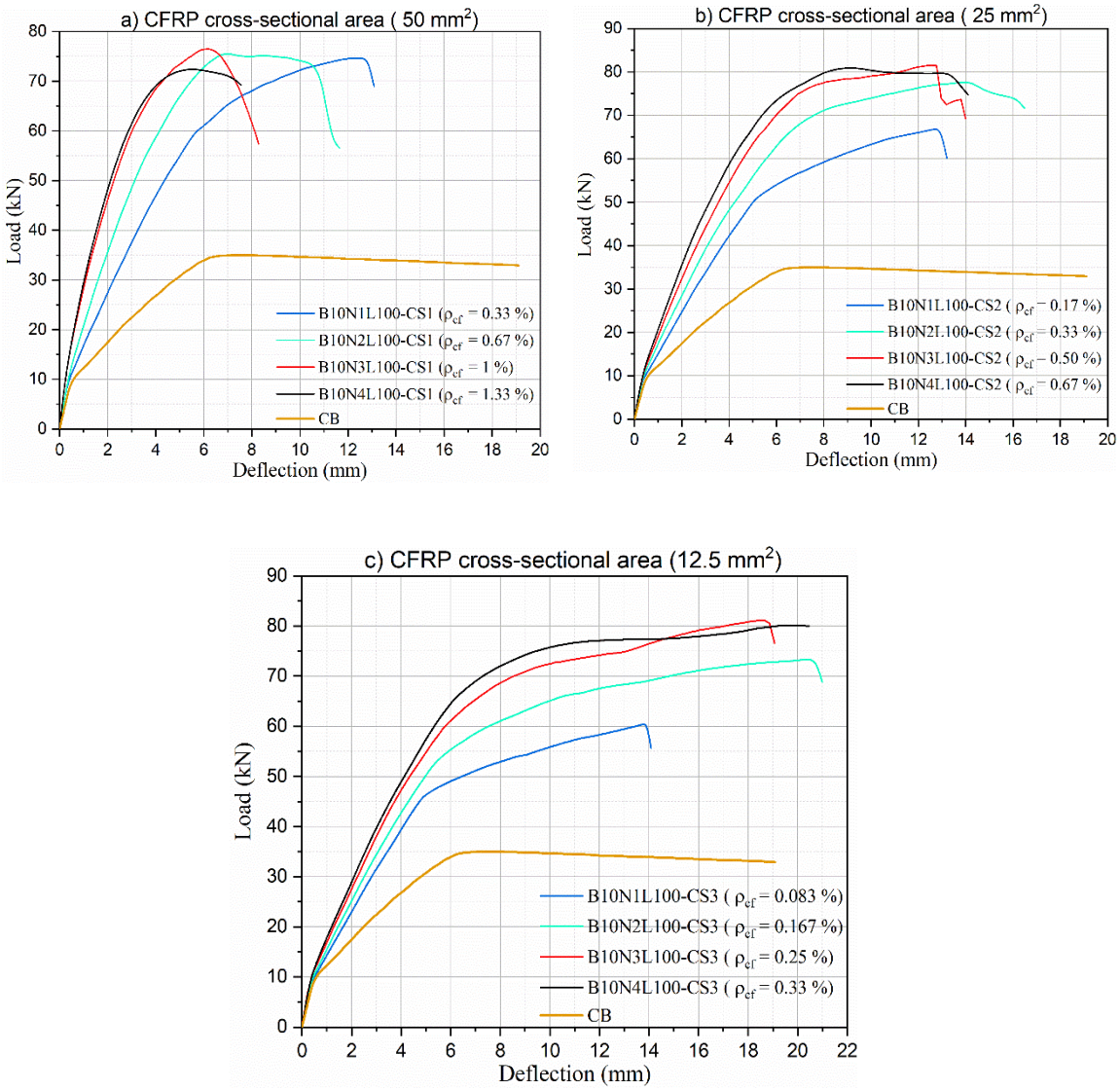

Figure 4.17 load-deflection curve for various CFRP ratios and cross-sectional area

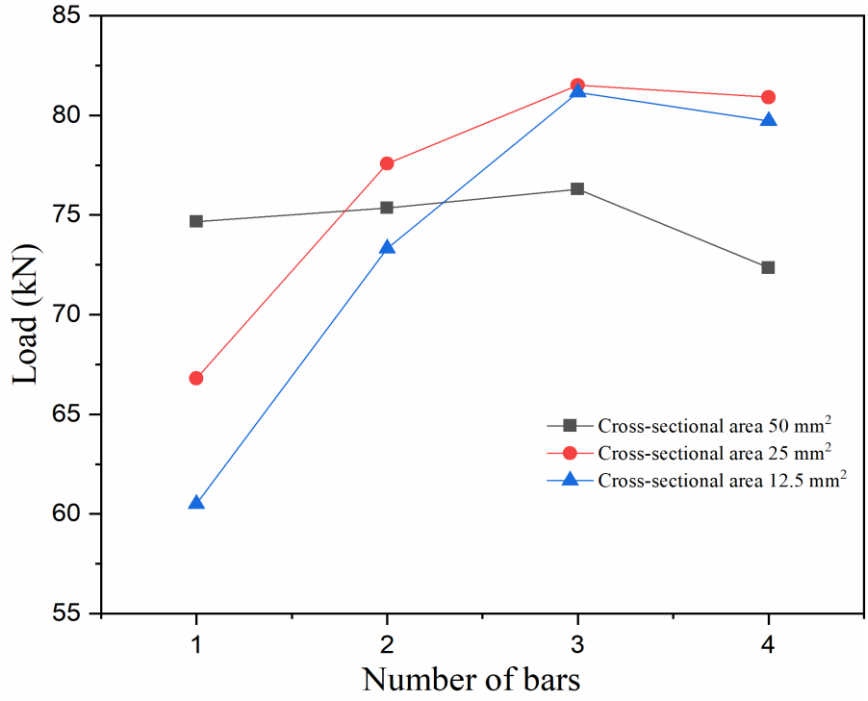

Figure 4.18 Effect of the CFRP cross-sectional area for different number of NSM bars

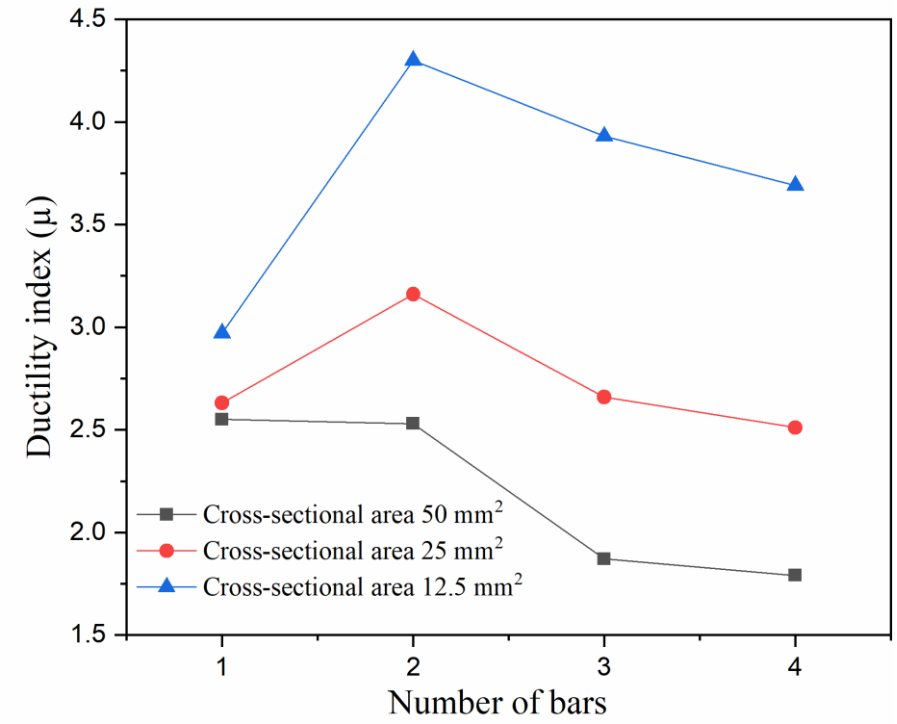

Figure 4.19 Effect of the CFRP cross-sectional area for different number of NSM bars on the ductility index

IV.6.4 Effect of FRP Reinforcement Method

In this section, the effect of bar positioning on the behavior of reinforced concrete beams was investigated using the side near-surface mounted (SNSM) technique. The SNSM technique involves placing the FRP bars on the sides of the beams instead of at the bottom, as shown in Figure 4.20. The study considered two concrete cover lengths of 10 mm and 30 mm and bond lengths ranging from 25% to 100% of the beam span. The results obtained from the study are summarized in Table 4.6. Figure 4.21 compares the load-deflection curves for NSM and SNSM techniques for different concrete cover and bond lengths. As discussed in the previous section, the beams showed typical three-phase behavior, with the SNSM technique showing better ductile behavior than the NSM technique.Figure 4.22.a shows a comparison of the ultimate load between NSM and SNSM techniques for different bond lengths. The most significant difference occurred for lower bond lengths, where the SNSM technique increased both the load and deflection in comparison with NSM

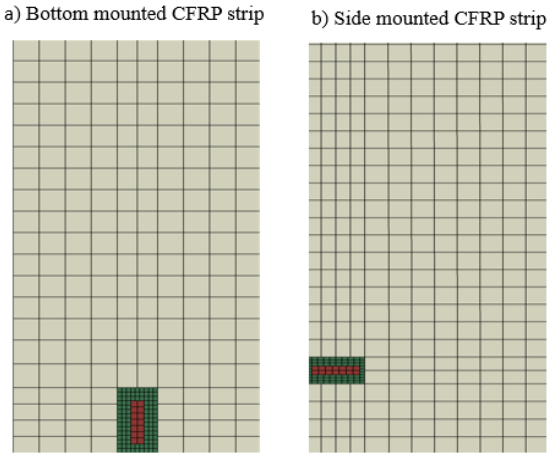

Figure 4.20 CFRP strip positioning for NSM and SNSM technique

Interestingly, for a bond length equal to the beam span, NSM strengthened beams had better load-bearing capacity, while SNSM had more ductility with a slight decrease in resistance. This behavior is due to the bars being placed higher than the area of the highest stress. Figure 4.22.a presents a detailed comparison of the ductility achieved by the NSM and SNSM techniques for different bond lengths. The results show that overall, the beams strengthened with the SNSM technique exhibited significantly better ductility performance than those strengthened with NSM, with improvements of (48%, 82%, and 34%) and (22%, 82%, and 32%) for bar lengths of (50% L, 75% L, and 100% L), and

concrete covers of 10 mm and 30 mm, respectively. In comparison with the NSM technique.

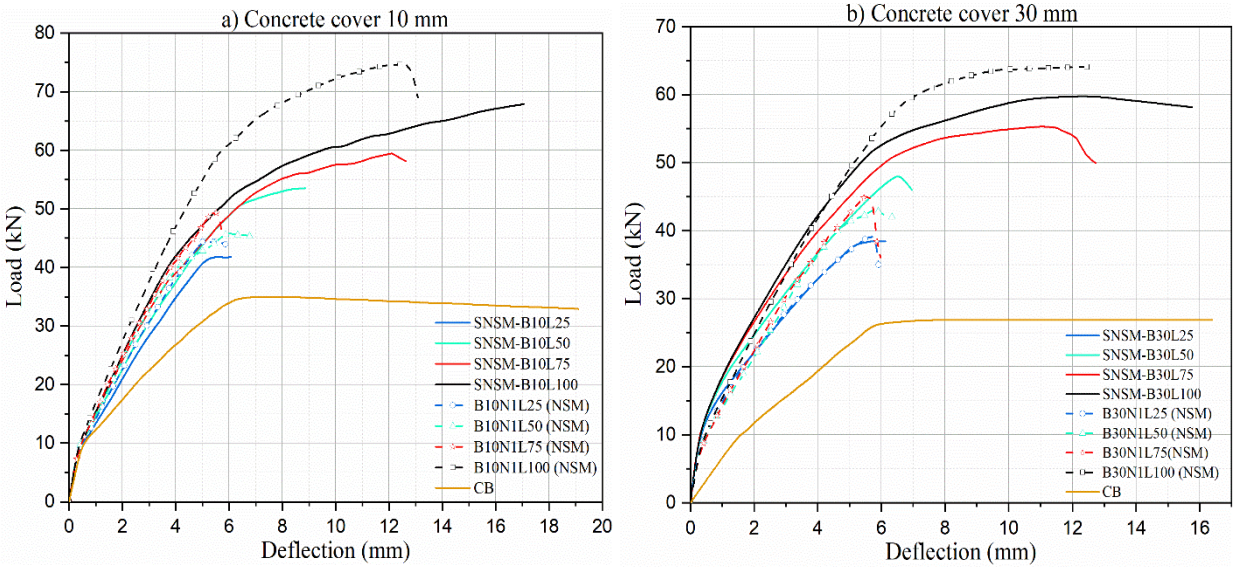

Figure 4.21 load-deflection curves for NSM and SNSM techniques

It is worth noting that the highest ductility was achieved at the full bond length for both strengthening techniques. This can be attributed to the fact that in this case, the bars are able to develop their full bond strength, leading to a better transfer of forces between the concrete and the bars. Overall, the results suggest that the SNSM technique is a more effective way to improve the ductility of reinforced concrete beams compared to NSM, especially when the bond length is relatively short.

Table 4.6 FE analysis results for NSM and SNSM techniques

Beam ID	Concrete cover	CFRP length	P_{cr} (kN)	P_y (kN)	Δ_y (mm)	P_u (kN)	Δ_u (mm)	P_u %	μ	FM
C30 (CB)		/	9.06	26.20	5.89	26.86	16.39	/	2.78	FF
SNSM-B30L25		0.25 L	11.12	35.67	4.55	38.41	6.12	43.00	1.34	ED
SNSM-B30L50	30	050 L	11.97	36.76	4.01	48.14	6.93	79.23	1.73	ED+CDC
SNSM-B30L75		0.75 L	12.36	44.34	4.86	55.30	12.72	105.88	2.62	CCS
SNSM-B30L100		L	12.43	48.32	5.04	59.75	15.75	122.45	3.13	ICD
C10 (CB)		/	9.35	33.60	5.81	35.90	19.10	/	3.29	FF
SNSM-B10L25		0.25 L	11.81	39.80	4.24	41.74	6.07	16.27	1.26	ED
SNSM-B10L50	10	050 L	12.38	39.77	4.25	53.54	8.85	49.14	2.08	ED+CDS
SNSM-B10L75		0.75 L	12.54	43.87	4.96	59.44	12.63	65.57	2.55	CCS
SNSM-B10L100		L	12.58	47.03	4.98	67.87	17.05	89.05	3.42	ICD

P_{cr} : cracking load , P_y and Δ_y : yielding and deflection load , P_u and Δ_u : ultimate load and deflection , P_u% is the percentage increase in the load carrying capacity in comparison with the control beam, μ (ductility index) : Δ_y/Δ_u , FM is the failure mode (FF: Flexural failure ,ED: FRP end debonding , CDC : Critical diagonal crack , CCS : Concrete cover separation , ICD : Intermediate crack debonding)

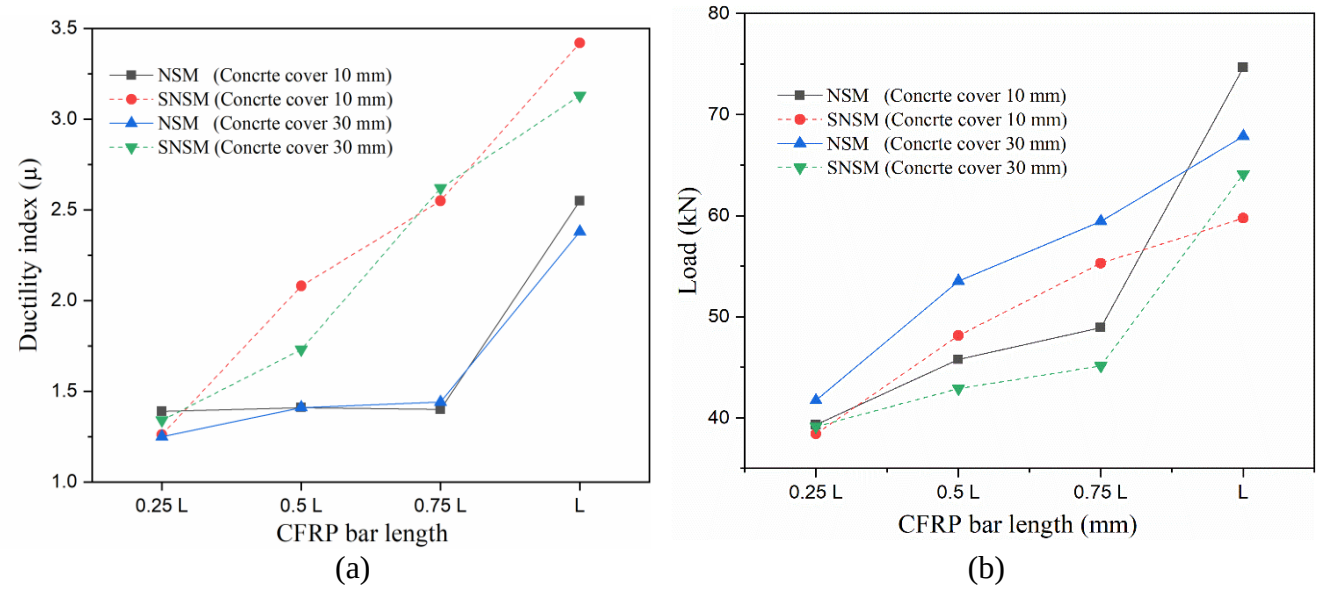

Figure 4.22 Effect of different bar lengths for NSM and SNSM techniques. a)Ultimate loads b) Ductility index.

IV.7 Conclution

This chapter presents a comprehensive investigation into the effectiveness of numerical modelling for evaluating the efficacy of NSM CFRP strip/rod reinforcement in RC beams. The investigation reveals key conclusions regarding the behaviour of strengthened beams. Firstly, the numerical model demonstrates remarkable accuracy in predicting both ultimate loads and failure modes, showcasing a robust correlation with experimental findings. Despite a slight decrease in ductility observed in NSM-strengthened beams compared to their reference counterparts, extending the length of NSM bars proves to be a significant enhancer of both load-carrying capacity and ductility, particularly noticeable when bars span the full length of the beam. Additionally, optimal positioning of smaller cross-sectional area FRP bars is identified as a strategy to improve beam performance and ductility. Furthermore, the influence of concrete strength on beam characteristics is elucidated, with CFRP emerging as the preferred choice for high-strength concrete applications. Conversely, while CFRP reinforcement leads to the highest increase in ultimate load, it exhibits lower ductility in low-strength concrete scenarios. Moreover, the prevalence of debonding of CFRP reinforcement is highlighted as the most common failure mode encountered in the study. Finally, the superiority of the SNSM technique over NSM, particularly in enhancing ductility for short bond lengths, is demonstrated to be a highly effective approach for structural strengthening.

Conclusions

The investigation of the effectiveness of the NSM CFRP strip/rod in strengthening RC beams provided valuable insights through the development of a sophisticated 3D nonlinear finite element model. The conclusions drawn from this study highlight the following key findings:

Strengthening reinforced concrete beams with NSM CFRP strips/rods significantly enhances their load-bearing capacity, showcasing the effectiveness of this reinforcement technique. Moreover, the process of cutting the lower part of steel stirrups to accommodate CFRP profiles does not compromise the ultimate load or deformability of the beams.

The evaluation of simulation accuracy in predicting the bond behavior of both externally bonded reinforcement (EBR) and near-surface-mounted (NSM) reinforcement systems showed remarkable agreement with experimental results. This close agreement serves to validate the reliability and robustness of these simulations, confirming their utility in effectively simulating and analyzing the behavior of reinforced structures.

The accuracy of the numerical model in predicting ultimate loads and failure modes of tested beams highlights its reliability as a structural analysis tool. This finding enhances our confidence in utilizing computational simulations for structural design and assessment.

While NSM-strengthened RC beams exhibit reduced ductility compared to their reference counterparts, extending NSM bars to the full span of the beam substantially improves both load-carrying capacity and ductility. This emphasizes the importance of considering NSM bar length in reinforcement design.

Optimizing the use of FRP bars by employing smaller cross-sectional areas with optimal positioning enhances the performance and ductility of reinforced concrete beams. This finding suggests potential cost-effective strategies for structural reinforcement.

The influence of concrete strength on beam characteristics underscores the interplay between material properties and structural performance. CFRP emerges as the preferred choice for high-strength concrete applications, while AFRP, GFRP, and BFRP offer cost-effective solutions for low-strength concrete.

Debonding of CFRP reinforcement emerges as the predominant failure mode in this study, highlighting the critical importance of robust bonding mechanisms in reinforcement design and implementation.

Furthermore, the SNSM technique demonstrates significant enhancement in the ductility of reinforced concrete beams compared to NSM, particularly for short bond lengths. The highest levels of ductility are achieved when bars are placed at full bond length for both techniques.

In conclusion, this study provides valuable insights into the optimization and effectiveness of NSM CFRP strip/rod for strengthening RC beams. These findings offer practical implications for structural engineering and construction practices, laying the groundwork for further research and development in the pursuit of more resilient concrete structures.

Perspectives for Future Research

Drawing upon the findings of this research and the reviewed literature, several potential avenues for future exploration are suggested:

Expanding the experimental scope to investigate the prolonged flexural performance of NSM CFRP RC beams under various sustained and fatigue loading conditions typical of real-world service conditions is imperative.

Furthermore, exploring the long-term flexural behavior of NSM CFRP RC beams under environmental challenges like freeze-thaw cycles and high temperatures is essential for comprehensive understanding.

Conducting numerical simulations through finite element analysis is crucial to examine the enduring effects of different influencing factors. This entails incorporating diverse

bond-slip models, nonlinear material properties, and time-dependent analyses to capture realistic scenarios accurately.

Moreover, there remains a significant gap in understanding the impact of factors such as concrete edge distance, groove spacing, and elevated temperatures on the bond behavior of NSM FRP-to-concrete joints, warranting further investigation.

Existing experimental studies have primarily focused on simply supported RC beams with NSM FRP reinforcement in sagging moment regions. Hogging moment regions, such as those in RC frames, have been overlooked. Future research should address this gap to elucidate potential differences in strengthening mechanisms.

Lastly, while a proposed numerical model for predicting cover separation failure shows promise, its accuracy requires validation through comprehensive parametric studies and experimental verification.

Bibliography

[1] Al-Saadi, N.T.K., Mohammed, A., Al-Mahaidi, R., Sanjayan, J., A state-of-the-art review: Near-surface mounted FRP composites for reinforced concrete structures, Construction and Building Materials. 209 (2019) 748–769.

[2] Bank, L.C., Composites for Construction: Structural Design with FRP Materials, John Wiley & Sons, 2007.

[3] Teng, J.G., Chen, J.F., Smith, S.T., Lam, L., FRP : Strengthened RC Structures, John Wiley & Sons, 2002.

[4] GangaRao, H.V.S., Taly, N., Vijay, P.V., Reinforced Concrete Design with FRP Composites, CRC Press, 2006.

[5] Hollaway, L.C., Teng, J.G., Strengthening and rehabilitation of civil infrastructures using fibre-reinforced polymer (FRP) composites, Woodhead Pubishing, 2008.

[6] Balaguru, P.N., Nanni, A., Giancaspro, J., FRP composites for reinforced and prestressed concrete structures: a guide to fundamentals and design for repair and retrofit, CRC Press, 2009.

[7] ISIS Canada, Reinforcing Concrete Structures with Fibre Reinforced Polymers Reinforcing, ISIS Canada Corporation, 2001.

[8] Banthia, N., Bisby, L., Cheng, R., Fallis, G., Hutchinson, R., Mufti, a., Neale, K.W., Newhook, J., Soudki, K., Wegner, L., An Introduction to FRP Composites for Construction, ISIS Canada Educational Module No. 2: FRP Composites for Construction. (2006) 25.

[9] Fédération Internationale du Béton (fib), externally bonded FRP reinforcement for RC structures, Task Group 9.3, Bulletin No. 14, 2001.

[10] De Lorenzis, L., Nanni, A., Characterization of FRP rods as near-surface mounted reinforcement, Journal of Composites for Construction. 5 (2001) 114–121.

[11] Parretti, R., Nanni, A., Strengthening of RC members using near-surface mounted FRP composites: Design overview, Advances in Structural Engineering. 7 (2004)

[12] Kotynia R, Baky HA, Neale KW, Ebead UA. Flexural Strengthening of RC Beams with Externally Bonded CFRP Systems: Test Results and 3D Nonlinear FE Analysis. Journal of Composite for Concstruction 2008; 12:190-201.

[13] Neale KW, Ebead UA, Baky HMA, Elsayed WE, Godat A. Modelling of Debonding Phenomena in FRP-Strengthened Concrete Beams and Slabs. Proceedings of the International Symposium on Bond Behavior of FRP in Structures 2005; 203:461-480.

[14] Wu YF, Wang ZY, Liu K, He W. Numerical analyses of hybrid-bonded FRP strengthened concrete beams. Computer Aided Civil & Infrastructure Engineering 2009; 24:371-384.

[15] Dai JG, Ueda TU, Sato Y. Modeling of tension stiffening behavior in FRP-strengthened RC members based on rigid body spring networks. Computer Aided Civil & Infrastructure Engineering 2012; 27:406-418.

[16] Niu, H.D., Wu, Z.S., Numerical analysis of debonding mechanisms in FRP-strengthened RC beams. Computer Aided Civil & Infrastructure Engineering. 2005,

[17] Mazzotti C, Savoia M, Ferracuti B. An experimental study on delamination of FRP plates bonded to concrete. Constr Build Mater 2008;22(7):1409–21.

[18] Nakaba K, Kanakubo T, Furuta T, Yoshizawa H. Bond behavior between fiber-reinforced polymer laminates and concrete. ACI Structural Journal 2002; 98(3): 359–367.

[19] Neubauer U, Rostasy FS. Design aspects of concrete structures strengthened with externally bonded CFRP plates. In: Proc. of 7th international conference on structural faults andrepair, vol. 2. Edinburgh (Scotland): ECS Publications 1997.

[20] Monti M, Renzelli M, Luciani P. FRP adhesion in uncracked and cracked concrete zones. Proc of 6th international symposium on FRP reinforcement for concrete structures. Singapore: World Scientific Publications 2003. p.183–92.

[21] Dai JG, Ueda T. Local bond stress slip relations for FRP sheets concrete interfaces. Proc of 6th international symposium on FRP reinforcement for concrete structures. Singapore: World Scientific Publications 2003. p. 143–52.

[22] Dai JG, Ueda T, Sato Y.Development of the nonlinear bond stress–slip model of fiber reinforced plastics sheet-concrete interfaces with a simple method. Journal of Composite for Concstruction 2005; 9(1):52–62.

[23] Lu XZ, Teng JG, Ye LP, Jiang JJ. Bond–slip models for FRP sheets/plates bonded to concrete. Engineering Structures 2005; 27(6): 920–937.

[24] Sun W, Ghannoum WM, Jirsa J O. Behavior of anchored carbon fiber reinforced polymer(CFRP) strips on strengthening reinforced concrete structures. ACI Structural Journal 2016; 113(2): 163-172.

[25] Sun W. Behavior of carbon fiber reinforced polymer (CFRP) anchors strengthening reinforced concrete structures [Doctoral thesis]. America: The University of Texas at Austin ; 2014.

[26] SAS. ANSYS 12.1 Finite element analysis system, SAS IP, Inc 2009.

[27] Wolanski AJ. Flexural behavior of reinforced and prestressed concrete beams using finite element analysis [Master Thesis]. America: Marquette University; 2004.

[28] ACI 440.2R-08, Guide for the design and construction of externally bonded frp systems for strengthening concrete structures. Farmington Hills, MI (USA): American Concrete Institute (ACI); 2008.

[29] Zhang HW, Smith ST. Fiber-reinforced polymer (FRP)-to-concrete joints anchored with FRP anchors: test and experimental trands. Canadian Journal of Civil Engineering 2013; 40(11): 1103-1116.

[30] I.A. Sharaky, A study of the bond and flexural behaviour of reinforced concrete elements strengthened with near surface mounted (NSM) FRP reinforcement

[31] Zhou YW. Analytical and experimental study on the strength and ductility of FRP-reinforced high strength concrete beam [Doctoral thesis]. China: Dalian University of Technology; 2009 [in Chinese].

[32] Takeo K, Matsushita H, Makizumi T, Nagashima G. Bond characteristics of CFRP sheets in the CFRP bonding technique. In: Proc. of Japan concrete institute 1997; 19(2): 1599–604.

[33] Zidani MB, Belakhdar K, Tounsi A, Bedia EAA. Finite element analysis of initially damaged beams repaired with FRP plates. Composite Structures 2015; 134:4209-

[34] Mohamed, N.A.A., Strength and drift capacity of GFRP-reinforced concrete shear walls, Université de Sherbrooke, 2013.

[35] Mukhtar, F.M., Faysal, R.M., A review of test methods for studying the FRP-concrete interfacial bond behavior, Constr. Build. Mater. 169 (2018) 877–887.

[36] Serbescu, A., Guadagnini, M., Pilakoutas, K., Standardised double-shear test for determining bond of FRP to concrete and corresponding model development, Compos. B Eng. 55 (2013) 277–297.

[37] Pellegrino, C., Tinazzi, D., Modena, C., Experimental study on bond behavior between concrete and FRP reinforcement, J. Compos. Constr. 12 (2) (2008) 180–189.

[38] Hallonet, A., Michel, L., Ferrier, E., Investigation of the bond behavior of flax FRP strengthened RC structures through double lap shear testing, Compos. B Eng. 100 (2016) 247–256.

[39] Liu, S., Zhang, J.W., Zhao, J.C., Liu, R.D., Li, K., Experimental study on performance of short-bonding interface between CFRP and concrete, Key Eng. Mater. 753 (2017) 331–336.

[40] Yun, Y., Wu, Y., Tang, W.C., Performance of FRP bonding systems under fatigue loading, Eng. Struct. 30 (11) (2008) 3129–3140.

[41] Ko, H., Sato, Y., Bond stress-slip relationship between FRP sheet and concrete under cyclic load, J. Compos. Constr. 11 (4) (2007) 419–426.

[42] Mukhtar, F.M., Customized shear test for bond-slip characterization of EBR FRP- concrete system: Influence of Substrate aggregate type, Compos. B Eng. 163 (2019) 606–621.

[43] Raoof, S.M., Bournas, D.A., Bond between TRM versus FRP composites and concrete at high temperatures, Compos. B Eng. 127 (2017) 150–165.

[44] Zheng, X.H., Huang, P.Y., Chen, G.M., Tan, X.M., Fatigue behavior of FRP–concrete bond under hygrothermal environment, Constr. Build. Mater. 95 (2015) 98–909.

[45] Mukhtar, F.M., Peiris, A., FRP-concrete bond performance under accelerated hygrothermal conditions, Constr. Build. Mater. 270 (2021) 121403.

[46] Tao, Y., Chen, J.F., Concrete damage plasticity model for modeling FRP-to-concrete bond behavior, J. Compos. Constr. 19 (1) (2015) 04014026.

[47] Dai JG, Ueda T, Sato Y. Development of the nonlinear bond stress–slip model of fiber reinforced plastics sheet-concrete interfaces with a simple method. J Compos Constr 2005;9(1):52–62..

[48] Zhang HW, Smith ST. Fiber-reinforced polymer (FRP)-to-concrete joints anchored with FRP anchors: test and experimental trands. Canadian Journal of Civil Engineering 2013; 40(11): 1103-1116.

[49] Neale K., FRPs for structural rehabilitation: a survey of recent progress, Structural Engineering and Materials. 2 (2000) 133–138.

[50] Li R, Teng JG, Yue QR. Experimental study on bond behavior of NSM CFRP strips- concrete Interface. Ind Constr 2005;35(8):31–5.

[51] Seracino R, Saifulnaz MRR, Oehlers DJ. Generic debonding resistance of EB and NSM plate-to-concrete joints. J Compos Constr ASCE 2007;11(1):62–70.

[52] Oehlers DJ, Haskett M, Wu CQ, Seracino R. Embedding NSM FRP plates for im- proved IC debonding resistance. J Compos Constr ASCE 2008;12(6):635–42.

[53] Sharma, S.K., Ali, M.S.M., Goldar, D., Sikdar, P.K., Plate-concrete interfacial bond strength of FRP and metallic plated concrete specimens, Composites Part B: Engineering. 37 (2006) 54–63.

[54] Yuan, H., Teng, J.G., Seracino, R., Wu, Z.S., Yao, J., Full-range behavior of FRP-to-concrete bonded joints, Engineering Structures. 26 (2004) 553–565.

[55] Siddiqui, N.A., Experimental investigation of RC beams strengthened with externally bonded FRP composites, Latin American Journal of Solids and Structures. 6 (2009) 343–362.

[56] Täljsten, B., Carolin, A., Nordin, H., Concrete beams strengthened with near surface mounted CFRP laminates, in: Proceedings FRPRCS, 2001: pp. 107–116.

[57] Chen, J.F., Yuan, H., Teng, J.G., Debonding failure along a softening FRP-to-concrete interface between two adjacent cracks in concrete members, Engineering Structures. 29 (2007) 259–270.

[58] Lu, X.Z., Teng, J.G., Ye, L.P., Jiang, J.J., Bond-slip models for FRP sheets/plates bonded to concrete, Engineering Structures. 27 (2005) 920–937.

[59] Yao, J., Teng, J.G., Plate end debonding in FRP-plated RC beams-I: Experiments, Engineering Structures. 29 (2007) 2457–2471.

[60] Yan, X., Miller, B., Nanni, A., Bakis, C.E., Characterization of CFRP rods used as near surface mounted reinforcement, in: 8th International Conference on Structural Faults and Repair, 1999: pp. 1–12.

[61] Galati, D., De Lorenzis, L., Effect of construction details on the bond performance of NSM FRP bars in concrete, in: Advances in Structural Engineering, 2009: pp. 683–700.

[62] Capozucca, R., Damage to reinforced concrete due to reinforcement corrosion, Construction and Building Materials. 9 (1995) 295–303.

[63] Tavakkolizadeh, M., Saadatmanesh, H., Strengthening of steel-concrete composite girders using carbon fiber reinforced polymers sheets, Journal of Structural Engineering. 129 (2003) 30–40.

[64] D. Lee, L. Cheng, J. Yan-Gee Hui, Bond characteristics of various NSM FRP reinforcements in concrete, Journal of Composites for Construction. 17 (2013) 117–129.

[65] El-Hacha, Raafat, and Sami H. Rizkalla. "Near-surface-mounted fiber-reinforced polymer reinforcements for flexural strengthening of concrete structures." Structural Journal 101.5 (2004): 717-726. [66] S.S. Zhang, J.G. Teng, T. Yu, Bond strength model for CFRP strips near-surface mounted to concrete, Journal of Composites for Construction. 18 (2014) A4014003.

[66] Foret, Gilles, and Oualid Limam. "Experimental and numerical analysis of RC two-way slabs strengthened with NSM CFRP rods." Construction and Building Materials 22.10 (2008): 2025-2030.

[67] Bilotta, Antonio, et al. "Bond efficiency of EBR and NSM FRP systems for strengthening concrete members." Journal of Composites for Construction 15.5 (2011): 757-772.

[68] Nian, Jun-Nan, and Hsisheng Teng. "Hydrothermal synthesis of single-crystalline anatase TiO2 nanorods with nanotubes as the precursor." The Journal of Physical Chemistry B 110.9 (2006): 4193-4198.

[69] De Lorenzis, Laura, and Antonio Nanni. "Bond between near-surface mounted fiber-reinforced polymer rods and concrete in structural strengthening." Structural Journal 99.2 (2002): 123-132.

[70] Seracino R., N.M. Jones, M.S.M. Ali, M.W. Page, D.J. Oehlers, Bond strength of near-surface mounted FRP strip-to-concrete joints, Journal of Composites for Construction. 11 (2007) 401–409.

[71] Yun Y., Y.F. Wu, W.C. Tang, Performance of FRP bonding systems under fatigue loading, Engineering Structures. 30 (2008) 3129–3140.

[72] Sena Cruz, José M., et al. "Bond behavior of near-surface mounted CFRP laminate strips under monotonic and cyclic loading." Journal of Composites for Construction 10.4 (2006): 295-303.

[73] Blaschko, M. "Bond behaviour of CFRP strips glued into slits." Fibre-Reinforced Polymer Reinforcement for Concrete Structures: (In 2 Volumes). 2003. 205-214. [71]

[74] Shield, C., Cathy French, and Emily Milde. "The effect of adhesive type on the bond of NSM tape to concrete." Special Publication 230 (2005): 355-372. Ebnesajjad, A.H. Landrock, Adhesives Technology Handbook, William Andrew, 2008.

[75] Thorenfeldt, E. "Bond capacity of CFRP strips glued to concrete in sawn slits." Proceedings, 8th international conference on fibre reinforced plastics for reinforced concrete structures. 2007.

[76] Haskett, Matthew, Deric John Oehlers, and MS Mohamed Ali. "Local and global bond characteristics of steel reinforcing bars." Engineering Structures 30.2 (2008): 376-383..

[77] Perera, Kalpana, et al. "Bond mechanisms of various shapes of NSM CFRP bars." Advanced Composites in Construction (ACIC 2009) (2009): 250-258.

[78] Hassan, T., and S. Rizkalla. "Bond mechanism of NSM FRP bars for flexural strengthening of concrete structures." ACI Structural journal 101.6 (2004): 830-839.

[79] Barros, Joaquim AO, and A. S. Fortes. "Flexural strengthening of concrete beams with CFRP laminates bonded into slits." Cement and Concrete Composites 27.4 (2005): 471-480.

[80] Barros, Joaquim A., and Débora R. Ferreira. "Assessing the efficiency of CFRP discrete confinement systems for concrete cylinders." Journal of Composites for Construction 12.2 (2008): 134-148.

[81] Teng, Jin-Guang, et al. "Debonding failures of RC beams strengthened with near surface mounted CFRP strips." Journal of composites for construction 10.2 (2006): 92-105.

[82] Aidoo, John. Flexural retrofit of reinforced concrete bridge girders using three CFRP systems. University of South Carolina, 2004..

[83] Yost, Joseph Robert, et al. "Flexural behavior of concrete beams strengthened with near-surface-mounted CFRP strips." ACI structural journal 104.4 (2007): 430.

[84] Khakimova, Regina, et al. "Buckling of axially compressed CFRP cylinders with and without additional lateral load: Experimental and numerical investigation." Thin-Walled Structures 119 (2017): 178-189.

[85] Kotynia, Renata, et al. "Pioneering strengthening of concrete bridge girders with pretensioned CFRP laminates in Poland." International Symposium of the International Federation for Structural Concrete. Cham: Springer Nature Switzerland, 2023.

[86] Novidis, D., Stavroula J. Pantazopoulou, and E. Tentolouris. "Experimental study of bond of NSM-FRP reinforcement." Construction and Building Materials 21.8 (2007): 1760-1770. [87] J. Yao, J.G. Teng, Plate end debonding in FRP-plated RC beams-I: Experiments, Engineering Structures.

[87] Takács, P. F., et al. "Non-linear analysis of prestressed concrete beams with a total strain based model: FEM model and full-scale testing." Finite Elements in Civil Engineering Applications. CRC Press, 2021. 201-208.

[88] Kalayci, Ahmet Serhat, Baris Yalim, and Amir Mirmiran. "Effect of untreated surface disbonds on performance of FRP-retrofitted concrete beams." Journal of Composites for Construction 13.6 (2009): 476-485.

[89] Tanarslan, H. M. "The effects of NSM CFRP reinforcements for improving the shear capacity of RC beams." Construction and Building Materials 25.5 (2011): 2663-2673.

[90] Hassan, Tarek, and Sami Rizkalla. "Investigation of bond in concrete structures strengthened with near surface mounted carbon fiber reinforced polymer strips." Journal of composites for construction 7.3 (2003): 248-257.

[91] Rizzo, Andrea, and Laura De Lorenzis. "Behavior and capacity of RC beams strengthened in shear with NSM FRP reinforcement." Construction and Building Materials 23.4 (2009): 1555-1567.

[92] Al-Mahmoud, Firas, et al. "Strengthening of RC members with near-surface mounted CFRP rods." Composite structures 91.2 (2009): 138-147.

[93] Wahab, Noran, Khaled A. Soudki, and Timothy Topper. "Mechanism of bond behavior of concrete beams strengthened with near-surface-mounted CFRP rods." Journal of composites for construction 15.1 (2011): 85-92.

[94] Kalayci, Ahmet Serhat, Baris Yalim, and Amir Mirmiran. "Construction tolerances and design parameters for NSM FRP reinforcement in concrete beams." Construction and building materials 24.10 (2010): 1821-1829.

[95] Barros, Joaquim AO, et al. "Assessing the effectiveness of embedding CFRP laminates in the near surface for structural strengthening." Construction and Building Materials 20.7 (2006): 478-491.

[96] Soliman, Ahmed Mohamed Abouzied. Flexural Behaviour of Rectangular FRP Tubes Fully Or Partially Filled with Reinforced Concrete. Diss. Université de Sherbrooke, 2016.

[97] I.A. Sharaky, R.M. Reda, M. Ghanem, M.H. Seleem, H.E.M. Sallam, Experimental and numerical study of RC beams strengthened with bottom and side NSM GFRP bars having different end conditions, Construction and Building Materials. 149 (2017) 882–903.

[98] I.A. Sharaky, M. Baena, C. Barris, H.E.M. Sallam, L. Torres, Effect of axial stiffness of NSM FRP reinforcement and concrete cover confinement on flexural behaviour of strengthened RC beams: Experimental and numerical study, Engineering Structures. 173 (2018) 987–1001.

[99] I.A. Sharaky, S.A.I. Selmy, M.M. El-Attar, H.E.M. Sallam, The influence of interaction between NSM and internal reinforcements on the structural behavior of upgrading RC beams, Composite Structures. 234 (2020) 111751.

[100] ACI 440 1R-15. Guide for the design and construction of structural concrete reinforced with FRP bars. American Concrete Institute (ACI), Farmington Hills, MI (2007).

[101] AASHTO, L. Bridge Design Guide Specifications for GFRP—Reinforced Concrete Bridge Decks and Traffic Railings. Washington (DC): American Association of State Highway and Transportation Officials, (2009).

[102] Banibayat, P. and A. Patnaik. Creep rupture performance of basalt fiber-reinforced polymer bars. Journal of Aerospace Engineering, 28(3) (2013) p. 04014074.

[103] Tetta, Z.C., L.N. Koutas, and D.A. Bournas. Shear strengthening of full-scale RC T-beams using textile-reinforced mortar and textile-based anchors. Composites Part B: Engineering, 95 (2016) 225- 239.

[104] Yeh, Y.-K. and Y. Mo. Shear retrofit of hollow bridge piers with carbon fiber-reinforced polymer sheets. Journal of Composites for Construction, 9(4) (2005) 327-336.

[105] Zhao, Xiao-Ling, Yu Bai, Riadh Al-Mahaidi, and Sami Rizkalla. Effect of dynamic loading and environmental conditions on the bond between CFRP and steel: state-of-the-art review. Journal of Composites for Construction, 18(3) (2013) p. A4013005.

[106] Liu Q, S.M., Parnas RS, McDonnell AM. Investigation of basalt fibre composite aging behaviour for applications in transportation. Polym Compos 27(5) (2006) 475–483.

[107] Abdel-Kareem, Ahmed H., Ahmed S. Debaiky, Mohamed H. Makhlouf, et al. "Shear strengthening of reinforced concrete beams using NSM/EBR techniques." Advances in Concrete Construction 12, no. 1 (2021): 63-74.

[108] Merdas, A., B. Fiorio, and N.-E. Chikh. "Aspects of bond behavior for concrete beam strengthened with carbon fibers reinforced polymers – near surface mounted." Journal of Reinforced Plastics and Composites 34, no. 6 (2015): 463-478.

[109] Douadi, A., A. Merdas, and Ł. Sadowski. "The bond of near-surface mounted reinforcement to low-strength concrete." Journal of Adhesion Science and Technology 33, no. 12 (2019): 1320-1336.

[110] Sadoun, O., A. Merdas, and A. Douadi. "The bond and flexural strengthening of reinforced concrete elements strengthened with near surface mounted prestressing steel (PS) bars." Journal of Adhesion Science and Technology 34, no. 19 (2020): 2120-2143.

[111] Pour, Arash K., Mehrdad Karami, and Moses Karakouzian. "Enhancing Flexural Strength of RC Beams with Different Steel–Glass Fiber-Reinforced Polymer Composite Laminate Configurations: Experimental and Analytical Approach." Infrastructures 9, no. 4 (2024): 73.

[112] Al-zu'bi, H., M. Abdel-Jaber, and H. Katkhuda. "Flexural Strengthening of Reinforced Concrete Beams with Variable Compressive Strength Using Near-Surface Mounted Carbon-Fiber-Reinforced Polymer Strips [NSM-CFRP]." Fibers 10 (2022): 86.

[113] Merdas, A. "Contribution à l'étude de l'adhérence renfort-béton et du comportement des poutres en B.A. renforcées par PRFC utilisant la technique NSM (Near Surface Mounted)."

[114] Abdesselam, A., A. Merdas, B. Fiorio, and N.-E. Chikh. "Experimental and Numerical Study on RC Beams Strengthened by NSM Using CFRP Reinforcements." Periodica Polytechnica Civil Engineering 67, no. 4 (2023): 1214-1233.

[115] De Lorenzis, Laura, Karin Lundgren, and Andrea Rizzo. "Anchorage length of near-surface mounted fiber-reinforced polymer bars for concrete strengthening-experimental investigation and numerical modeling." ACI Structural Journal 101.2 (2004): 269-278.

[116] Barros, Joaquim AO, et al. "Near surface mounted CFRP strips for the flexural strengthening of RC columns: Experimental and numerical research." Engineering Structures 30.12 (2008): 3412-3425.

[117] Lundqvist, Joakim, et al. "A probability study of Finite Element analysis of Near Surface Mounted Carbon Fiber Reinforced Polymer bonded to reinforced concrete." International Symposium on Fiber Reinforced Polymer Reinforcement for Concrete Structures: 16/07/2007-18/07/2007. FRPRCS-8 Symposium Secretariat, 2007.

[118] Lindquist, J., Nordin, H., Täljsten, B., Olofsson, T. "Numerical analysis of concrete beams strengthened with CFRP: a study of anchorage lengths", In: International Symposium on Bond Behaviour of FRP in Structures, Hong Kong, China. , 2005, pp. 239-246.

[119] Hassan, T., and S. Rizkalla. "Bond mechanism of NSM FRP bars for flexural strengthening of concrete structures." ACI Structural journal 101.6 (2004)

[120] Vasquez, D., Seracino, R. "Assessment of the Predictive Performance of

Existing Analytical Models for Debonding of Near-Surface Mounted FRP Strips", Advances in Structural Engineering, 13(2), pp. 299–308, 2010.

[121] Kalayci, Ahmet Serhat, Baris Yalim, and Amir Mirmiran. "Effect of untreated surface disbonds on performance of FRP-retrofitted concrete beams." Journal of Composites for Construction 13.6 (2009): 476-485.

[122] Soliman, S. M., et al. "Experimental and numerical investigation of RC beams strengthened in bending with near surface mounted CFRP." 5th International conference on Advanced Composite Materials in Bridges and Structures (ACMBSV). 2008.

[123] Barros, J.A.O., Varma, R.K., Sena-Cruz, J.M., Azevedo ,A.F.M."Near surface mounted CFRP strips for the flexural strengthening of RC columns:

Experimental and numerical research", Engineering Structures, 30(12), pp. 3412–3425, 2008.

[124] Obaidat, Y.T., Heyden, S., Dahlblom, O. "The effect of CFRP and CFRP/concrete interface models when modelling retrofitted RC beams with FEM", Composite Structures, 92(6), pp. 1391–1398, 2010.

[125] Hawileh, R. A. "Nonlinear finite element modeling of RC beams strengthened with NSM FRP rods", Construction and Building Materials, 27(1), pp. 461–471, 2012.

[126] Rezazadeh, M., Cholostiakow, S., Kotynia, R., Barros, J."Exploring new NSM reinforcements for the flexural strengthening of RC beams: Experimental and numerical research", Composite Structures, 141, pp. 132–145, 2016.

[128] NF “NF P18-406, Essai de compression [Compression test] “, French Standardization Association, Paris, France, 1981. (in French)

[129] NF “NF P18-408, Essai de traction [Tensile test]”, French Standardization Association, Paris, France, 1981. (in French)

[130] EN " 10002-1:2001, Metallic materials - Tensile testing - Part 1: Method of test at ambient temperature", European Committee for Standardization, 2001.

[131] ISO " ISO 527-1:2012 Plastics - Determination of tensile properties — Part 1: General principles", International Organization for Standardization, Geneva, Switzerland, 2012.

[132] ISO "ISO-527-2:2012. Plastics – determination of tensile properties – part 2: test conditions for moulding and extrusion plastics", international Organization for Standardization, Geneva, Switzerland, 2012.

[133] Lu XZ, Teng JG, Ye LP, Jiang JJ. Bond–slip models for FRP sheets/plates bonded to concrete. Engineering Structures 2005; 27(6): 920–937.

[134] Neubauer, U., and F. S. Rostasy. "Design aspects of concrete structures strengthened with externally bonded CFRP-plates." Proceedings of the Seventh International Conference on Structural Faults and Repair, 8 July 1997. Volume 2: Concrete and Composites. 1997.

[135] Brosens, K., and D. Van Gemert. "Anchorage of externally bonded reinforcements subjected to combined shear/bending action." Proceedings of the international Conference on FRP composites in Civil Engineering. 2001.

[136] Dai JG, Ueda T, Sato Y.Development of the nonlinear bond stress–slip model of fiber reinforced plastics sheet-concrete interfaces with a simple method. Journal of Composite for Concstruction 2005; 9(1):52–62.

[137] Nakaba K, Kanakubo T, Furuta T, Yoshizawa H. Bond behavior between fiber-reinforced polymer laminates and concrete. ACI Structural Journal 2002

[138] Cruz, José Sena, and Joaquim Barros. "Modeling of bond between near-surface mounted CFRP laminate strips and concrete." Computers & Structures 82.17-19

[139] Focacci, Francesco, Antonio Nanni, and Charles E. Bakis. "Local bond-slip relationship for FRP reinforcement in concrete." Journal of composites for construction 4.1 (2000): 24-31.

[140] De Lorenzis, Laura, and Antonio Nanni. "Bond between near-surface mounted fiber-reinforced polymer rods and concrete in structural strengthening." Structural Journal 99.2 (2002): 123-132.

[141] Borchert, Kurt, and Konrad Zilch. "Bond behaviour of NSM FRP strips in service." Structural Concrete 9.3 (2008): 127-142.

[142] Zhang, S.S., Teng, J.G., Yu T."Bond–slip model for CFRP strips near-surface mounted to concrete", Engineering Structures, 56, pp. 945–953, 2013.

[143] Fib "Model Code 2010-Final draft: Volume 1". International Federation for Structural Concrete, Lausanne, Switzerland, 2012.

[144] ABAQUS "Analysis User's Manual, Version 6.14", [Online] Available at:

[145] Carreira, D.J., Chu, K.H. "Stress-Strain Relationship for Plain Concrete in Compression ", ACI Journal Proceedings, 82(6), pp.797–804,1985

[146] Aydın, E., Boru, E., Aydın, F. "Effects of FRP bar type and fiber reinforced concrete on the flexural behavior of hybrid beams", Construction and Building Materials, 279, pp.122–407, 20.